NASA CR-132476

REARWARD-FACING STEPS IN LAMINAR SUPERSONIC

FLOWS WITH AND WITHOUT SUCTION

by

A. K. Jakubowski and C. H. Lewis

Virginia Polytechnic Institute and State University

FOREWORD

This research was sponsored by the NASA Langley Research Center under Grant No. NGR-47-004-070. The authors gratefully acknowledge contribution of Mr. R. T. Swann who was the technical monitor on the research grant and who made possible arrangements for the experiments conducted in the NASA Langley arc heated wind tunnels and Mr. R. D. Brown who performed wind tunnel measurements in the Thermal Facility Unit. The assistance of Mr. R. D. Kirchner with the data reduction and numerical calculations is gratefully appreciated.

ABSTRACT

An experimental investigation of heat-transfer and pressure distributions within regions of laminar separated flows produced by two-dimensional rearward-facing steps has been carried out at freestream Mach numbers of around 4 in the range of step height-to-boundary layer thickness (h/δ) varying from 0.1 to 2.4. With no suction from the separated area, the ratio of the maximum post-step heat transfer to the attached-flow values ($\dot{q}_{max}/\dot{q}_{fp}$) was less than unity and decreased slowly with h/δ or Reynolds number based on the step height, $Re_{\infty,h}$. A minimum values of $\dot{q}_{max}/\dot{q}_{fp}$ was predicted to occur in the range $10^3 < Re_{\infty,h} < 10^4$. The maximum heating-rate region was located far downstream of the reattachment plate stagnation point. Mass suction from the separated area increased the local heating rates, this effect was however relatively weak for purely laminar flow conditions and the competing effect of the step height clearly predominated. At step heights comparable with boundary-layer thickness, even removing the entire approaching boundary layer was not sufficient to raise the post-step heating rates above the flat-plate values.

The base pressure in the no-suction, solid-step case correlates reasonably well with the parameters $Re_{\infty,h}$ and h/δ, displaying an initial decrease followed by a tendency to level-off in the upper range of $Re_{\infty,h}$ and h/δ tested. Our experimental evidence indicates that entrainment conditions at separation may have a significant effect on the pressure distribution and flow field behind the step. The experimental results and trends observed in this investigation are discussed and explained qualitatively in terms of physical flow field models believed to be characteristic for separated flows with thick approaching boundary layers.

TABLE OF CONTENTS

TABLES

PRECEDING PAGE BLANK NOT FILMED

ILLUSTRATIONS

SYMBOLS

b	Width of model
h	Step height
H	Enthalpy
L	Length of surface ahead of step
$\dot{m}$	Mass flow rate
M	Mach number
P	Pressure
$\dot{q}$	Heat flux

$Re_{\infty,h} = U_\infty h/\nu_\infty$, Reynolds number based on h

$Re_{\infty,L} = U_\infty L/\nu_\infty$, Reynolds number based on L

T	Absolute temperature
U	Velocity

$w = \dot{m}_s/\rho_\infty U_\infty bh$, nondimensional mass-suction rate

X	Distance downstream of leading edge
ΔX	Distance downstream of step
X_e	Distance downstream of nozzle exit
y	Transverse distance measured from centerline; distance from surface
δ	Boundary-layer thickness
δ^*	Boundary-layer displacement thickness
ρ	Density
ν	Kinematic viscosity
$\overline{x}$	Interaction parameter

Subscripts:

b	Base
BL	Boundary layer
fp	Flat plate
max	Maximum value
ns	No suction
o	Stagnation conditions
ref	Reference conditions
s	Suction; static
step	Step location on the flat plate

t	Total, pitot
ts	Test section
w	Wall conditions
∞	Freestream conditions

INTRODUCTION

The flow field downstream of a rearward facing step at supersonic
speeds has been of much interest during the past several years. The
problem has become important because of the current interest in flares
and control surfaces for various flight configurations at hypersonic
speeds and because of possible application of sliding metallic heat-
shield panels for future space shuttle structures. One of the possible
flow regimes which may be encountered by some of these applications
concerns the conditions characterized by (a) laminar flow throughout
the separation, (b) thick boundary layer (i.e., when its thickness δ is
comparable to or larger than the step height h), and (c) mass suction
from the separated area. It is our intention to investigate heat-
transfer and pressure distributions for such flow configurations.

The flow field in the step region under no-suction conditions is
determined by a strong interaction between the viscous recirculating
region at the step base and the external inviscid flow. The studies
of various aspects of a rearward-facing step or wedge are numerous;
however, the vast majority of published works have centered on the case
where the boundary-layer thickness is smaller than the step height,
including investigations by Rom and Seginer[1], Weiss and Weinbaum[2,3],
Scherberg and Smith[4,5], Hama[6], Batt and Kubota[7], and more recent works
by Erdos and Zakkay[8], Wu and Su[9], and Ohrenberger and Baum.[10] Experi-
mental information or the case of $h/\delta \leq 1$ is almost nonexistent and,
to our knowledge, no experiments have been made that would include
mass suction from the separated area.

When the boundary-layer thickness is comparable to or larger than
the step height, then: a) downstream effects can be easily transmitted
upstream through the subsonic portion of the boundary or shear layer,
b) viscous effects may increase their range of influence, and c) the
effects characteristic of supersonic, thin boundary-layer flow such as
expansion at the corner, well defined location of compression near the
reattachment point, and configuration of lip and trailing shocks will
be substantially modified. Further modification and/or complexity will

1

be introduced by application of the mass suction from the base area.
Such a suction may conceivably result in an intense heating at reattach-
ment and, therefore, knowledge of poststep heat-transfer dis⁺ ⁻   ion,
when the mass-suction is applied, may be of considerable ⊦ ⌐tical
importance. In addition, it is felt that a study of pressure and heat-
transfer distributions may provide information which can be used to
define preliminary flowfield models amenable to analytical studies.

Our experiments were conducted at $M_\infty \approx 4$ in an arc-heated wind
tunnel of Thermal Facility Unit at NASA Langley. The ratio h/δ varied
from 0.1 to 2.4 and the ratio of wall temperature to freestream temp-
erature, T_w/T_o, varied between 0.055 and 0.11. The effects on surface
pressure and heating rates of step height, slot mass-flow rate, and
freestream flow parameters are presented and discussed for a range of
$Re_{\infty,h}$ (Reynolds number based on freestream conditions and step height)
between 40 and 2200. The present data on base pressure and maximum
poststep heating rates are correlated and compared with available
theoretical predictions. Part of the experimental results presented in
this report was published in Ref. 11.

APPARATUS AND PROCEDURES

Wind Tunnel

The arc-heated wind tunnel used for the experiments consists of
a magnetically-stabilized alternating current arc heater, plenum
chamber, a 15 degree conical supersonic nozzle, test cabin, diffuser
and vacuum pumping system. The water-cooled supersonic nozzle has a
7 cm (2.75 in.)-diameter throat and a 22.8 cm (9 in.)-diameter exit
section. The size of uniform gas core at the model location is no less
than 17 cm (6.7 in.). The test medium was air heated by copper elec-
trodes and the nominal range of test conditions was: $P_o = 1.82 \times 10^4$ -
1.99×10^5 N/m^2 (0.18 - 1.96 atm), T_o = 2700 - 5500 K, M_∞ = 3.95 - 4.27,
Re_∞/cm = 160 - 2200. Figure 1 presents a simplified diagram of the
experimental setup used in this investigation.

Models and Instrumentation

Two basic models were used in this investigatic.. Model I was designed for no-suction tests, Model II was designed and used primarily for suction tests. Both models were two-dimensional and provided with sharp leading edges. The models were made of copper and were water-cooled.

Model I (Fig. 2) had 12.5 cm (4.91 in.) long section upstream of the step. This section was provided with two pressure orifices, one located 3.1 cm (1.22 in.) ahead of the step and the other located on the vertical surface of the step. Varying the step height was accomplished by inserting or removing spacers beneath the reattachment plates which were mounted immediately behind the step. The interchangeable reattachment plates were instrumented for either heat-transfer or pressure measurements.

Model II (Fig. 3) was designed as an integral part of a structure containing the step model itself, retractable supporting strut and air suction duct. Under the conditions of thick approaching boundary-layers and low pressures in the recirculating region, a large suction ' area was required in order to remove a significant portion, or poss _ , the entire boundary-layer flow. Therefore, nearly the entire area of the vertical step face was used as a suction slot. The slot was connected to a R-6000 Heraeus Mechanical Blower via a sjust em of flexible hoses which allowed for rapid injection of the model into the test stream. The section upstream of the step was 10 cm (3.925 in.) long. The step height was varied by changing the spacers beneath the interchangeable plates, instrumented for either pressure or heat-transfer measurements.

Heat-transfer plates (separate for Models I and II) consisted of a 0.74 mm (0.029 in.) thick stainless steel sheet with chromel-alumel thermocouples spot-welded to the undersurface. The outputs from the thermocouples were recorded at 0.025-second intervals.

Water-cooled pressure plates (made of copper) were instrumented with 1.2 mm (0.047 in.) diameter pressure orifices which were connected to CEC strain-gauge pressure transducers. The electrical outputs from the transducers were recorded at intervals of about 1 second.

Mass Suction Installation

An arrangement employed for suction experiments on Model II is shown schematically in Fig. 1. The hot air removed from the separated region behind the step was passed through flexible hoses, vacuum pump, and an instrumented section and then reintroduced into the test cabin. The instrumented section connected to the discharge side of the vacuum pump was equipped with several pressure and temperature sensors to provide information neces ary for evaluation of suction mass-flow rates.

Procedures

The test conditions were varied by changing the tunnel mass flow-rate and the power input to the arc heater. At the beginning of each run, pitot pressure and stagnation heat transfer rate in the freestream flow were determined by using standard retractable devices (impact pressure probe and hemispherical calorimeter) injected sequentially into the stream. These measurements, combined with that of the pressure in the plenum chamber, served to establish stagnation and freestream conditions for each individual run.

In the experiments involving mass suction (Model II), the vacuum pump in the suction circuit was started before the model was injected into the jet. It was found that, for most of the tests, a period of time needed to stabilize pressure in the suction circuit after the model had been injected, was less than about 0.8 second.

Heat-transfer data were obtained from measurements of transient skin temperatures resulting from a stepwise increase in stagnation temperature. The model, initially at room temperature, was suddenly (in less than 0.25 sec.) exposed to the hot air flow where it remained from 1 to 3 seconds. Heat-transfer data were computer reduced according to a simplified heat-balance equation

$$\dot{q} = c_w \rho_w d_w \frac{dT_w}{dt}$$

where c_w is the specific heat of the wall material, ρ_w is the density of the wall material, d_w is the wall thickness, T_w is the wall temperature, and t is time. The equation above presupposes a constant temperature through the model skin, negligible lateral heat flow, negligible

heat flow to the interior of the model, and no heat losses through radiation. In these experiments, the slope dT_w/dt remained very nearly constant for at least 3 seconds, i.e., for a period longer than that required to stabilize the flow in the suction duct (less than 0.8 sec.).

Instrumentation and experimental procedures are discussed in more detail in Ref. 12.

TEST CONDITIONS

In the absence of detailed data on the flow conditions in the test section of the 22.8 cm (9 in.) arc heated tunnel, extensive work had to be done to determine, as accurately as possible, the actual freestream conditions and boundary-layer parameters along the surface of the models used. This work amounted to a partly independent study which is summarized below.

Freestream Properties

A survey of the pitot pressure along the jet axis showed that a significant pressure gradient was present in the jet expanding freely from the nozzle. The tunnel flow properties at any location in the test stream were then evaluated from both measurements and calculation. As mentioned previously, during each experiment the pitot pressure and stagnation-point heat-transfer rate were measured at the model location and the plenum pressure was measured in the arc chamber. The stagnation enthalpy was then determined for dissociated air in thermochemical equilibrium using a correlation developed by Fay and Riddell (Ref. 13). The values of the plenum pressure and the stagnation temperature (the latter obtained from a Mollier diagram using the appropriate stagnation enthalpy) were used as input data to a computer program for chemically frozen, isentropic flow expansions (Ref. 14). The solution was terminated at the station where the computed pitot pressure matched the experimental value of the pitot pressure established for the step location.

The assumption of the frozen flow model was based on examination of numerical solutions[14] to (a) nonequilibrium, (b) frozen, and (c)

5

equilibrium nozzle expansions for a number of test conditions spanning the entire range of the nominal conditions. In all cases, the flow properties defined from frozen flow expansions were very close to the properties determined from nonequilibrium flow expansions, thus indicating only a minimal amount of chemical recombination during the expansions. Consequently, the use of simple frozen expansions should be considered as a reasonable assumption. An additional argument on behalf of this assumption was provided by close agreement between the experimental wall pressure distributions on the flat-plate configuration and the theoretical predictions based on frozen flow properties. In making such predictions, account was made for the existence of a longitudinal pressure gradient in the test section which was identified from pitot pressure surveys.

Complete records of test conditions in heat-transfer and pressure measurements are presented in Tables I through IV.

Boundary Layer Parameters

Parameters of the boundary layer at the step location were predicted for nonequilibrium flow-equilibrium catalytic wall conditions and assuming that there was no upstream influence of the base pressure. The calculations were performed by using a program developed by Blottner[15] and included the effect of the freestream pressure gradient along the plate. The selection of nonequilibrium flow-equilibrium catalytic wall conditions was based on a critical evaluation of numerical predictions of flat-plate heat-transfer distributions obtained for the following models: (a) nonequilibrium flow-equilibrium catalytic wall, (b) nonequilibrium flow-noncatalytic wall, and (c) perfect gas flow. Typical results of the comparison between theoretical and experimental data are shown in Fig. 4. It was found that in practically all cases being compared (sixteen different test conditions), the predictions based on model (a) were in good agreement with the experimental data, whereas the predictions using the other two models underestimated heating rates by a large margin. The major difference between the catalytic and noncatalytic solutions tended to indicate the significant influence of surface recombination effects on the heating rates.

6

The assumption of no upstream influence of the base pressure which, of course, is not valid in the case of a thick boundary layer, means simply that the boundary-layer parameters correspond to a flat-plate configuration. As such, they can be conveniently used as reference parameters when making comparisons or presenting correlations.

The values of boundary-layer thickness (δ) and displacement thickness (δ^*), predicted for the step location, are listed in Tables I through IV.

Flow Uniformity

Initial measurements of pressure distribution on the flat-plate configuration revealed strong departures from constant longitudinal pressure conditions which could not be explained in terms of viscous interaction effects. Subsequent pitot pressure surveys indicated the presence of an axial pressure gradient in the jet stream, as shown in Fig. 5. By properly adjusting the test-chamber pressure (controlled by the rate of additional air blown into the test chamber) it was possible to maintain the jet underexpansion unchanged from one test to another at the same stagnation conditions. The presence of the pressure gradient was accounted for in defining freestream conditions and parameters of the boundary layer along the surface of the models.

Because of limitations on the model size and a desire to produce a boundary layer as thick as possible, the models selected for this investigation had relatively small widths as compared with the lengths of the section upstream of the step. This raised a question concerning two-dimensionality of the flow along the instrumented section. To answer this question, pressure measurements were made which included transverse pressure distributions at a few stations along the instrumented plate. The results of this examination, shown in Figs. 6a and 6b, indicate that the flow near the centerline was essentially two-dimensional over a distance of at least 6.5 cm ($\sim$ 2.5 in.). In view of longitudinal pressure gradients in the jet and limited width of the models, great caution must be exercised when interpreting data collected far downstream of the step ($\Delta x > 6.5$ cm ($\sim$ 2.5 in.)). In addition, under some flow conditions, the rear part of the model was influenced by

7

back pressure effects or a shock wave system generated by the support-
ing strut. Since the main object of this investigation was to study
separated flow region immediately downstream of the step, the flow
structure downstream of the reattachment was of secondary interest in
this work.

Concerning the influence of longitudinal pressure gradients, it
may be argued that these gradients should affect different step geo-
metries in essentially the similar way, at least over a relatively
short distance just behind the step. Hence, the data collected (at
$\Delta x < 6.5$ cm (~ 2.5 in.)) appear to be well suited for interpretation
based upon comparison of various configurations under similar test
conditions.

Viscous Interactions

Combination of supersonic Mach numbers and low Reynolds numbers
in these experiments may possibly result in boundary-layer-induced
interactions which could affect the inviscid pressure distribution
along the model surface. The interaction parameter $\bar{\chi} = M^2 \sqrt{C}/\sqrt{Re_x}$
(where C is the factor of proportionality in the linear viscosity-temp-
erature relation $u = CT$) has been estimated for several test conditions
at the step location and has been found to vary between 0.2 and 0.75
indicating that only a weak interaction was present. Using the data
presented in Ref. 16, the interaction induced pressure, P/P_∞, can be
estimated as varying between 1.05 and 1.25. For several test cases,
freestream static pressure distributions have been calculated from
frozen-flow expansions taking into account the actual pitot pressure
gradient in the test stream. These distributions have been found to
be in reasonably close agreement with experimental static wall pressures
except for the highest pressure case, in which case some disagreement
occurred toward the downstream end of the plate. It has been, there-
fore, concluded that viscous interaction did not play any important
role in the heat-transfer and pressure distributions discussed in this
report.

8

RESULTS AND DISCUSSION

A. No-Suction Case (Model I)

Typical heating-rate distributions along the centerline of the plate behind the steps of different height are presented in Figs. 7a-7e. The h = 0 data correspond to a flat-plate geometry. The data shown in each of these figures were obtained at similar, but not necessarily identical, freestream conditions. Typical scatter and standard deviation are indicated in Fig. 8. Dashed lines in Figs. 7a-7e refer to data which might be influenced by possible side effects or the effects of disturbances in the external flow.

For the 1.02 cm (0.4 in.) step, the heating rates are initially significantly lower than the attached-flow values obtained with the flat-plate and they gradually recover to somewhat less than the attached-flow values near the approximate reattachment region. For the 0.51 cm (0.2 in.) and 0.16 cm (0.063 in.) steps, the heating rates downstream of the reattachment region are approximately equal to the attached-flow readings. Figures 9a-9c show the effect of pressure variation on the heat-transfer distribution for each of the configurations and for various enthalpy levels. We may note that for the large step (h = 1.02 cm) the low heating rate just behind the step remains essentially unaffected by the stagnation pressure change by a factor as large as eight. This insensitivity to pressure variation gradually disappeared when the step height was decreased. By crossplotting, heating rates were determined (Figs. 10a-10c) which correspond to a given pressure level and different stagnation enthalpies. The heating rates vary roughly in proportion to the stagnation temperature which, besides the step height, plays the dominant role in establishing heating rates. Effects of Reynolds number based on the length of the plate preceding the step ($Re_{\infty,L}$) can be seen in Figs. 11a and 11b showing a few representative curves for the steps h = 1.02 and 0.51 cm.

Typical wall pressure distributions behind the steps of different height (h = 0, 0.2, 0.51, 0.71 and 1.02 cm) are displayed in Figs. 12a and 12b. Figures 13a and 13b show distributions of the wall pressure

normalized by the value of the reference pressure measured upstream of the step (P_{ref}). The pressure at the step location ($\Delta x = 0$) was measured on the vertical surface of the step. Because of the model design limitaticns, this pressure was not measured for the small step height (~ 0.2 cm). Examination of the pressure distributions shows a small region of low pressure along the surface immediately dcw.stream of the step. The length of this region increased with the step height, h, and freestream Reynolds number, Re_∞. Downstream of the "constant" pressure plateau, the pressure increased and, at distances of several step heights, the pressure recovered to approximately the attached-flow values for the flat plate. Since the low-pressure region at the step base is, most likely, associated with a recirculating flow, we may infer that for the conditions of laminar flow and thick incoming boundary layers, the extension of the recirculating area is very small, being less than one step height in most of these experiments.

The changes in surface pressure and heat-transfer rates in the separated flow area behind the step can be explained qualitatively by referring to a hypothetical schematic of the flowfield, believed to be characteristic for the case of a thick laminar boundary layer (boundary-layer thickness, δ, comparable with the step height, h) as shown in Fig. 14. A relatively thick subsonic portion of the approaching boundary layer allows the base pressure to communicate upstream of the step over a significant distance. This results in both streamwise and transverse pressure gradients upstream of the step and, consequently, a significant portion of the pressure drop across the step (p_b/p_∞) may take place before the step itself.[*] The expanding flow near the corner

---

[*] In a rough approximation, the subsonic layer may be considered as a single "streamtube." On expanding to low pressures, this streamtube reaches sonic velocity (with the average Mach number of unity) at a "throat," while the thickness and shape of the streamtube vary in compatability with the pressure variation in the outer supersonic flow. The only physically consistent solution which satisfies continuity of flow angle and pressure is to have the "throat" right at the corner. Thus, for sufficiently strong expansions (i.e., for sufficiently low base pressures) most of the subsonic flow is expanded to nearsonic or supersonic conditions at the corner.

turns sharply and is likely to undergo an overexpansion[*] followed by a recompression to the nearly constant base pressure. In the region of recompression, the flow separates from the vertical surface of the step and forms a recirculating region. The recirculating flow is entrained by the shear layer which eventually reattaches downstream of the step. The overexpansion and recompression as well as aligning the flow parallel to the dividing streamline may be the cause of the compression waves which coalesce to form a lip shock. For the low Reynolds numbers in these experiments, the lip shock is expected to be very weak, perhaps it may even vanish almost completely for the very thick approaching boundary layers.

An increase of the step height results in a) an increased expansion around the step corner leading to a rather sharp drop in the base pressure and hence a lower density at the step base and b) an increased thickness of the recirculating region which causes a reduction of temperature gradients near the wall. Both these effects are responsible for a significant drop in heating rates behind the step when its height is increased. In addition, at a higher step, the shear layer is subject to mixing with relatively cool recirculating air over a longer period and length which leads to a "cooling" and some additional lateral expansion of the shear layer, and, as a consequence, the temperature gradients and levels near the wall in the recompression zone are reduced and so are the heating rates. In consistency with the presence of a very small recirculating region in these tests, heating rates (and pressures) started to recover from low base values almost immediately downstream of the step. The maximum heating rate is expected to occur in the neighborhood of the maximum convergence (neck) of the reattaching shear layer, where both the temperature gradient and mass flux are likely to attain their maximum values. Thus, according to this suggestion, the maximum heat transfer may occur far downstream of the stagnation point (i.e., the point where the dividing streamline meets the surface of the plate)

---

[*]In the immediate vicinity of the corner, very large, theoretically infinite, pressure gradients are possible and this may play some role in the overexpansion below the step corner.

and this is in some variance with the commonly accepted model for heat-transfer distribution in separated flows.

Figures 15-17 present the correlations of the peak heating rates against the parameters $Re_{\infty,h}$ and h/δ. The peak heating rates, $\dot{q}_{max}$, are referenced to heating rates at the step location obtained from flat-plate measurements, $\dot{q}_{step}$, (Figs. 15 and 16) or to local flat-plate values, $\dot{q}_{fp}$ (Fig. 17). At a given Mach number, the parameter $Re_{\infty,h}$ combines the effects of the freestream Reynolds number Re_{∞} and the step height, h. For a given model geometry (L/h) and a laminar boundary layer, the parameter $Re_{\infty,h}$ varies as $(h/\delta)^2$. This emphasizes the potential effectiveness of $Re_{\infty,h}$ as a scaling parameter because the step height and the boundary layer thickness are the length scales which control the flowfield in the separated region. Figures 15 and 17 include data obtained by Rom and Seginer[1], Smith[5], and several points evaluated on the basis of measurements reported by Holloway, Sterrett, and Creekmore.[17] The combination of our results with the results of Smith and those of Holloway et al. provides a continuous variation of peak heating rates over the range $10^2 < Re_{\infty,h} < 10^5$. The results of Rom and Seginer depart very strongly from other reported results. It should be pointed out that Rom's measurements were made in a shock tube using very small models. A line traced through the experimental points represents "average" $\dot{q}_{max}/\dot{q}_{step}$ or $\dot{q}_{max}/\dot{q}_{fp}$ values at supersonic speeds (M < ~ 6). According to this line, a flat minimum may occur somewhere around $Re_{\infty,h} \approx 10^4$. The magnitude of this minimum may depend on the freestream Mach number M_{∞}; however, we do not expect any strong effect of M_{∞} in the range $Re_{\infty,h} < 10^3$. A physical explanation of the peak heating-rate variation shown in Fig. 15 can be given in terms of the combined effects of Re_{∞} and h as follows:

1) In the range of low Re_{∞} covered by our experiments ($Re_{\infty,h} < 2 \times 10^3$) and for a given geometry (L,h), an increase of the unit Reynolds number is equivalent to a reduction of the boundary-layer thickness δ, which, in turn, results in an extension of the recirculating region and moving the location of the peak heat transfer $\dot{q}_{max}$ further downstream. Consequently, the ratio $\dot{q}_{max}/\dot{q}_{step}$ reduces somewhat when Re_{∞} increases (note that $\dot{q}_{max}$ values were near or less than flat-plate heating rates

12

and the latter decreased in the downstream direction). The effect of the step height in the low Re_∞-range, discussed previously, can be briefly summarized as follows: The larger h is, the lower the base heating will be, the further downstream the heat-transfer reducing influence of h extends, and consequently $\dot{q}_{max}$ occurs further downstream resulting in lower values of $\dot{q}_{max}/\dot{q}_{step}$. Hence, both Re_∞ and h, when being increased, affect $\dot{q}_{max}/\dot{q}_{step}$ in the same direction, and, as the parameter $Re_{\infty,h}$ increases from very small values, the ratio $\dot{q}_{max}/\dot{q}_{step}$ gradually decreases from the initial value of unity.

2) As the Reynolds number and/or step height increase $(Re_{\infty,h} > \sim 10^3)$ the effects of Re_∞ and h tend first to stabilize and then become reversed. For this we offer an explanation as follows: When the boundary-layer thickness becomes several times smaller than the step height (due to increasing Re_∞ at a given h), then the upstream penetration of base pressure will be reduced, the recirculating region will expand, and the regions of expansions and recompressions become relatively contracted streamwise and separated by a free shear layer of nearly constant pressure (Fig. 18). Along with these changes, a lip shock of moderate strength may appear, a nearly-constant pressure zone develops immediately behind the step (associated with an increased recirculating region; cf. Fig. 12b), and the recompression zone moves downstream. Because the recompression region becomes more confined streamwise and its thickness relative to the step height decreases, the heating rates must increase above the flat-plate values if the boundary layer continues to decrease in thickness. This of course will be followed by an increase in $\dot{q}_{max}/\dot{q}_{step}$ values. As for the effect of the step height itself, it has been shown in our experiments (cf. Fig. 19) that above $Re_{\infty,h} \approx 10^3$, the base pressure tends to stabilize and becomes rather insensitive to the step height (in a purely laminar flow). This should be followed by a somewhat similar behavior of heating rates. At sufficiently large Reynolds number, we may expect an onset of transition effects in the separated area, and this will bring about some new and possibly drastic changes in the variation of $\dot{q}_{max}/\dot{q}_{step}$.

The base pressure ratios, P_b/P_∞, determined in our experiments are plotted against parameters $Re_{\infty,L}$, $Re_{\infty,h}$, and h/δ in Figs. 19, 20, and 21,

13

respectively. The values of P_∞ correspond to the step location and were taken from the experimental pressure distributions along the flat-plate configuration.* The variation of P_b/P_∞ displays an initial decrease with a tendency toward leveling-off in the upper ranges of $Re_{\infty,L}$, $Re_{\infty,h}$, and h/δ tested. The plot of P_b/P_∞ against h/δ demonstrates clearly that, for laminar separated flows, h and δ are the length scales which control the base pressure. Figure 21 includes theoretical predictions recently published by Inger (Ref. 18). His predictions on the initial slope of the base pressure variation with h/δ (i.e., for $h/\delta < 1$) agree well with our results (note that our data in the range $h/\delta < 1$ correspond to $Re_{\infty,L} < 10^3$). Our results seem to indicate that the conclusion of Chapman et al.[19] and Denison and Baum[20] that the base pressure is independent of Re_∞ for laminar flow may be essentially correct at $Re_{\infty,L} > 10^4$, even in the case of thick boundary layers.** The base pressure predicted by the laminar theory of Chapman[21] is shown in Fig. 20. Measurements performed by Smith[5] showed that at the lowest Reynolds number in his tests ($Re_{\infty,L} \approx 2 \times 10^5 - 4 \times 10^5$), i.e., when the separated flow was laminar throughout, the base pressure appeared to be approaching a constant pressure plateau, and this behavior was especially pronounced in the case of a large step (1.9 cm) and $M = 5$. These findings, if extended to lower Reynolds numbers, may be in good general agreement with our results. It may be pointed out that several investigators who studied laminar near wakes behind slender wedges and cones [22-24] reported the same trend in the base pressure variation as the one observed in our experiments. At the same time, conclusions of Kavanau[25] and Weiss[26] who predicted an increase of P_b/P_∞ until $Re_{\infty,L} \approx 10^4$, are at variance with our results.

----

*Because of some uncertainty involved in measurements of P_b at small step height ($h \leq 0.51$ cm), we do not include the data for $h \leq 0.51$ cm. It should be mentioned, however, that the data for small steps followed the same trends as shown in Figs. 19 thru 21.

**Chapman's model assumes a zero initial boundary-layer thickness, whereas Denison and Baum's model assumes a finite, but relatively small, boundary-layer thickness.

14

B. Suction Case (Model II)

Figures 22a-22d and 23a-23d show heat-transfer distributions downstream of 1.02 cm and 0.6 cm (0.4 in. and 0.235 in.) step heights, respectively. The data obtained at the downstream end of the reattachment plate were discarded as they were strongly influenced by a shock wave system produced by the supporting strut. The results obtained for 'suction' and 'no suction' cases are compared with 'reference' heat-transfer distribution of a flat-plate configuration under similar free-stream conditions. The 'no suction' measurements were made with the suction duct blanked off at the model outlet-port, thus leaving a large internal cavity connected to the suction slot. The nondimensional mass-suction rate (w) is defined as the ratio of the mass flow rate through the slot $(\dot{m}_s)$ to a mass flow rate based on freestream conditions and the step surface $(\rho_\infty U_\infty bh)$. An inspection of the stagnation conditions in the tests being compared shows that the stagnation pressure in the suction tests was a little lower (usually about 7 - 8%) than the stagnation pressure in the corresponding no-suction tests. Consequently, the suction heating rates should be somewhat increased whenever a quantitative comparison is made with the no-suction heating rates. A necessary correction may be roughly estimated by using data collected at different pressures but nearly constant temperature (such corrections have been applied in the presentation of data displayed in Fig. 27). Figures 22 and 23 indicate that, in general, mass suction from the separated area increases the local heating rates. The relative increase depends on (a) freestream conditions of the main flow, (b) rate of mass suction, (c) step height, and (d) location behind the step. The relative increase is most significant over a distance of a few step heights downstream of the step. The maximum heating rate occurred at distances of 4 to 6 step heights behind the 1.02-cm step and 7 to 9 step heights behind the 0.6-cm step. In terms of the maximum heating rate, even large suction rates, applied in this investigation, did not produce any spectacular peaks and the effect of mass suction seemed to be weaker than might be expected. Nevertheless, at sufficiently large values of w, local heating rates due to mass suction approached or exceeded the corresponding values of the flat plate configuration. Figures 24a-24c

present a direct comparison of post-step heat-transfer distribution for the cases of 1.02-cm and 0.6-cm steps and for approximately the same freestream conditions and mass suction rates ($\dot{m}_s$). It appears that the suction case is governed primarily by two parameters, h and $\dot{m}_s$. The heating rates decrease with increasing h, but increase with increasing $\dot{m}_s$. Of these two competing effects, the former clearly predominates for the flow configuration and freestream Reynolds number range studied.

No-suction heat-transfer distributions obtained on the slotted-step model (Model II) differed somewhat from those obtained on the solid-step model (Model I), the main difference being a slower recovery of heating rates downstream of the base and, correspondingly, slightly lower peak values in the slotted-step case. Only part of the difference can be ascribed to different lengths preceding steps in Models I and II. The main origin of the observed difference seems to be associated with different entrainment conditions at separation (cf. Figs. 14 and 26b). This inference can be reached on examination of pressure distributions downstream of the slotted step (measured with and without mass suction, Figs. 25a-25c*) and comparing them with solid-step pressure distributions. At low stagnation pressures, no-suction data coincided practically with the suction data. As the pressure level increased, the no-suction pressure distributions departed from the suction case, exhibiting a relatively small pressure drop around the step, followed by a slow and gradual pressure increase behind the step base.

The trends observed in heat-transfer and pressure distributions can be explained in terms of hypothetical flowfield models as sketched in Fig. 26. When the mass suction is applied (Fig. 26a), the flow downstream of the step base is formed by a boundary layer which develops along the surface while remaining under a strong influence of the recompression occurring in the adjacent outer flow. In essence, pressure and heat-transfer distribution in the suction case are similar to those

---

*Pressure distributions with mass suction applied were measured on one step configuration (h = 1.02 cm) only because a failure of the vacuum pump prevented further continuation of suction tests. In addition, the readings recorded by two pressure taps near the step location had to be discarded because of leaks which developed in the corresponding pressure lines.

observed in the no-suction solid-step case (Model I), the main differ-
ence being a somewhat smaller streamwise extension of the recompression
zone in the suction case. In the case of no-suction open slot step, a
system of vortices may develop as sketched in Fig. 26b. The pressure
at the step base, and correspondingly, the amount of expansion in the
flow over the step, may be strongly affected by a relatively extended
viscous-flow region beneath the step and shear layer and by the amount
of pressure differential which can be maintained across this region.
Since no large pressure difference can be sustained by a low-energy
flow, hence at stream pressures higher than a certain value, the "base-
pressure" departs strongly from the value cor   onding to a solid-step
configuration and remains only somewhat lowe·   the freestream static
pressure. In contrast, in the no-suction solid-step case (cf. Fig. 14),
the viscous dominated region is very limited and the base pressure
seems to be governed primarily by the properties of the outer inviscid
flow (and the geometry of the step), even at low Reynolds numbers char-
acteristic of these experiments.

From the viewpoint of potential practical applications of step con-
figurations involving mass suction, the most important property may be
the maximum post-step heating rate. Figure 27 illustrates how the maxi-
mum heating rate recorded with suction applied, $\dot{q}_{max_s}$, and normalized
by the maximum heating rate without suction, $\dot{q}_{max_{ns}}$, (using the same
configuration, i.e., slotted-step model) varies with the ratio of mass-
suction rate, $\dot{m}_s$, to the boundary-layer mass flow rate, $\dot{m}_{BL}$. The latter
was calculated from $\dot{m}_{BL} = \int_0^\delta \rho u \, dy$ for a number of test conditions. As
we mentioned previously, the stagnation conditions in the tests being
compared usually differed somewhat and corrections had to be applied to
values of $\dot{q}_{max_s}/\dot{q}_{max_{ns}}$. This involved some degree of uncertainty and,
consequently, most of the experimental points are indicated in the form
of bars which span from the minimum to the maximum of expected values.
The most complete and, perhaps, most reliable data were collected in
runs 4 and 7 with the steps of 0.6 and 1.02 cm, respectively. These
results, displayed in Fig. 27 as shaded areas, indicate that as the
mass removal increases and approaches $\dot{m}_{BL}$, the ratio $\dot{q}_{max_s}/\dot{q}_{max_{ns}}$ tends
to level off. Such a behavior should be expected on the grounds of

temperature distribution across the boundary layer. A subsequent small reduction in $\dot{q}_{max_s}/\dot{q}_{max_{ns}}$, which can be seen in the results of runs 4 and 7, may or may not be fortuitous and we see no simple explanation of such a variation. In Fig. 28 we plotted the ratio $\dot{q}_{max_s}/\dot{q}_{step}$ against the nondimensional mass-suction rate w for the case of $h/\delta \approx 0.5$. For this particular case of h/δ, theoretical predictions have been recently published in Ref. 27. A very strong departure of these predictions from the experimental results is evident, particularly if one notes that theoretical plots corresponding to T_w/T_o values in our experiments (0.06 - 0.08) would lie above those depicted in Fig. 28. Figure 29 presents an attempt to correlate all suction data by using the parameter $w(h/L)Re_{\infty,h}$ as the scaling factor. At very small values of this parameter including the case of no suction [i.e., $w(h/L)Re_{\infty,h} = 0$], the ratio $\dot{q}_{max_s}/\dot{q}_{max_{ns}}$ is close to unity. As the parameter increases above about 5, the heating-rate amplitude $(\dot{q}_{max_s}/\dot{q}_{max_{ns}})$ starts to increase. We may note that the parameter $w(h/L)Re_{\infty,h}$ is roughly proportional to suction-mass flow rate and it increases rapidly with the step height $[w(h/L)Re_{\infty,h} \sim h^2]$. thus pointing to the fact that the step height plays a dominant role in establishing heating rates at the step base.

CONCLUSIONS

An experimental study was conducted to determine heat-transfer and pressure distributions in laminar supersonic flows downstream of rear-ward-facing steps with and without mass suction from the separated region. Flow and test conditions varied in the ranges as follows: $M_\infty \approx 4$, $40 < Re_{\infty,h} < 2200$, $0.1 < h/\delta < 2.4$, $0.05 < T_w/T_o$ 0.11, and $0.1 < w < 0.8$. The more important results of this study are presented below.

1) For both suction and no-suction cases, an increase in the step height caused a sharp drop in the initial heating rates (at the step base) which then gradually recovered to less or near the attached-flow values. The height f the step controlled the heating rates at the step base, clearly dominating effects of stagnation temperature and pressure.

2) In the Re_∞-range studied, the ratio of the maximum heat-transfer in the recompression zone to the attached-flow value at the step ($\dot{q}_{max}/\dot{q}_{step}$) was less than unity and decreased slowly with h/δ or $Re_{\infty,h}$. It is anticipated that in the no-suction case, $\dot{q}_{max}/\dot{q}_{step}$ attains a minimum somewhere around $Re_{\infty,h} \sim 10^4$. The variation of the maximum heat transfer referenced to the local attached-flow value ($\dot{q}_{max}/\dot{q}_{fp}$) was very similar to the variation of $\dot{q}_{max}/\dot{q}_{step}$.

3) Mass suction from the separated area increased the local heating rates, the relative increase being most significant immediately behind the step. In general, however, the effect of mass suction on heat transfer at all-laminar flows was relatively weak and a mass suction rate exceeding the mass flow rate of the entire incoming boundary layer was needed to raise the post-step heating rates above the flat-plate values. Mass-suction data expressed in terms of the ratio $\dot{q}_{max_s}/\dot{q}_{max_{ns}}$ (peak heating rate with suction ratioed to the peak heating rate without suction) was correlated by using a parameter $w(h/L)Re_{\infty,h}$.

4) Pressure distribution downstream of the step was found to be dependent on the entrainment conditions at separation. In the no-suction solid-step case, the base pressure correlated reasonably well with the parameters $Re_{\infty,h}$ and h/δ, displaying an initial decrease followed by a tendency to level-off in the upper range of $Re_{\infty,h}$ and h/δ tested. The length of a pressure plateau behind the step was very small and tended to increase somewhat with Re_∞ and h. In the mass-suction case, the post-step pressure distributions resembled generally those obtained on no-suction solid-step configuration.

REFERENCES

1. Rom, J. and Seginer, A., "Laminar Heat Transfer to a Two-Dimensional Backward Facing Step from the High-Enthalpy Supersonic Flow in the Shock Tube," AIAA Journal, Vol. 2, No. 2, pp. 251-255, Feb. 1964.
2. Weiss, R. and Weinbaum, S., "Hypersonic Boundary Layer Separation and the Base Flow Problem," AIAA Journal, Vol. 4, No. 8, pp. 1321-1330, Aug. 19--

3. Weiss, R. F., "A New Theoretical Solution of the Laminar, Hyper-
   sonic Near Wake," AIAA Journal, Vol. 5, No. 12, pp. 2142-2149,
   Dec. 1967.

4. Scherberg, M. G. and Smith, H. E., "An Experimental Study of Super-
   sonic Flow Over a Rearward Facing, Step," AIAA Journal, Vol. 5,
   No. 1, pp. 51-56, Jan. 1967.

5. Smith, H. E., "The Flow Field and Heat Transfer Downstream of a
   Rearward Facing Step in Supersonic Flow," ARL 67-0056, March 1967,
   Wright-Patterson Air Force Base, Ohio.

6. Hama, F. R., "Experimental Studies on the Lip Shock," AIAA Journal,
   Vol. 6, No. 2, pp. 212-219, Feb. 1968.

7. Batt, R. G. and Kubota, T., "Experimental Investigation of Laminar
   Near Wakes Behind 20° Wedges at M = 6," AIAA Journal, Vol. 6,
   No. 11, pp. 2077-2083, November 1968.

8. Erdos, J. I. and Zakkay, V., "Inviscid Solution of the Steady,
   Hypersonic Near Wake by a Time-Dependent Method," AIAA Journal,
   Vol. 9, No. 7, pp. 1287-1293, July 1971.

9. Wu, J. M. and Su, M. W., "Measurements on Separated Supersonic
   Boundary Layer Flows After an Expansion Corner," Proceedings of
   the Ninth International Symposium on Space Technology and Science,
   Tokyo, Japan, 1971.

10. Ohrenberger, J. T. and Baum, E., "A Theoretical Model of the Near
    Wake of a Slender Body in Supersonic Flow," AIAA Journal, Vol. 10,
    No. 9, pp. 1165-1172, Sept. 1972.

11. Jakubowski, A. K. and Lewis, C. H., "Experimental Study of Super-
    sonic Laminar Base Flow with and without Suction," AIAA Journal,
    Vol. 11, No. 12, pp. 1670-1677, Dec. 1973.

12. Brown, R. D. and Jakubowski, A. K., "Heat-Transfer and Pressure
    Distribution in Laminar Separated Flows Downstream of Rearward
    Facing Steps with and without Mass Suction," NASA TN-D 7430, 1974.

13. Fay, J. A. and Riddell, F. R., "Theory of Stagnation Point Heat
    Transfer in Dissociated Air," J. Aeronaut. Sci., Vol. 25, No. 2,
    Feb. 1958, pp. 73-85.

14. Lordi, J. A., Mates, R. E. and Moselle, J. R., "Computer Program for
    the Numerical Solution of Nonequilibrium Expansions of Reacting Gas
    Mixtures," Cornell Aeronautical Lab, Report AD-1689-A-6, Oct. 1965.

15. Blottner, F. G., "Nonequilibrium Laminar Boundary Layer Flow of Ionizing Air," General Electric Report R64SD56, Nov. 1964.

16. Hays, W. D. and Probstein, R. F., "Hypersonic Flow Theory," Academic Press, New York, 1959.

17. Holloway, P. F., Sterrett, J. R. and Creekmore, H. S., "An Investigation of Heat Transfer within Regions of Separated Flow at a Mach Number of 6.0," NASA TN D-3074, November 1965.

18. Inger, G. R., "Theory of Supersonic Laminar Non-Adiabatic Boundary Layer Flow Past Small Rearward-Facing Steps Including Viscous-Inviscid Interaction," AIAA Paper No. 73-668, July 1973.

19. Chapman, D. R., Kuehn, D. M. and Larson, H. K., "Investigation of Separated Flows in Supersonic and Subsonic Streams with Emphasis on the Effect of Transition," NASA Rept. 1356, 1958.

20. Denison, M. R. and Baum, E., "Compressible Free Shear Layer with Finite Initial Thickness," AIAA Journal, Vol. 1, No. 1, pp. 342-349, January 1963.

21. Chapman, D. R., "An Analysis of Base Pressure at Supersonic Velocities and Comparison with Experiments," NACA TR 1051, 1951.

22. Dewey, C. F., Jr., "The Near Wake of a Blunt Body at Hypersonic Speeds," AIAA Journal, Vol. 3, No. 6, pp. 1001-1010, June 1965.

23. Softley, E. J. and Graber, B. C., "An Experimental Study of the Pressure and Heat Transfer on the Base of Cones in Hypersonic Flow," AGARD Conference Proceedings, No. 19, Vol. 1, May 1967.

24. Bauer, A. B., "Some Experiments in the Near Wake of Cones," AIAA Journal, Vol. 5, No. 7, pp. 1356-1358, July 1967.

25. Kavanau, L. L., "Base Pressure Studies in Rarefied Supersonic Flows," Journal of the Aeronautical Sciences, Vol. 23, No. 3, pp. 193-208, March 1956.

26. Weiss, R. F., "Base Pressure of Slender Bodies in Laminar, Hypersonic Flow," AIAA Journal, Vol. 4, No. 9, pp. 1557-1559, Sept. 1966.

27. Telionis, D. P., "Heat Transfer at Reattachment of a Compressible Flow over a Backward Facing Step with a Suction Slot," AIAA Journal, Vol. 10, No. 8, pp. 1108-1110, August 1972.

TABLE I.- TEST CONDITIONS IN HEAT-TRANSFER MEASUREMENTS: MODEL I

RUN	MODEL CONDITIONS		STAGNATION CONDITIONS			FREESTREAM CONDITIONS AT THE STEP LOCATION*							BOUNDARY LAYER AT THE STEP**		
	h cm	Tw/To	Po atm	Ho MJ/kg	To K	P∞ atm x10³	ρ∞ kg/m³ x10³	T∞ K	u∞ m/sec	M∞	Re∞,L x10³	Re∞,h x10³	δ cm	δ* cm	h/δ
180-03-03	0.0	0.133	0.178	3.95	2900	0.91	0.38	790	2274	4.01	3.11	0.0	1.25	0.47	0.0
180-03-06	0.0	0.098	0.204	4.28	3400	1.01	0.37	856	2531	4.09	3.11	0.0	1.29	0.48	0.0
180-03-09	0.0	0.377	0.221	6.47	3900	1.03	0.32	897	2770	4.27	2.75	0.0	1.33	0.52	0.0
180-03-12	0.0	0.073	0.233	7.96	4100	0.96	0.30	922	2855	4.19	2.73	0.0	1.36	0.53	0.0
180-03-15	0.0	0.364	0.253	10.23	4600	1.16	0.31	1071	3051	4.25	2.53	0.0	1.40	0.56	0.0
180-03-18	0.0	0.058	0.262	11.62	5200	1.17	0.29	1150	3262	4.25	2.52	0.0	1.41	0.56	0.0
180-03-21	0.0	0.055	0.277	12.79	5500	1.22	0.28	1168	3380	4.29	5.28	0.0	1.41	0.55	0.0
180-03-24	0.0	0.093	0.360	5.01	3230	1.82	0.74	831	2445	4.12	5.54	0.0	0.99	0.35	0.0
180-03-27	0.0	0.087	0.380	5.51	3700	1.84	0.67	874	2535	4.09	5.41	0.0	0.98	0.37	0.0
180-03-30	0.0	0.241	0.400	7.90	4200	1.99	0.63	897	2667	4.15	5.25	0.0	1.01	0.37	0.0
180-03-33	0.0	0.371	0.440	7.90	4200	1.94	0.64	979	2876	4.19	5.25	0.0	1.03	0.40	0.0
180-03-36	0.0	0.366	0.467	9.33	4550	2.07	0.58	1024	3010	4.21	5.05	0.0	0.99	0.37	0.0
180-03-39	0.0	0.061	0.495	10.06	4950	2.14	0.53	1158	3262	4.24	4.62	0.0	0.69	0.27	0.0
180-04-03	0.0	0.104	0.645	3.49	2880	3.17	1.38	792	2266	4.02	10.89	0.0	0.67	0.25	0.0
180-04-06	0.0	0.095	0.696	4.18	3160	3.36	1.30	856	2397	4.03	10.57	0.0	0.68	0.25	0.0
180-04-09	0.0	0.092	0.722	4.68	3320	3.50	1.30	869	2437	4.04	10.72	0.0	0.72	0.27	0.0
180-04-12	0.0	0.382	0.775	6.51	3660	3.66	1.25	932	2623	4.11	10.65	0.0	0.73	0.29	0.0
180-04-15	0.0	0.376	0.810	7.00	3925	3.97	1.24	974	2804	4.16	21.70	0.0	0.51	0.19	0.0
180-04-18	0.0	0.372	0.870	7.90	4300	4.75	2.63	873	2391	4.02	20.61	0.04	0.50	0.19	0.111
180-11-03	2.16	0.094	1.304	4.53	3175	7.03	2.57	907	2468	4.03	20.37	0.04	1.26	0.57	0.124
180-11-06	2.16	0.090	1.470	5.11	3350	7.18	2.63	945	2611	4.08	19.72	0.04	1.47	0.48	0.105
180-11-09	2.16	0.082	1.490	6.04	3650	1.06	0.41	835	2415	4.14	3.36	0.04	1.37	0.62	0.114
180-05-09	2.16	0.094	0.210	7.21	3400	1.17	0.42	894	2529	4.08	3.41	0.04	1.37	0.55	0.170
180-05-12	2.16	0.087	0.238	8.16	3750	1.20	0.38	898	4695	4.14	3.10	0.08	0.93	0.35	0.159
180-05-15	2.16	0.090	0.258	10.23	4575	1.20	0.33	1059	3016	4.18	2.86	0.04	1.00	0.39	0.162
180-05-18	2.16	0.063	0.270	9.76	4775	1.26	0.33	1103	3291	4.21	2.81	0.04	1.05	0.39	0.151
180-05-21	2.16	0.055	0.293	12.55	5050	1.33	0.32	1143	3196	3.99	6.13	0.07	1.01	0.39	0.157
180-06-03	2.16	0.100	0.364	4.68	3000	1.90	0.78	825	2318	4.02	6.06	0.08	0.96	0.25	0.106
180-06-06	2.16	0.094	0.385	5.58	3200	1.97	0.76	858	2415	4.02	6.53	0.08	0.68	0.25	0.235
180-06-09	2.16	0.388	0.407	6.39	3400	2.35	0.82	917	2498	3.96	5.90	0.07	0.68	0.26	0.233
180-06-12	2.16	0.078	0.448	7.40	3850	2.09	0.68	925	2730	4.15	5.40	0.07	0.74	0.27	0.214
180-06-15	2.16	0.063	0.473	8.18	4400	2.16	0.62	1025	2950	4.19	11.02	0.14	0.73	0.28	0.214
180-06-18	2.16	0.063	0.561	10.23	4750	2.28	0.60	1096	3079	4.20	5.23	0.07	0.74	0.27	0.166
180-06-21	2.16	0.111	0.639	3.69	2700	3.24	1.18	769	2180	4.00	11.83	0.15	0.66	0.25	0.235
180-06-24	2.16	0.103	0.660	4.07	2900	3.48	1.49	806	2269	4.00	11.63	0.15	0.68	0.26	0.233
180-06-27	2.16	0.096	0.710	4.88	3175	3.58	1.36	868	2394	4.02	11.02	0.14	0.74	0.27	0.214
180-06-30	2.16	0.090	0.766	6.00	3475	3.78	1.34	909	2540	4.19	10.91	0.11	0.73	0.28	0.214
180-06-36	2.16	0.075	0.808	6.97	3750	3.78	1.31	931	2673	4.13	10.61	0.13	0.72	0.28	0.220
180-10-03	2.16	0.092	1.360	4.65	3250	6.74	2.56	866	2425	4.03	20.15	0.26	0.51	0.19	0.312
180-10-06	2.16	0.087	1.420	5.23	3450	6.95	2.48	922	2517	4.05	19.82	0.26	0.44	0.19	0.364
180-10-09	2.16	0.082	1.490	6.00	3675	7.12	2.60	951	2624	4.09	19.58	0.25	0.52	0.19	0.306

22

TABLE I. TEST CONDITIONS IN HEAT-TRANSFER MEASUREMENTS: MODEL I - Concluded

RUN	MODEL CONDITIONS		STAGNATION CONDITIONS			FREESTREAM CONDITIONS AT THE STEP LOCATION*							BOUNDARY LAYER AT THE STEP**		
	h cm	T_w/T_o	P_o atm	H_o MJ/kg	T_o K	P_e atm $\times 10^{-3}$	ρ_e kg/m³ $\times 10^{-3}$	T_e K	U_e m/sec	M_e	$Re_{e,t}$ $\times 10^{-3}$	$Re_{e,h}$ $\times 10^{-3}$	δ cm	δ^* cm	h/δ
180-07-03	0.51	0.115	0.183	4.18	2725	0.92	0.42	742	2200	4.03	3.33	0.14	1.22	0.45	0.417
180-07-06	0.51	0.097	0.202	6.04	3100	1.03	0.41	826	2377	4.03	3.32	0.13	1.20	0.44	0.424
180-07-09	0.51	0.090	0.214	7.09	3350	1.06	0.39	892	2565	4.08	3.29	0.13	1.26	0.47	0.435
180-07-12	0.51	0.080	0.224	4.14	3750	1.07	0.36	898	2696	4.14	3.11	0.12	1.42	0.57	0.381
180-07-15	0.51	0.069	4.53	11.62	4350	1.21	0.35	1032	2926	4.12	3.30	0.12	1.33	0.50	0.381
180-07-18	0.51	0.061	0.253	11.62	4900	1.22	0.31	1123	3139	4.20	2.66	0.11	1.44	0.55	0.354
180-07-21	0.51	0.059	0.273	12.79	5074	1.26	0.31	1147	3208	4.21	2.70	0.11	1.37	0.53	0.372
180-07-24	0.51	0.102	0.345	4.65	2950	1.60	0.60	815	2296	3.94	5.87	0.25	0.94	0.36	0.538
180-07-27	0.51	0.095	0.380	5.35	3150	1.96	0.76	852	2391	4.01	6.39	0.25	1.00	0.38	0.513
180-07-30	0.51	0.092	0.395	6.04	3270	2.03	0.76	868	2451	4.03	6.39	0.25	0.99	0.38	0.513
180-07-33	0.51	0.086	0.431	7.67	3750	2.10	0.70	921	2686	4.11	5.42	0.24	0.93	0.34	0.546
180-07-36	0.51	0.070	0.457	9.07	4300	2.12	0.62	1006	2912	4.18	5.36	0.22	1.00	0.38	0.507
180-07-39	0.51	0.067	0.464	9.42	4500	2.21	0.63	1057	3032	4.18	5.67	0.22	1.01	0.36	0.501
180-07-42	0.51	0.100	0.640	3.60	2750	3.33	1.51	768	2200	3.99	11.75	0.46	0.66	0.26	0.761
180-07-45	0.51	0.104	0.640	4.34	3175	3.51	1.44	826	2315	4.14	11.27	0.46	0.70	0.26	0.728
180-07-48	0.51	0.094	0.711	6.97	3725	3.24	1.22	926	2540	4.06	10.04	0.41	0.70	0.26	0.728
180-07-51	0.51	0.081	0.797	6.97	3725	3.13	1.11	884	2481	4.30	9.05	0.39	0.72	0.27	0.703
180-07-54	0.51	0.075	0.832	7.92	4075	3.78	1.15	965	2796	4.17	13.20	0.41	0.53	0.19	1.010
180-07-57	0.51	0.096	1.360	4.18	3115	6.76	2.68	862	2366	4.02	25.96	0.86	0.52	0.22	0.936
180-09-03	0.51	0.086	1.420	6.35	3675	6.81	2.21	973	2750	4.05	19.65	0.75	0.54	0.20	0.819
180-09-06	0.51	0.111	1.552	5.74	3675	6.91	2.66	983	2750	4.11	18.45	0.72	1.24	0.45	0.846
180-09-09	1.02	0.398	0.178	3.95	2700	0.91	0.43	767	2183	3.99	3.18	0.27	1.20	0.44	0.726
180-01-03	1.02	0.092	0.257	6.74	3675	1.05	0.43	775	2163	4.02	3.44	0.24	1.40	0.56	0.807
180-01-06	1.02	0.081	0.276	6.74	3700	1.11	0.42	844	2465	4.06	3.53	0.20	1.26	0.48	0.754
180-01-09	1.02	0.067	0.240	7.90	4450	1.15	0.36	891	2672	4.14	3.37	0.24	1.35	0.50	0.717
180-01-12	1.02	0.063	0.294	9.76	4600	1.19	0.33	1034	2971	4.18	2.92	0.23	1.42	0.54	0.739
180-01-15	1.02	0.058	0.265	11.16	4800	1.23	0.30	1103	3101	4.19	2.79	0.23	1.37	0.53	1.066
180-01-18	1.02	0.107	0.274	13.25	5150	1.24	0.30	1152	3238	4.23	2.65	0.22	0.55	0.42	1.066
180-01-21	1.02	0.094	0.358	4.65	2950	1.87	0.77	861	2294	3.99	6.14	0.50	1.01	0.39	1.001
180-01-24	1.02	0.092	0.390	5.58	3200	2.01	0.77	870	2416	4.00	6.10	0.50	0.93	0.34	1.093
180-01-27	1.02	0.067	0.442	6.34	3275	2.00	0.77	876	2454	4.33	6.21	0.47	0.46	0.37	1.038
180-02-03	1.02	0.064	0.470	8.60	4150	2.17	0.66	978	2854	4.17	5.73	0.43	0.95	0.36	1.065
180-02-06	1.02	0.064	0.500	10.00	4700	2.27	0.61	1086	3041	4.20	5.27	0.43	0.67	0.25	1.559
180-02-09	1.02	0.135	0.640	3.95	2850	2.80	1.43	792	2246	4.03	11.17	0.91	0.68	0.26	1.488
180-02-12	1.02	0.102	0.680	4.18	2950	3.48	1.46	815	2291	4.00	11.42	0.93	0.70	0.27	1.493
180-02-15	1.02	0.094	0.710	4.88	3200	3.58	1.38	873	2438	4.02	10.92	0.89	0.75	0.28	1.355
180-02-18	1.02	0.087	0.760	5.81	3450	3.82	1.36	911	2526	4.04	10.59	0.89	0.73	0.28	1.389
180-02-24	1.02	0.073	0.860	8.16	4125	3.84	1.19	981	2838	4.18	10.28	0.84	0.56	0.10	1.389
180-04-03	1.02	0.093	1.460	4.53	3225	6.94	2.66	883	2413	4.02	20.87	1.70	0.55	0.10	2.031
180-08-06	1.02	0.087	1.460	5.23	3450	7.12	2.55	922	2517	4.05	20.33	1.65	0.50	0.18	2.020
180-08-09	1.02	0.080	1.530	6.28	3750	7.24	2.46	953	2658	4.10	19.71	1.60	0.5	0.19	1.972

*FREE STREAM CONDITIONS BASED ON FROZEN FLOW MODEL

**BOUNDARY LAYER PREDICTIONS BASED ON NONEQUILIBRIUM FLOW-EQUILIBRIUM CATALYTIC WALL CONDITIONS

TABLE II. TEST CONDITIONS IN PRESSURE MEASUREMENTS: MODEL I

RUN	MODEL CONDITIONS		STAGNATION CONDITIONS			FREESTREAM CONDITIONS AT THE STEP LOCATION*							BOUNDARY LAYER AT THE STEP**			
	h cm	T_w/T_o	P_o atm	H_o MJ/kg	T_o K	P_∞ atm x10^3	ρ_∞ kg/m^3 x10^3	T_∞ K	U_∞ m/sec	M_∞	$Re_{\infty,L}$ x10^3	$Re_{\infty,h}$ x10^3	δ cm	δ^* cm	h/δ

*FREE STREAM CONDITIONS BASED ON FROZEN FLOW MODEL

**BOUNDARY LAYER PREDICTIONS BASED ON NONEQUILIBRIUM FLOW-EQUILIBRIUM CATALYTIC WALL CONDITIONS

TABLE III.- TEST CONDITIONS IN HEAT-TRANSFER MEASUREMENTS: MODEL II

RUN	MODEL CONDITIONS			STAGNATION CONDITIONS			FREESTREAM CONDITIONS AT THE STEP LOCATION*							BOUNDARY LAYER AT THE STEP**		
	h cm	w	T_w/T_o	P_o atm	H_o MJ/kg	T_o K	P_∞ atm $\times10^3$	ρ_∞ kg/m³ $\times10^3$	T_∞ K	U_∞ m/sec	M_∞	$Re_{\infty,L}$ $\times10^{-3}$	$Re_{\infty,h}$ $\times10^{-3}$	δ cm	δ^* cm	h/δ
190-10-03	0.0	0.0	0.682	0.226	7.90	3650	1.13	0.39	804	2645	4.10	2.61	0.0	1.24	0.45	0.0
190-12-06	0.0	0.0	0.092	0.251	12.50	4750	1.24	0.32	1110	3076	4.15	2.19	0.0	1.24	0.45	0.0
190-10-32	0.0	0.0	0.092	0.385	5.81	3253	2.66	0.77	877	2435	3.99	4.87	0.0	0.79	0.30	0.0
190-13-15	0.0	0.0	0.078	0.450	7.96	3850	2.24	0.72	943	2722	4.10	4.87	0.0	0.82	0.31	0.0
190-10-18	0.0	0.0	0.065	0.477	9.15	4175	2.32	0.60	1038	2931	4.14	4.67	0.0	0.86	0.33	0.0
190-13-21	0.0	0.0	0.103	0.409	3.96	2900	3.78	1.59	515	2262	3.96	9.72	0.0	0.58	0.22	0.0
190-10-24	0.0	0.0	0.087	0.775	6.57	3650	4.08	1.54	622	2520	4.21	9.08	0.0	0.60	0.23	0.0
190-13-27	0.0	0.0	0.081	0.875	7.44	3725	4.24	1.36	644	2655	4.08	9.28	0.0	0.61	0.23	0.0
190-13-30	0.110	0.0	0.077	0.221	7.96	3900	1.24	1.35	965	2735	4.11	8.99	0.0	0.61	0.23	0.0
190-05-03	0.0	0.0	0.081	0.727	7.60	3494	1.11	1.36	935	2645	4.09	2.55	0.015	1.23	0.49	0.487
190-04-03	0.60	0.0	0.082	0.263	7.60	3840	1.11	0.48	994	2645	4.10	2.57	0.015	1.12	0.42	0.535
190-04-09	0.0	0.0	0.063	0.260	11.36	4800	1.16	0.34	1116	3096	4.16	2.04	0.012	1.71	0.44	0.493
190-09-06	0.0	0.0	0.063	0.252	11.16	4775	1.61	0.51	1116	3044	4.15	2.17	0.013	1.22	0.46	0.491
190-04-12	0.611	0.0	0.097	0.355	5.58	3144	2.60	0.75	862	2398	3.99	4.54	0.028	0.82	0.33	0.728
190-05-12	0.58	0.0	0.093	0.383	7.81	3237	2.10	0.79	878	2420	3.98	4.75	0.028	0.87	0.36	0.731
190-03-12	0.0	0.0	0.093	0.383	7.21	3560	2.10	0.79	907	2589	3.98	4.93	0.030	0.82	0.30	0.687
190-04-15	0.606	0.0	0.061	0.410	7.56	3700	2.16	1.72	921	2656	4.06	4.76	0.029	0.82	0.30	0.728
190-05-15	0.593	0.0	0.081	0.432	7.72	3765	2.18	1.72	943	2723	4.08	4.42	0.029	0.84	0.31	0.712
190-09-15	0.0	0.0	0.076	0.439	9.07	4315	2.43	0.64	1245	2611	4.14	4.73	0.029	0.83	0.31	0.720
190-05-18	0.612	0.0	0.102	0.464	4.07	2928	3.47	1.66	627	2276	3.95	4.37	0.026	0.86	0.33	0.694
190-04-21	0.700	0.0	0.107	0.600	4.07	2935	3.71	1.64	626	2278	3.95	8.95	0.057	0.59	0.22	1.704
191-05-21	0.708	0.0	0.103	0.691	3.65	3000	3.76	1.54	819	2262	3.96	9.41	0.058	0.58	0.22	1.015
190-09-21	0.0	0.0	0.082	0.722	6.34	3437	3.48	1.27	910	2515	4.31	9.67	0.058	0.58	0.22	1.031
190-04-27	0.725	0.0	0.077	0.763	6.74	3857	3.96	1.30	961	2622	4.05	8.64	0.051	0.62	0.23	0.960
190-09-24	0.0	0.0	0.077	0.770	7.81	3650	4.06	1.41	927	2570	4.01	7.03	0.054	0.66	0.22	0.999
190-05-24	0.786	0.0	0.084	0.227	7.90	3675	4.17	1.41	923	2664	4.31	5.96	0.055	0.60	0.22	0.999
191-03-27	0.777	0.0	0.093	0.348	5.81	3217	4.40	1.40	982	2596	4.06	9.05	0.055	0.60	0.22	0.965
190-09-30	0.0	0.0	0.077	0.379	5.52	3185	2.60	0.71	967	2735	3.98	8.44	0.051	0.62	0.23	0.984
190-09-03	0.0	0.0	0.081	0.402	7.44	3560	2.11	0.71	905	2664	4.11	2.56	0.026	1.47	0.57	0.717
188-05-03	0.251	0.0	0.087	0.227	7.90	3695	1.67	0.36	982	2664	4.09	2.53	0.026	1.23	0.49	0.829
190-07-12	0.224	0.0	0.093	0.348	5.81	3217	1.80	0.71	872	2419	3.98	4.48	0.040	0.96	0.34	1.130
190-08-12	0.284	0.0	0.064	0.379	5.90	3560	2.60	0.71	867	2433	3.98	4.65	0.052	0.88	0.34	1.153
190-07-15	0.264	0.0	0.068	0.402	8.14	4405	2.18	0.66	980	2734	4.05	4.47	0.048	0.90	0.31	1.217
190-03-06	0.0	0.0	0.076	0.425	9.30	4405	2.11	0.59	860	2763	4.11	4.47	0.046	0.90	0.31	1.134
190-07-18	0.264	0.0	0.078	0.435	7.60	3846	2.18	0.70	962	2946	4.14	3.09	0.041	0.91	0.34	1.119
190-08-15	0.0	0.0	0.069	0.620	9.62	4320	2.17	0.70	942	2721	4.11	4.70	0.044	0.83	0.31	1.225
188-04-18	0.337	0.0	0.099	0.620	9.42	3030	2.26	0.65	1026	2911	4.14	4.39	0.045	0.86	0.32	1.186
188-04-15	0.346	0.0	0.100	0.664	4.36	2990	3.35	1.34	837	2323	3.96	8.27	0.095	0.68	0.25	1.502
190-07-21	0.337	0.0	0.100	0.660	4.36	2990	3.45	1.41	837	2305	3.97	8.66	0.089	0.66	0.22	1.692
190-08-21	0.0	0.0	0.104	0.690	3.65	2894	3.75	1.58	817	2267	3.96	9.67	0.099	0.58	0.22	1.754

TABLE III.- TEST CONDITIONS IN HEAT-TRANSFER MEASUREMENTS: MODEL II - Concluded

RUN	MODEL CONDITIONS			STAGNATION CONDITIONS			FREESTREAM CONDITIONS AT THE STEP LOCATION							BOUNDARY LAYER AT THE STEP**		
	h cm	w	T_w/T_o	P_o atm	H_o MJ/kg	T_o K	P_∞ atm $\times 10^{-3}$	ρ_∞ kg/m³ $\times 10^{-3}$	T_∞ K	U_∞ m/sec	M_∞	$Re_{\infty,st}$* $\times 10^{-3}$	$Re_{\infty,h}$ $\times 10^{-3}$	δ cm	δ^* cm	h/δ
190-07-24	1.02	0.358	0.088	0.714	5.88	3420	3.74	1.33	915	2526	4.01	8.42	0.86	0.62	0.23	1.642
190-07-18	1.02	0.407	0.089	0.750	5.68	3376	3.55	1.42	911	2463	4.00	8.95	0.52	0.60	0.22	1.701
190-07-27	1.02	0.394	0.086	0.755	6.07	3732	3.67	1.27	951	2676	4.06	8.28	0.85	1.63	0.23	1.603
190-08-24	1.02	0.3	0.087	0.766	5.91	3460	4.02	1.42	920	2516	4.21	8.38	0.92	0.80	0.22	1.701
190-07-30	1.02	0.435	0.076	0.802	7.67	3930	3.91	1.23	968	2751	4.11	8.21	0.84	0.63	0.24	1.610
190-23-12	1.02	0.491	0.079	0.805	7.18	3775	3.98	1.28	943	2681	4.10	8.48	0.47	0.62	0.23	1.634
190-08-27	1.02	0.3	0.080	0.815	6.97	3790	4.02	1.32	946	2667	4.28	8.71	0.89	0.61	0.23	1.675
188-02-09	1.02	0.442	0.077	0.865	7.56	3600	4.03	1.34	965	2735	4.11	8.90	0.71	0.61	0.23	1.667
190-04-33	1.02	0.3	0.077	0.870	7.56	26	4.25	1.34	972	2747	4.10	8.94	0.92	0.61	0.23	1.658

*FREE STREAM CONDITIONS BASED ON FROZEN FLOW MODEL

**BOUNDARY LAYER PREDICTIONS BASED ON NONEQUILIBRIUM FLOW-EQUILIBRIUM CATALYTIC WALL CONDITIONS

TABLE IV.- TEST CONDITIONS IN PRESSURE MEASUREMENTS: MODEL II

RUN	MODEL CONDITIONS h cm	MODEL CONDITIONS w	MODEL CONDITIONS T_w/T_o	STAGNATION CONDITIONS P_o atm	STAGNATION CONDITIONS H_o MJ/kg	STAGNATION CONDITIONS T_o K	FREESTREAM P_∞ atm $\times10^{-3}$	FREESTREAM ρ_∞ kg/m³ $\times10^{-3}$	FREESTREAM T_∞ K	FREESTREAM U_∞ m/sec	FREESTREAM M_∞	$Re_{\infty,L}$ $\times10^{-3}$	$Re_{\infty,\theta}$ $\times10^{-3}$	BL δ cm	BL δ^* cm	N/s
197-05-06	0.0	0.0	0.071	0.236	9.24	4250	1.18	0.34	1009	2869	4.12	2.33	0.0	1.19	0.45	0.0
197-05-12	0.0	0.0	0.054	0.160	5.52	3175	1.94	0.74	865	2399	3.98	4.45	0.0	0.82	0.30	0.0
197-05-15	0.0	0.0	0.076	0.421	8.14	3925	2.68	0.66	951	2756	4.11	4.45	0.0	0.86	0.32	0.0
197-05-18	0.0	0.0	0.070	0.451	8.07	4300	2.11	0.61	1010	2910	4.16	4.23	0.0	0.87	0.33	0.0
197-05-21	0.0	0.0	0.101	0.680	4.18	2960	3.68	1.52	832	2290	3.96	9.28	0.0	0.58	0.22	0.0
197-05-24	0.0	0.0	0.087	0.770	5.93	3452	4.06	1.43	922	2520	4.01	9.03	0.0	0.61	0.27	0.0
197-05-27	2.0	0.0	0.081	0.813	6.40	3700	4.14	1.37	947	2661	4.06	8.91	0.0	0.61	0.23	0.0
197-05-30	2.0	0.0	0.097	1.420	4.18	3082	7.65	3.02	870	2339	3.96	16.38	0.0	0.42	0.16	0.0
197-05-36	0.0	0.0	0.082	1.570	5.81	3675	7.99	2.65	968	2615	4.04	16.84	0.0	0.44	0.16	0.0
197-05-39	2.0	0.0	0.085	1.895	5.35	3550	9.69	3.32	958	2553	4.02	20.78	0.0	0.44	0.16	0.0
197-01-03	1.02	0.276	0.082	0.226	7.90	3650	1.13	0.39	896	2639	4.10	2.61	0.27	1.23	0.49	0.829
197-04-03	1.02	0.237	0.054	0.240	6.22	3200	1.28	0.69	856	2419	4.00	3.11	0.32	1.10	0.43	0.926
197-03-06	1.02	0.0	0.077	0.242	6.37	3900	1.20	0.38	936	2753	4.12	4.62	0.27	1.10	0.41	0.921
197-01-12	1.02	0.318	0.101	0.367	4.77	2960	2.00	0.81	814	2302	3.95	5.01	0.51	0.79	0.29	1.292
197-03-12	1.02	0.0	0.098	0.364	5.00	3050	1.99	0.78	846	2337	3.96	4.90	0.50	0.80	0.30	1.272
197-04-12	1.02	0.384	0.094	0.368	5.70	3200	2.12	0.76	872	2410	3.98	4.75	0.50	0.81	0.30	1.263
197-01-15	1.02	0.396	0.085	0.422	6.97	3650	2.15	0.73	900	2577	4.07	4.87	0.49	0.83	0.30	1.221
197-03-15	1.02	0.0	0.082	0.475	7.32	3650	2.14	0.68	916	2632	4.04	4.81	0.48	0.84	0.31	1.217
197-04-15	1.02	0.430	0.078	0.431	7.90	3875	2.14	0.68	937	2713	4.10	4.64	0.44	0.84	0.34	1.149
197-01-18	1.02	0.461	0.069	0.450	9.17	4353	2.19	0.62	1033	2924	3.98	4.25	0.44	0.88	0.30	1.258
197-03-18	1.02	0.0	0.075	0.553	6.77	4020	2.23	0.65	989	2795	4.12	4.66	0.44	0.87	0.36	1.161
197-03-21	1.02	0.474	0.070	0.675	4.07	2920	2.21	0.64	1021	2906	3.95	4.39	0.96	0.59	0.22	1.776
197-01-21	1.02	0.0	0.103	0.675	3.84	2825	3.68	1.60	798	2271	3.94	9.78	1.00	0.58	0.22	1.754
197-04-21	1.02	0.385	0.101	0.680	4.16	2963	3.68	1.57	832	2290	3.96	9.28	0.95	0.59	0.22	1.745
197-03-24	1.07	0.392	0.092	0.765	5.11	3250	3.51	1.34	893	2472	3.98	9.42	0.97	0.58	0.21	1.764
197-06-24	1.02	0.0	0.090	0.765	2.46	3350	3.51	1.43	900	2472	4.02	9.02	0.93	0.59	0.22	1.736
197-04-24	1.02	0.381	0.087	0.768	5.93	3452	4.05	1.42	922	2520	3.99	9.01	0.92	0.60	0.22	1.701
197-03-27	1.02	0.417	0.086	0.800	5.84	3475	4.18	1.46	925	2532	4.02	9.28	0.95	0.59	0.22	1.718
197-04-27	1.02	0.0	0.084	0.810	6.34	3575	4.22	1.44	938	2580	4.03	9.20	0.94	0.59	0.22	1.709
197-03-30	1.02	0.379	0.081	0.810	6.97	3700	4.12	1.37	947	2641	4.06	8.88	0.91	0.63	0.23	1.667
197-01-30	1.02	0.0	0.000	1.495	4.88	3790	3.51	1.82	921	2464	4.00	11.44	1.79	0.41	0.16	2.381
197-04-30	1.02	0.381	0.092	0.768	4.65	3250	7.80	2.97	901	2418	3.99	18.01	1.85	0.41	0.15	2.451
197-01-36	1.02	0.410	0.087	1.505	5.23	3460	7.87	2.76	942	2513	4.00	17.16	1.76	0.44	0.16	2.331
197-04-33	1.02	0.482	0.083	1.565	5.81	3630	7.93	2.67	962	2595	4.03	16.91	1.73	0.44	0.16	2.331
197-03-33	1.02	0.412	0.080	1.585	6.28	3750	8.01	7.61	977	2650	4.35	16.68	1.71	0.45	0.16	2.331
197-04-36	1.02	0.362	0.083	1.595	5.75	3630	8.07	2.71	962	2599	4.04	17.20	1.76	0.45	0.16	2.252
197-03-36	1.07	0.0	0.084	1.905	5.11	3460	9.90	3.45	951	2518	4.00	21.40	2.20	0.45	0.15	2.237

*FREE STREAM CONDITIONS BASED ON FROZEN FLOW MODEL

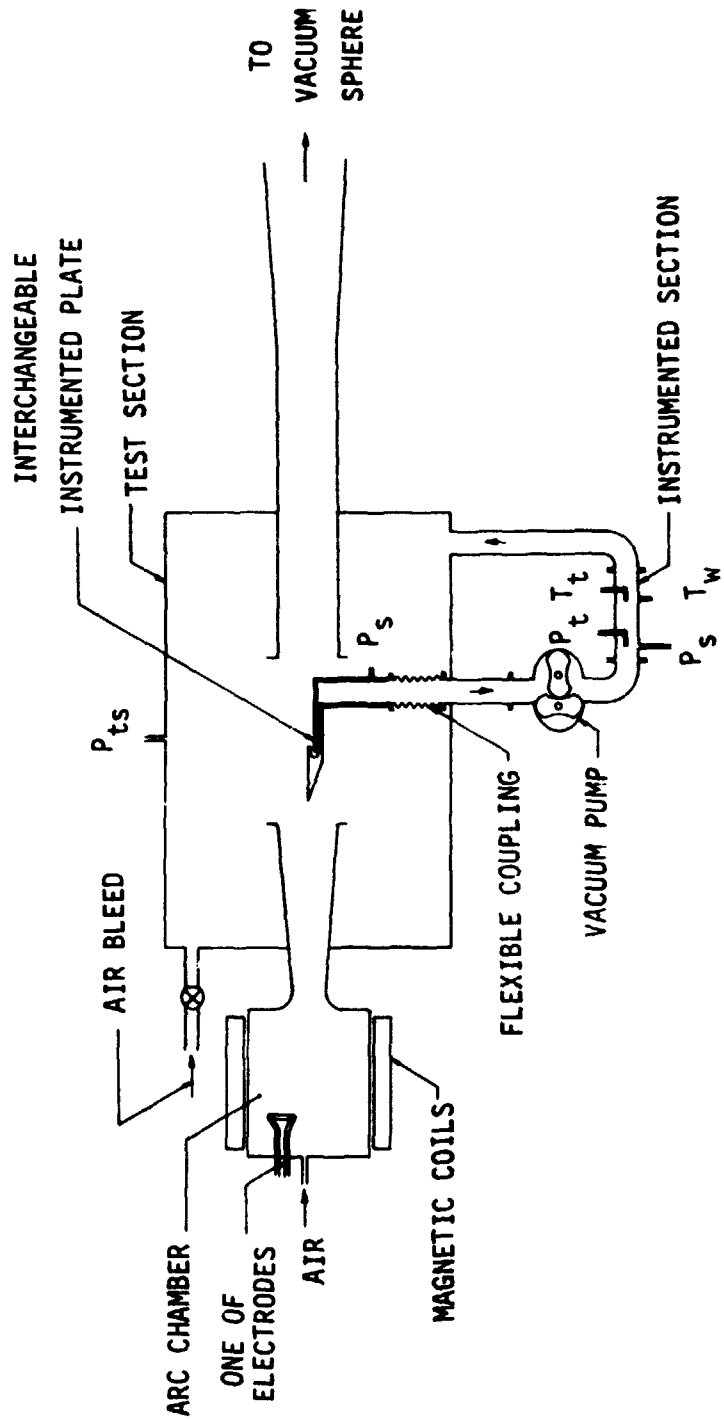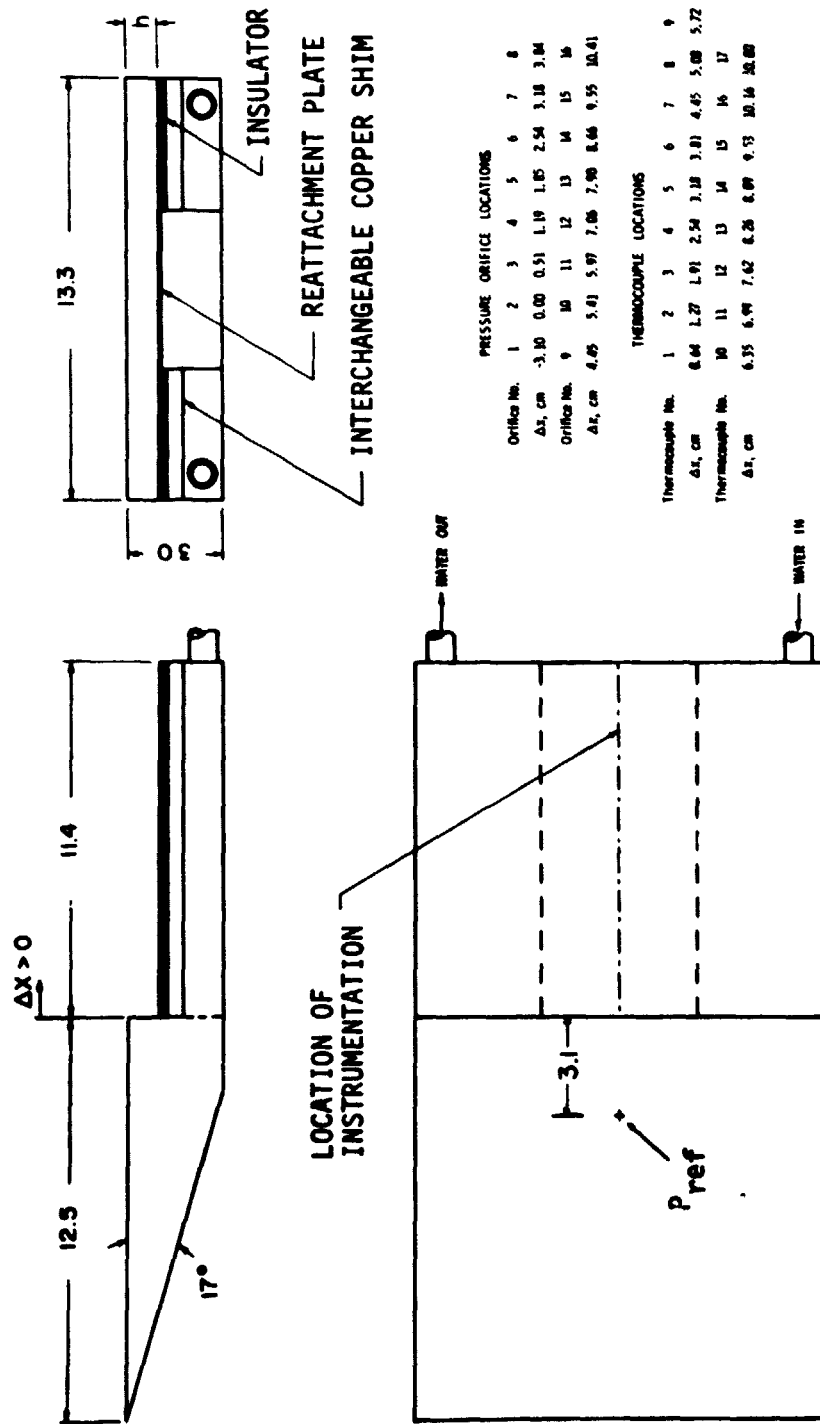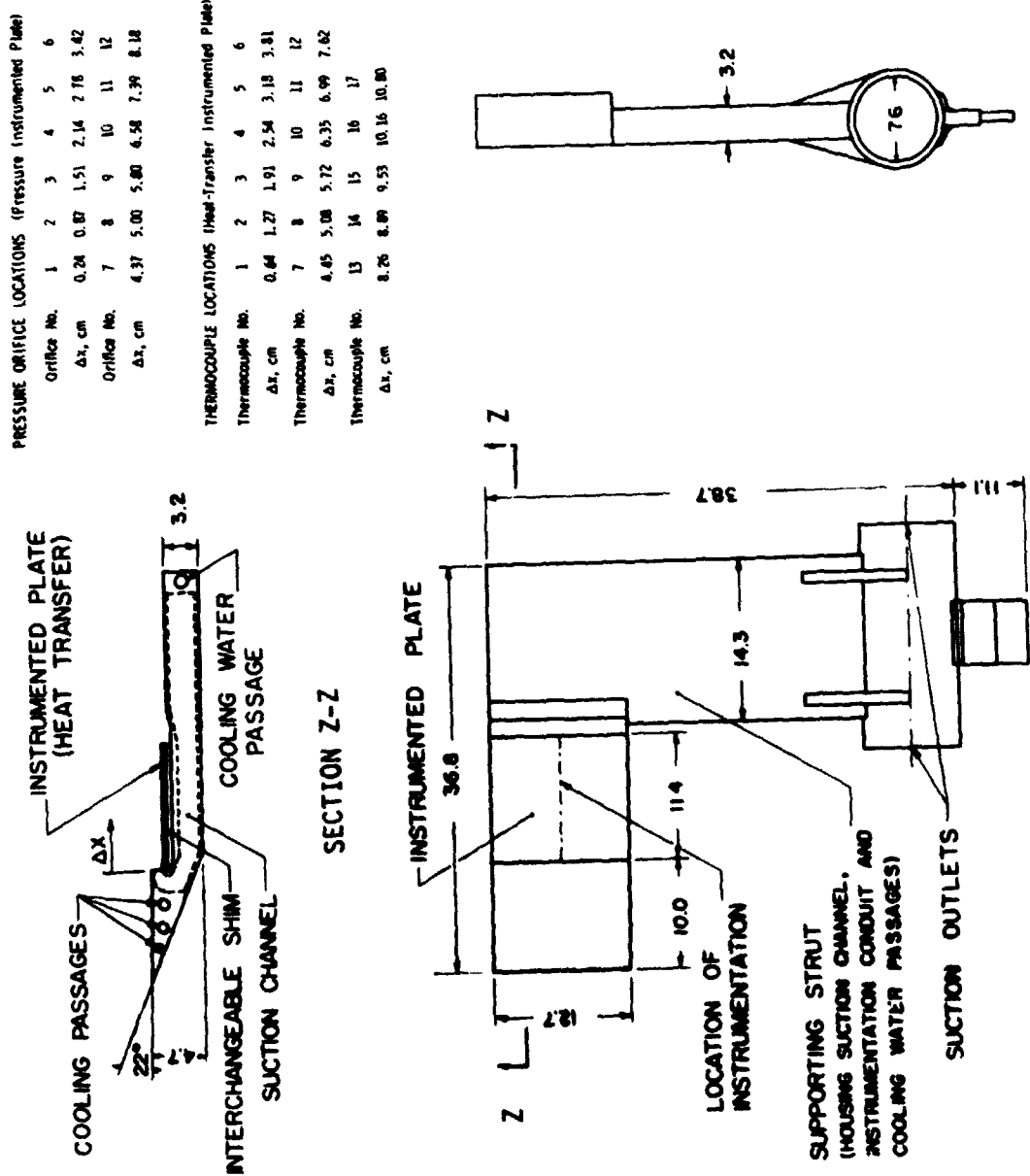**BOUNDARY LAYER PREDICTIONS BASED ON NONEQUILIBRIUM FLOW-EQUILIBRIUM CATALYTIC WALL CONDITIONS

27

Figure 1. Schematic diagram of experimental set-up with Model II.

PRESSURE ORIFICE LOCATIONS

Orifice No.	1	2	3	4	5	6	7	8
Δx, cm	-3.10	0.00	0.51	1.19	1.85	2.54	3.18	3.84
Orifice No.	9	10	11	12	13	14	15	16
Δx, cm	4.45	5.41	5.97	7.06	7.90	8.66	9.55	10.41

THERMOCOUPLE LOCATIONS

Thermocouple No.	1	2	3	4	5	6	7	8	9
Δx, cm	0.64	1.27	1.91	2.54	3.18	3.81	4.45	5.08	5.72
Thermocouple No.	10	11	12	13	14	15	16	17	
Δx, cm	6.35	6.99	7.62	8.26	8.89	9.53	10.16	10.80	

All linear dimensions are in centimeters.

Figure 2. Model I.

PRESSURE ORIFICE LOCATIONS (Pressure Instrumented Plate)

Orifice No.	1	2	3	4	5	6
Δx, cm	0.24	0.87	1.51	2.14	2.78	3.42
Orifice No.	7	8	9	10	11	12
Δx, cm	4.37	5.00	5.80	6.58	7.39	8.18

THERMOCOUPLE LOCATIONS (Heat-Transfer Instrumented Plate)

Thermocouple No.	1	2	3	4	5	6
Δx, cm	0.64	1.27	1.91	2.54	3.18	3.81
Thermocouple No.	7	8	9	10	11	12
Δx, cm	4.45	5.08	5.72	6.35	6.99	7.62
Thermocouple No.	13	14	15	16	17	
Δx, cm	8.26	8.89	9.53	10.16	10.80	

INSTRUMENTED PLATE (HEAT TRANSFER)

COOLING WATER PASSAGE

SECTION Z-Z

COOLING PASSAGES

INTERCHANGEABLE SHIM

SUCTION CHANNEL

22°

3.2

INSTRUMENTED PLATE

INSTRUMENTED PLATE

36.8

38.7

14.3

11.4

10.0

LOCATION OF INSTRUMENTATION

SUPPORTING STRUT
(HOUSING SUCTION CHANNEL,
INSTRUMENTATION CONDUIT AND
COOLING WATER PASSAGES)

SUCTION OUTLETS

3.2

76

ALL LINEAR DIMENSIONS ARE IN CENTIMETERS

Figure 3. Model II.
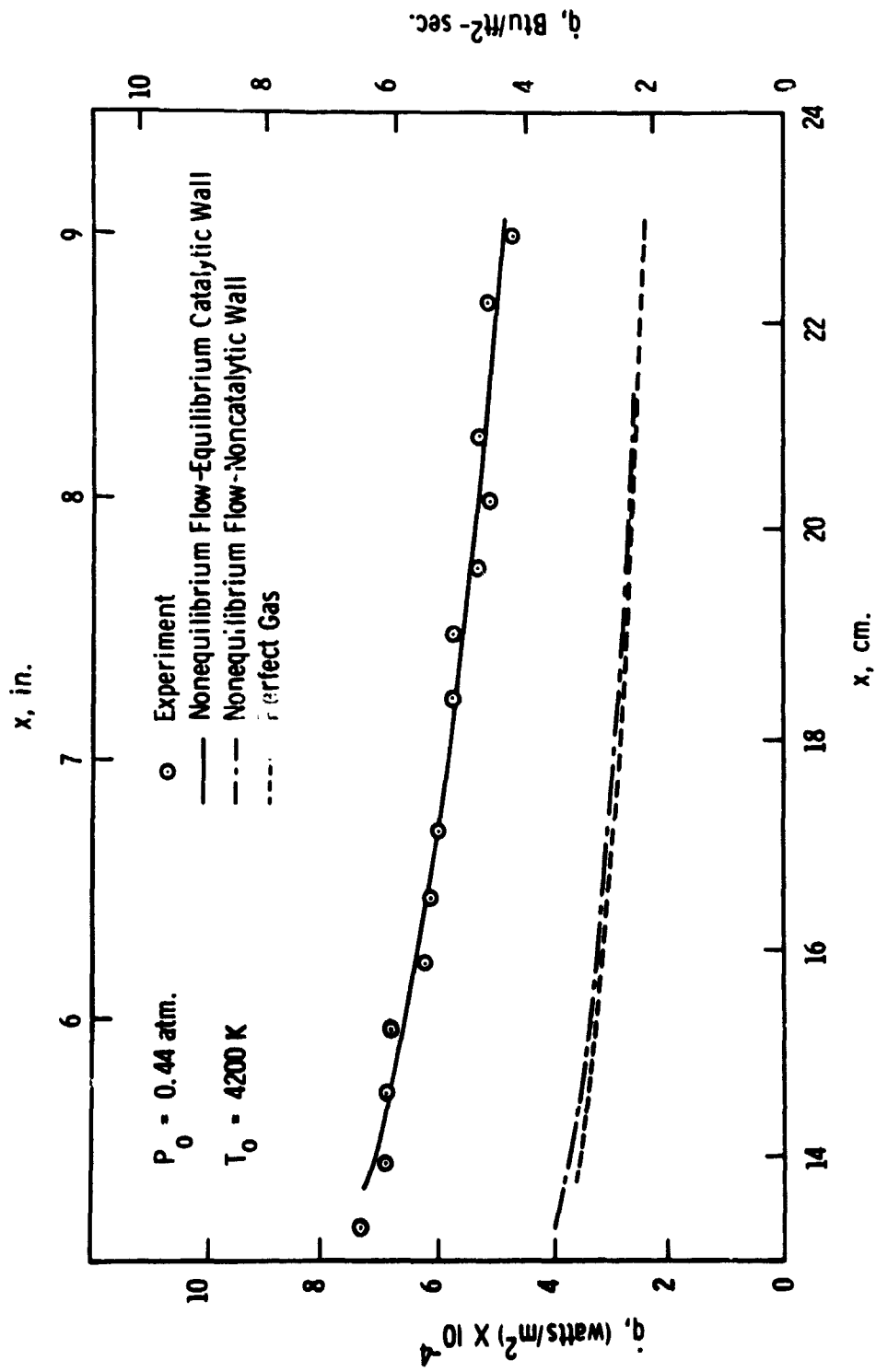
Figure 4. Heat-transfer distribution along flat-plate surface.
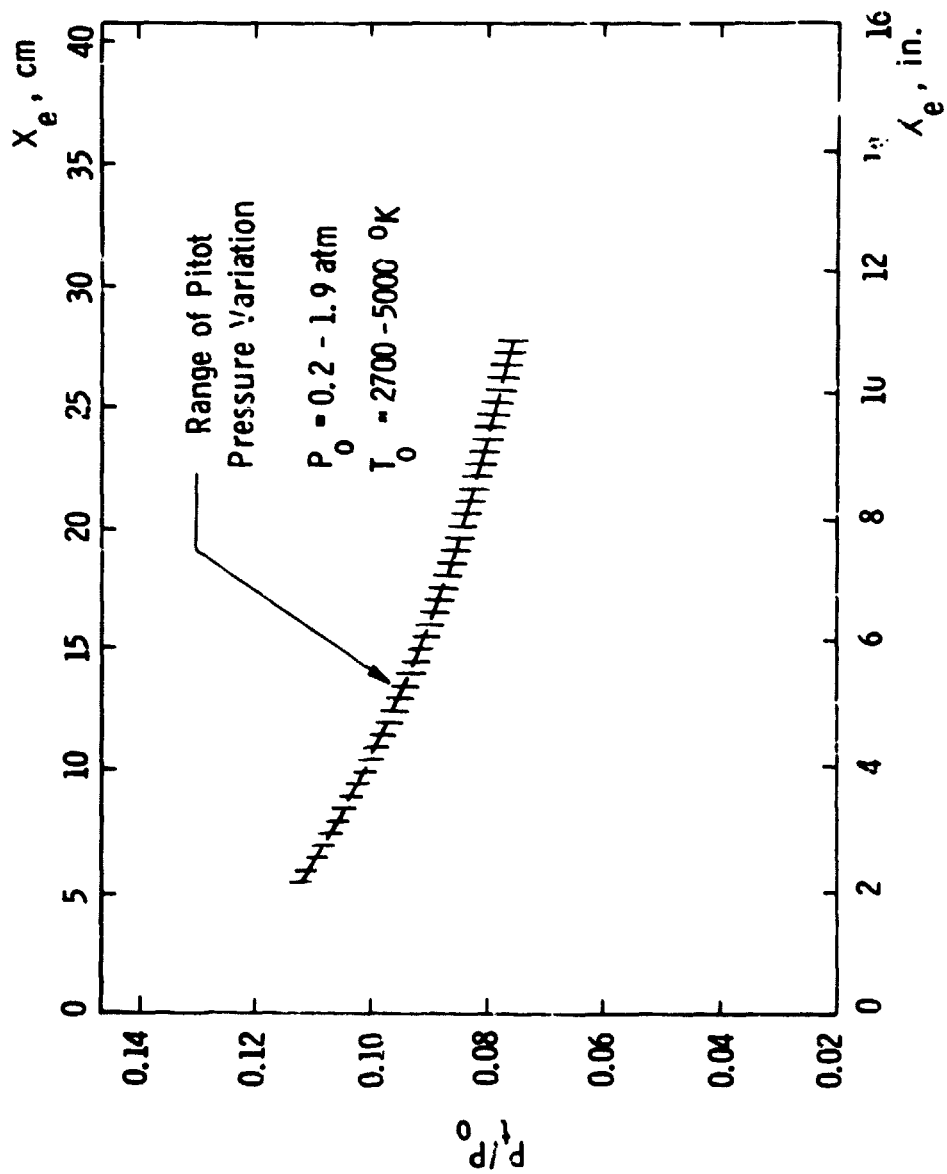
Figure 5. Axial distribution of pitot pressure in test section.

32
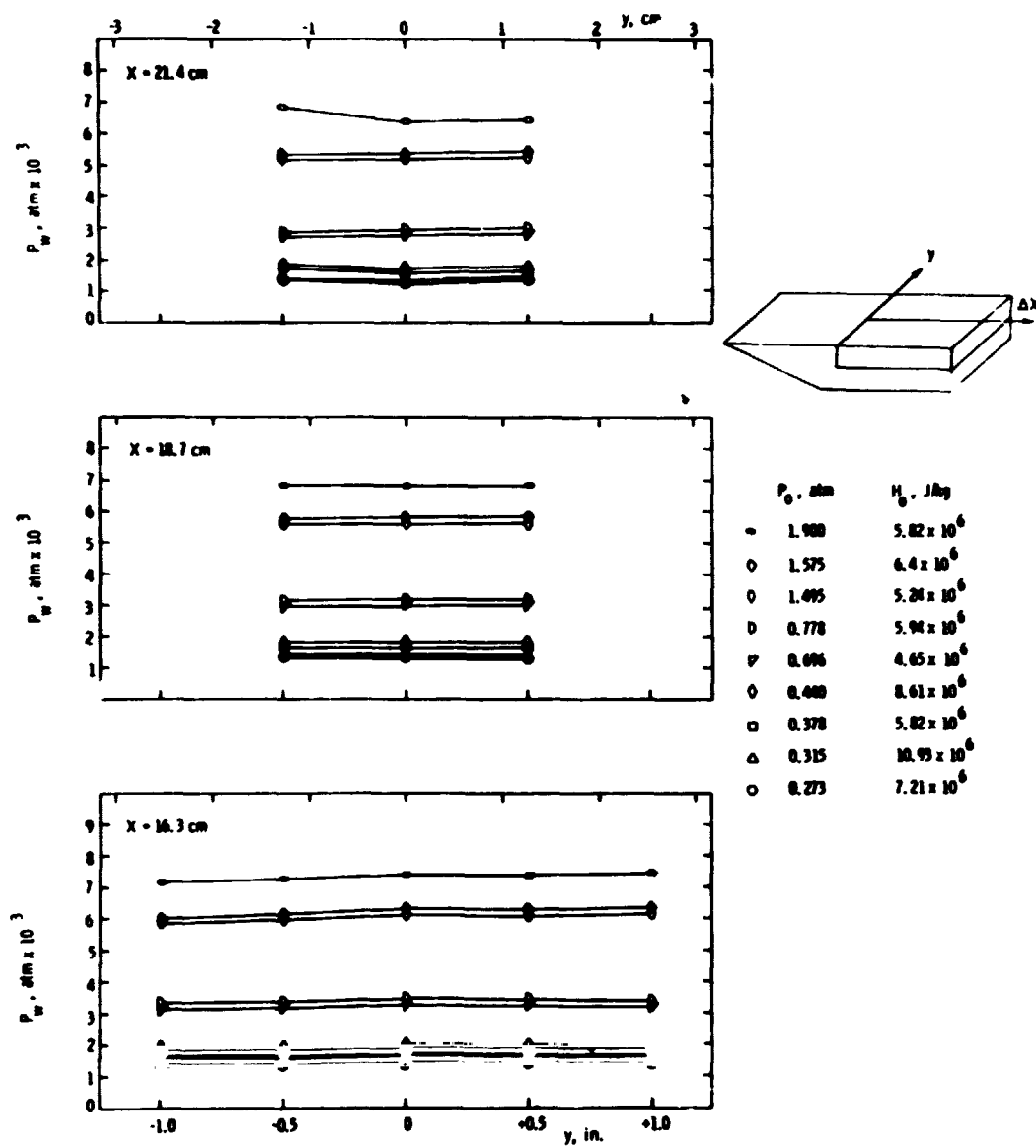
Figure 6a.   Transverse distribution of surface pressure on
the instrumented plate.
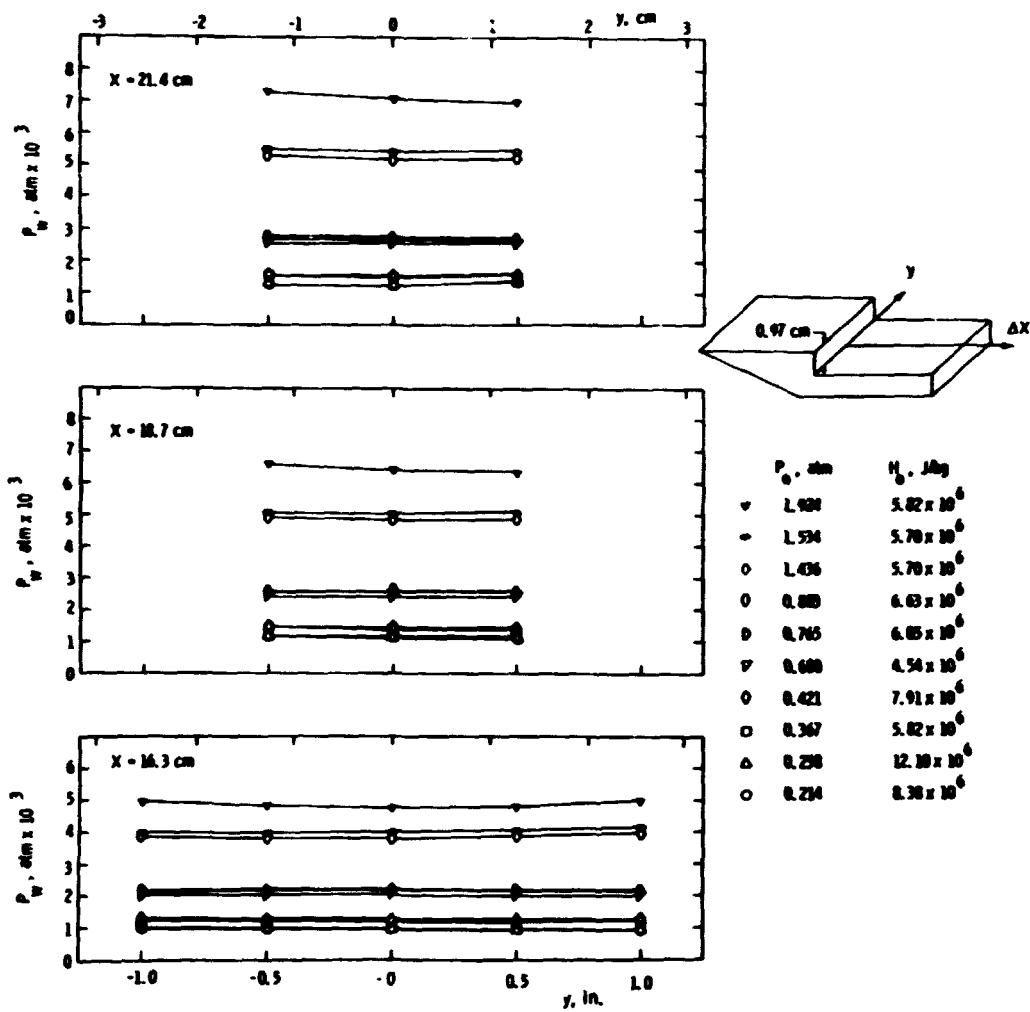
Figure 6b. Transverse distribution of surface pressure on
the instrumented plate.

Figure 7a. Heat-transfer distribution downstream of the step: Model I.

Run	h, cm	P_0, atm	T_0, °K	Re_∞/cm	M_∞
180-3-6	0.00	0.205	3400	249	4.09
180-5-6	0.16	0.210	3175	269	4.05
180-7-6	0.51	0.202	3100	265	4.03
180-1-6	1.02	0.207	3075	275	4.02

Figure 7b. Heat-transfer distribution downstream of the step: Model I.

Run	h, cm	P_o, atm	T_o, °K	Re_∞/cm	M_∞
● 180-3-18	0.00	0.265	5195	202	4.25
▲ 180-5-18	0.16	0.270	4775	229	4.19
◆ 180-7-18	0.51	0.259	4900	213	4.20
■ 180-1-18	1.02	0.265	4800	223	4.19

36

Figure 7c. Heat-transfer distribution downstream of the step: Model I.

Run	h, cm	P_o, atm	T_o, °K	Re_∞/cm	M_∞
180-3-39	0.00	0.495	4895	369	4.24
180-6-18	0.16	0.501	4750	418	4.20
180-7-39	0.51	0.484	4500	438	4.19
180-2-6	1.02	0.500	4700	422	4.20
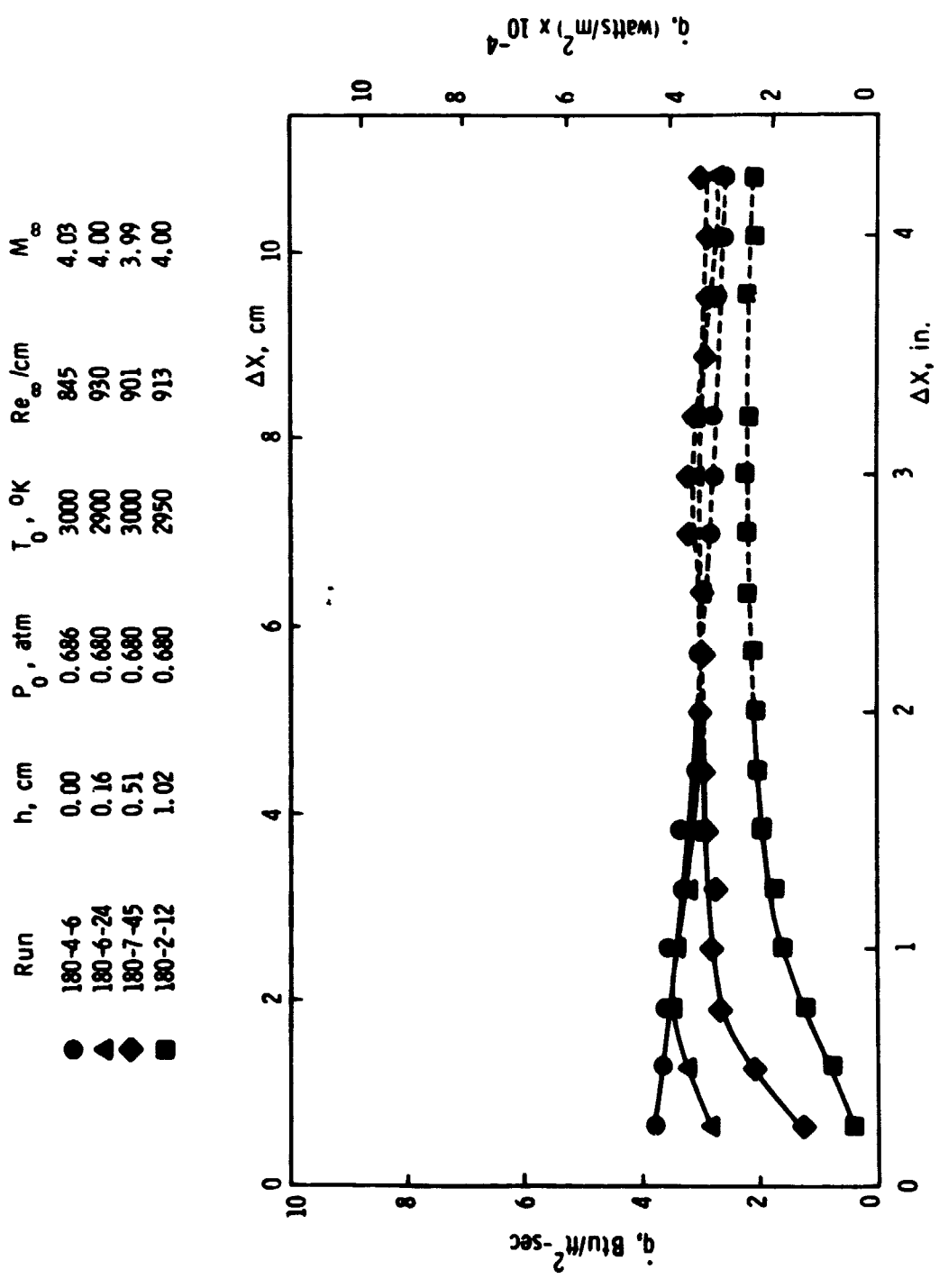
Figure 7d. Heat-transfer distribution. downstream of the step: Model I.

Run	h, cm	P_0, atm	T_0, $^\circ K$	Re_∞/cm	M_∞
180-4-6	0.00	0.686	3000	845	4.03
180-6-24	0.16	0.680	2900	930	4.00
180-7-45	0.51	0.680	3000	901	3.99
180-2-12	1.02	0.680	2950	913	4.00
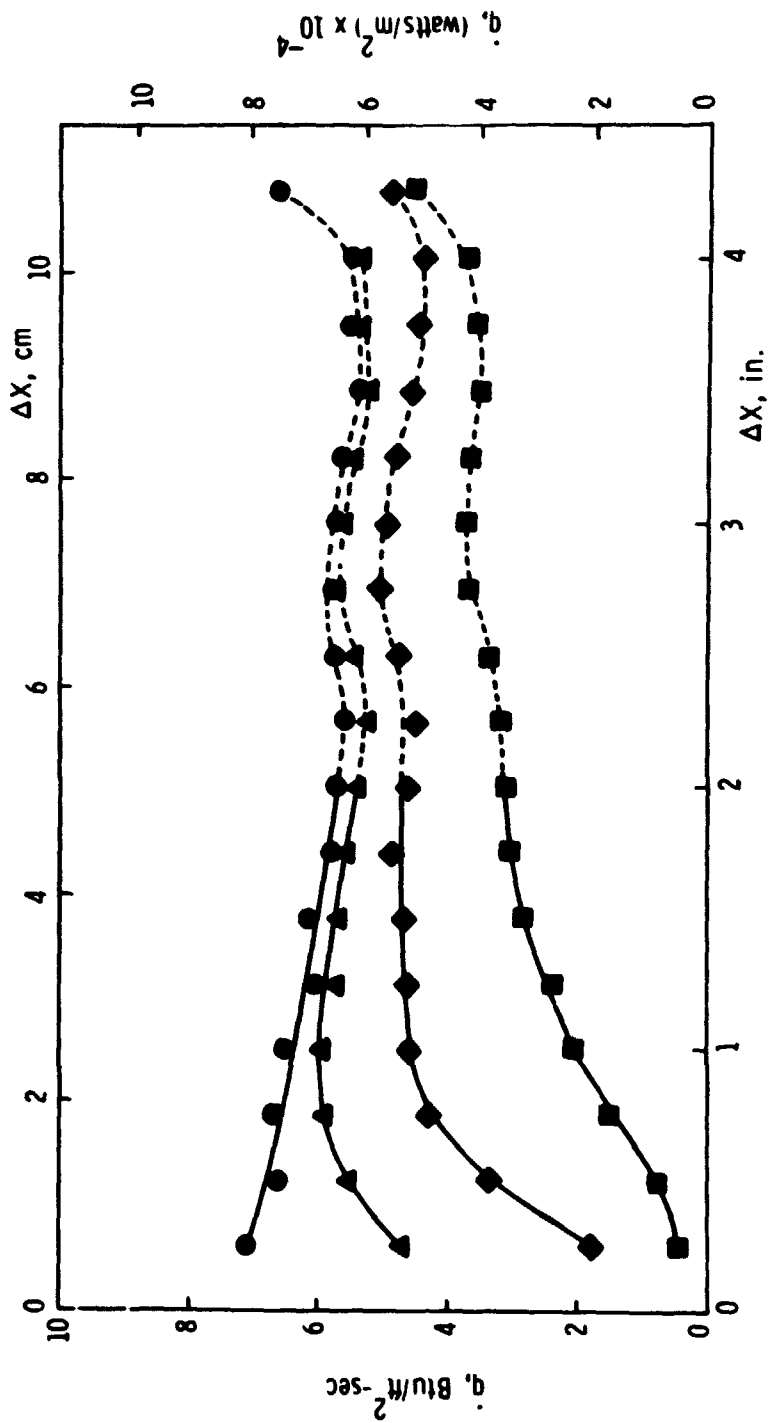
Figure 7e. Heat-transfer distribution downstream of the step: Model I.
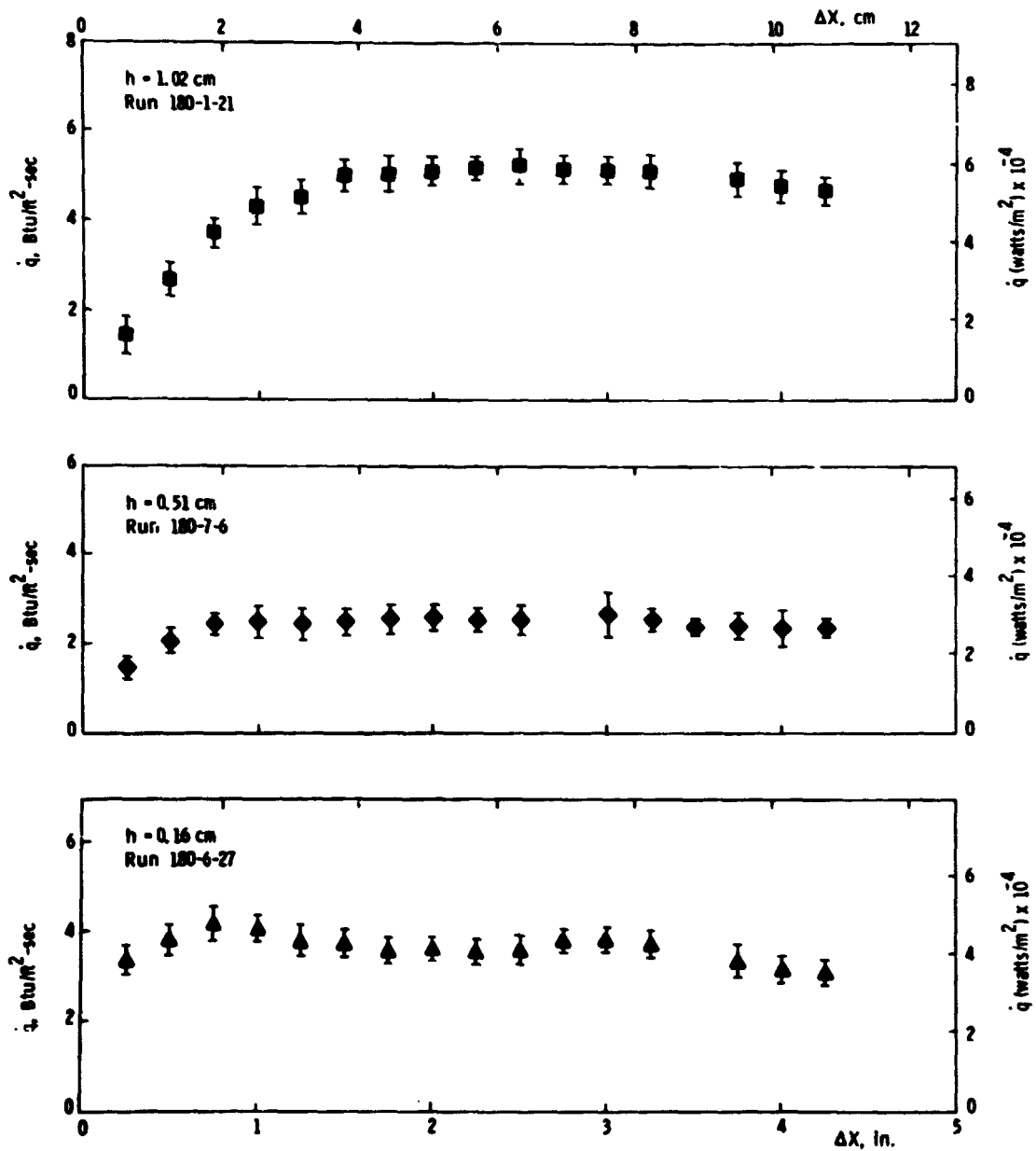
Figure 8. Standard deviation in heat-transfer measurements.
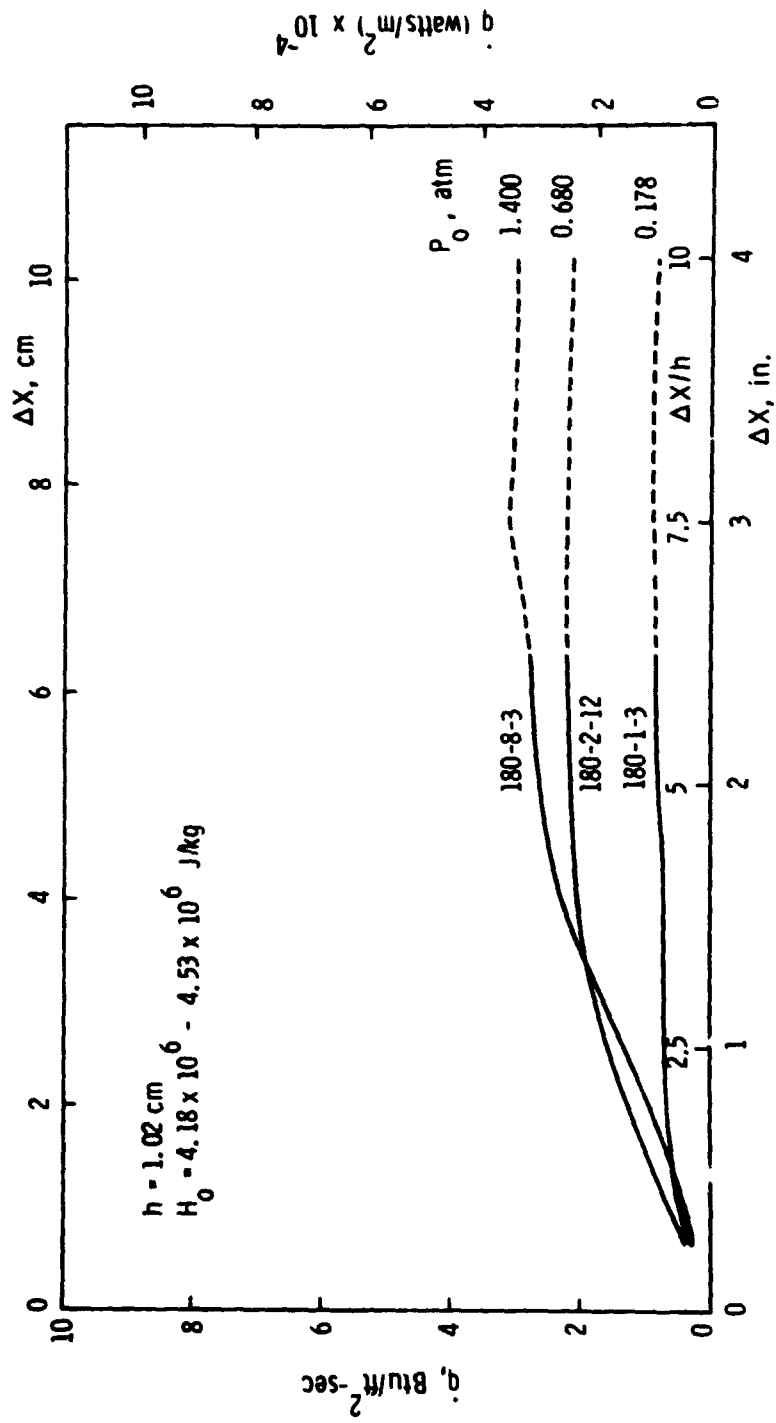
Figure 9a. Effect of pressure variation on heat-transfer distribution: Model I.

41
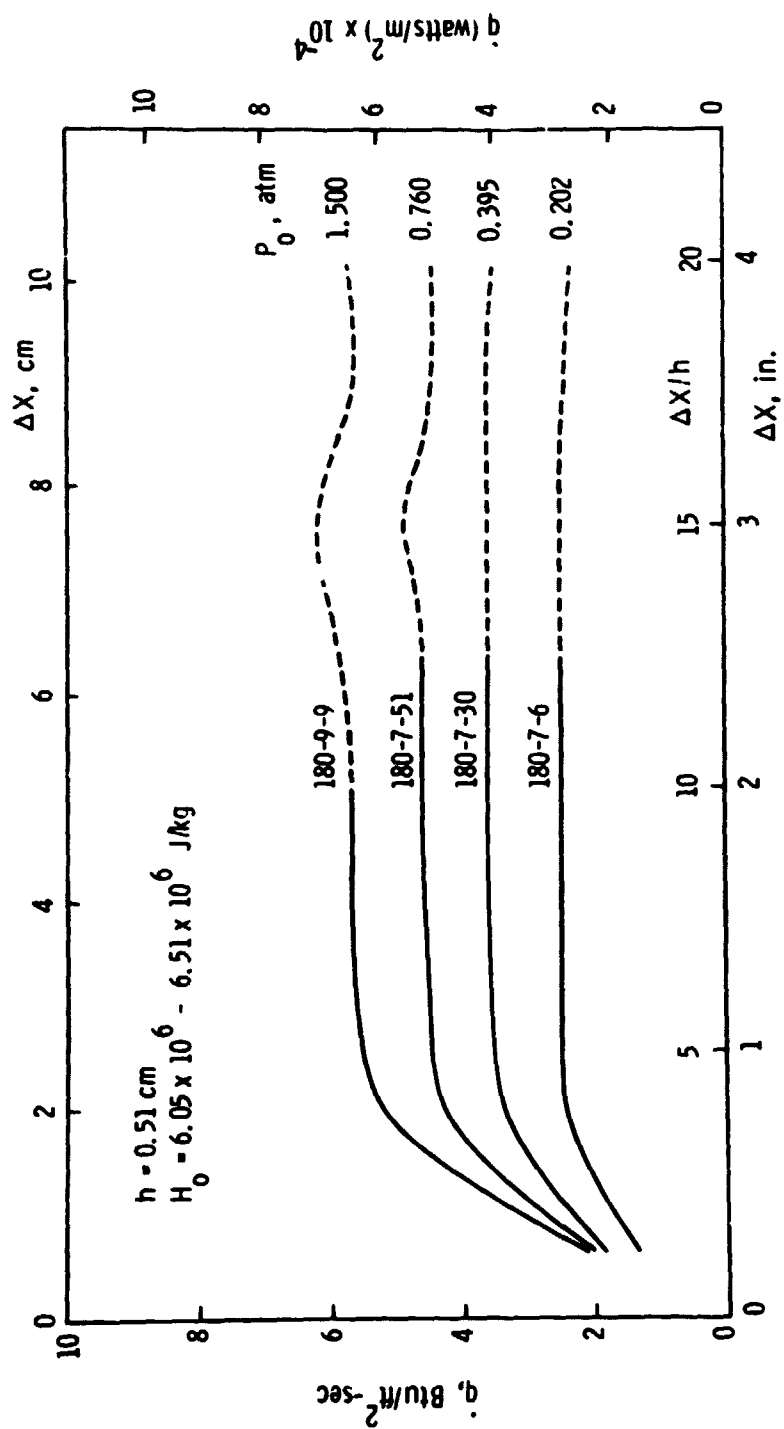
Figure 9b. Effect of pressure variation on heat-transfer distribution: Model I.
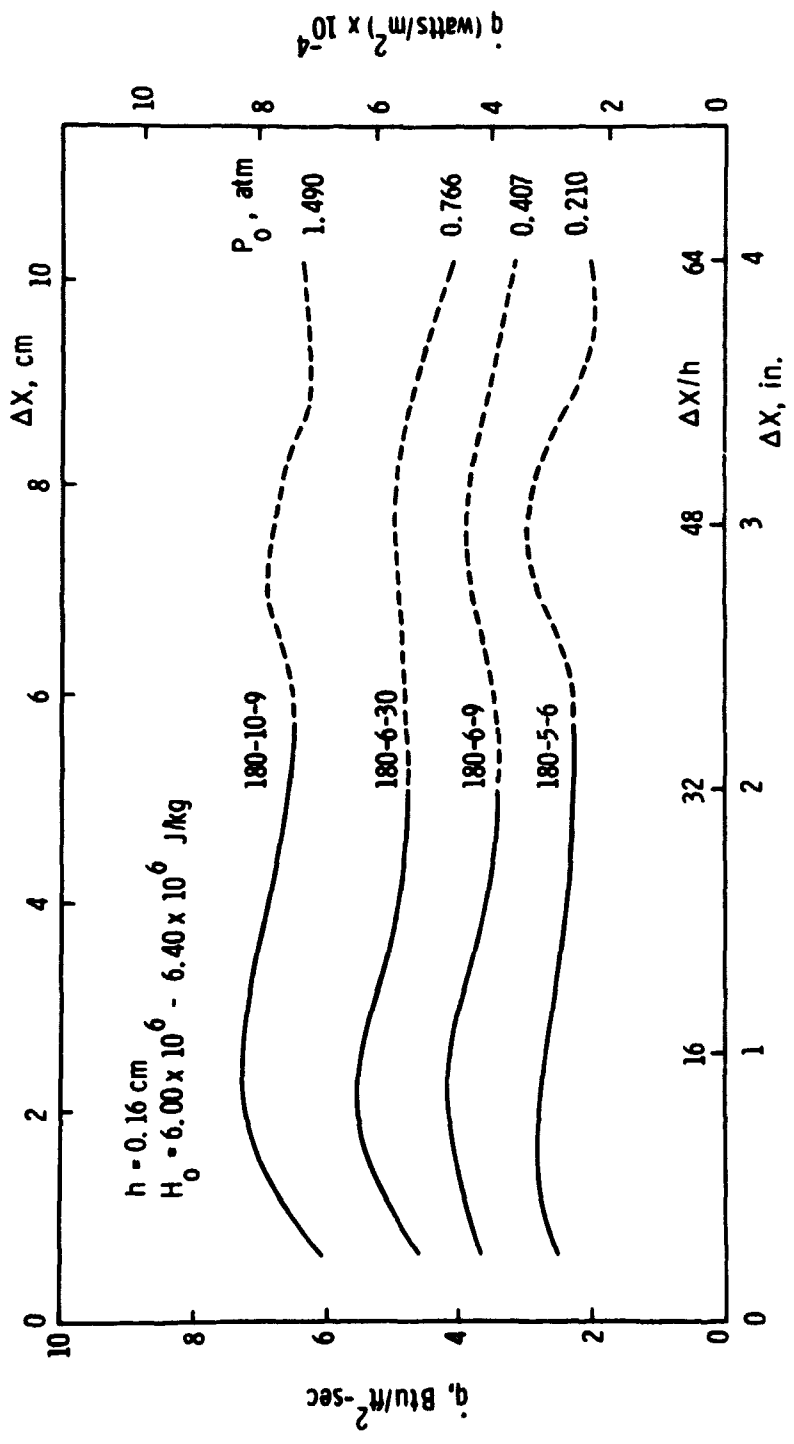
Figure 9c. Effect of pressure variation on heat-transfer distribution: Model I.

43
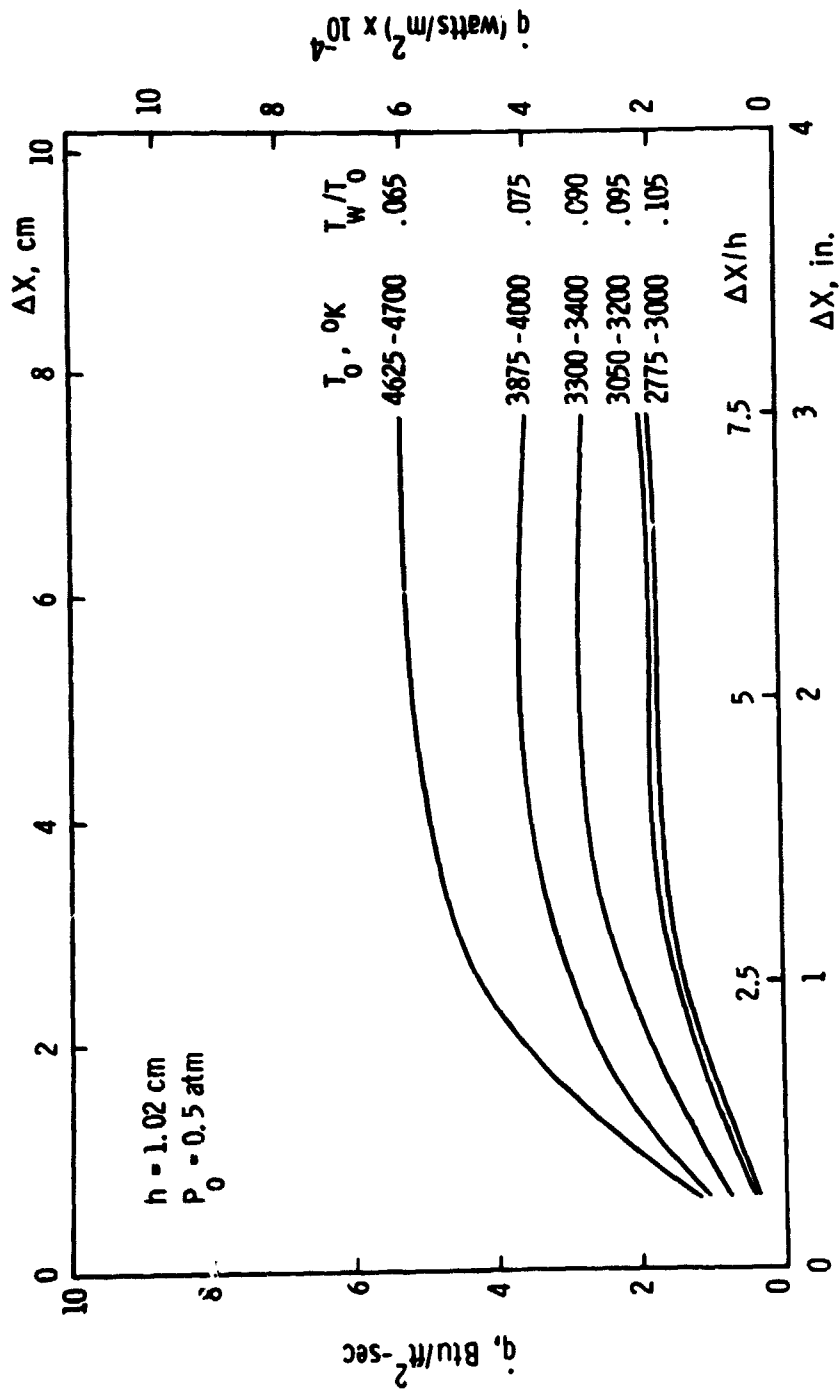
Figure 10a. Effect of enthalpy variation on heat-transfer distribution: Model I.

44
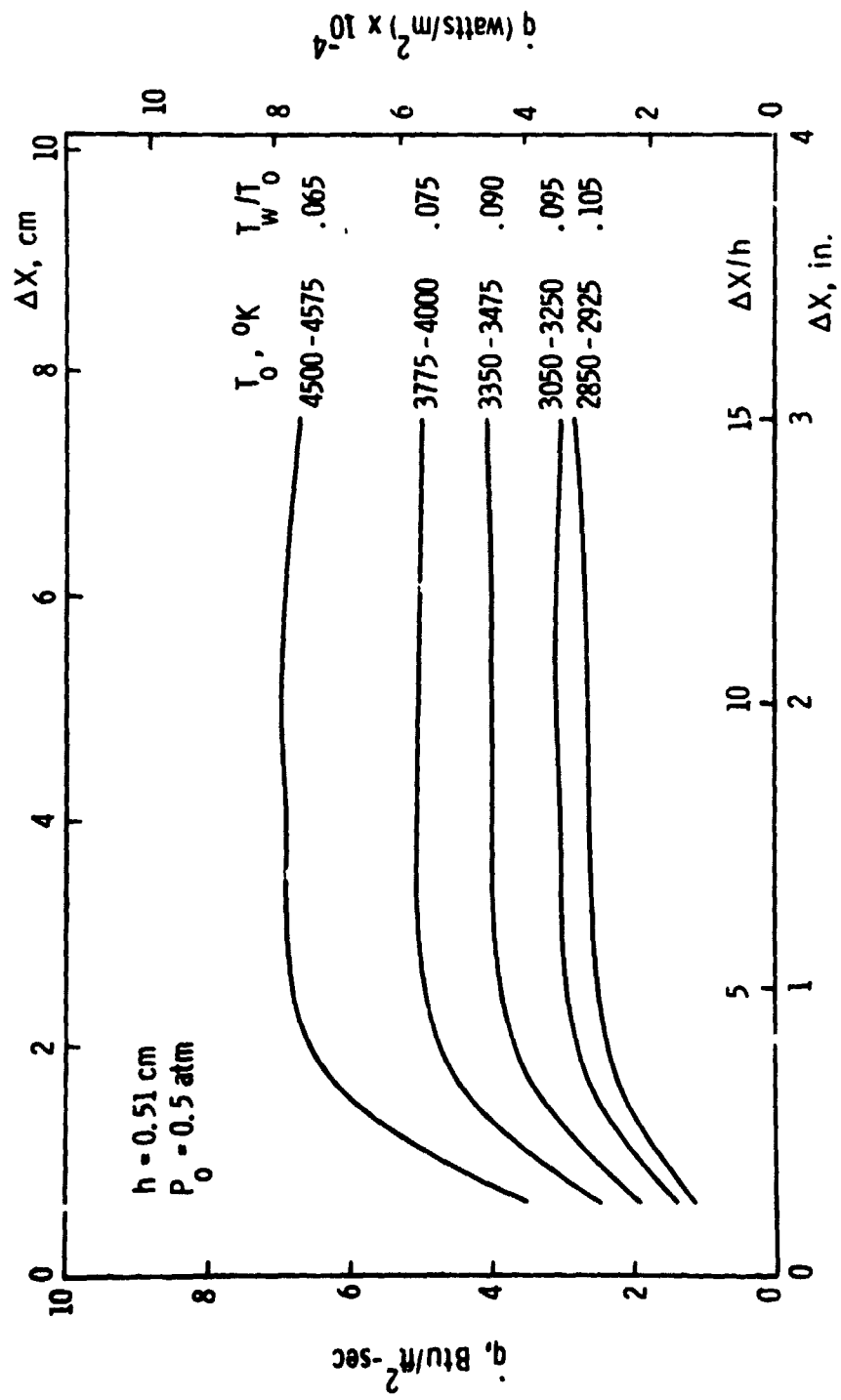
Figure 10b. Effect of enthalpy variation on heat-transfer distribution: Model I.
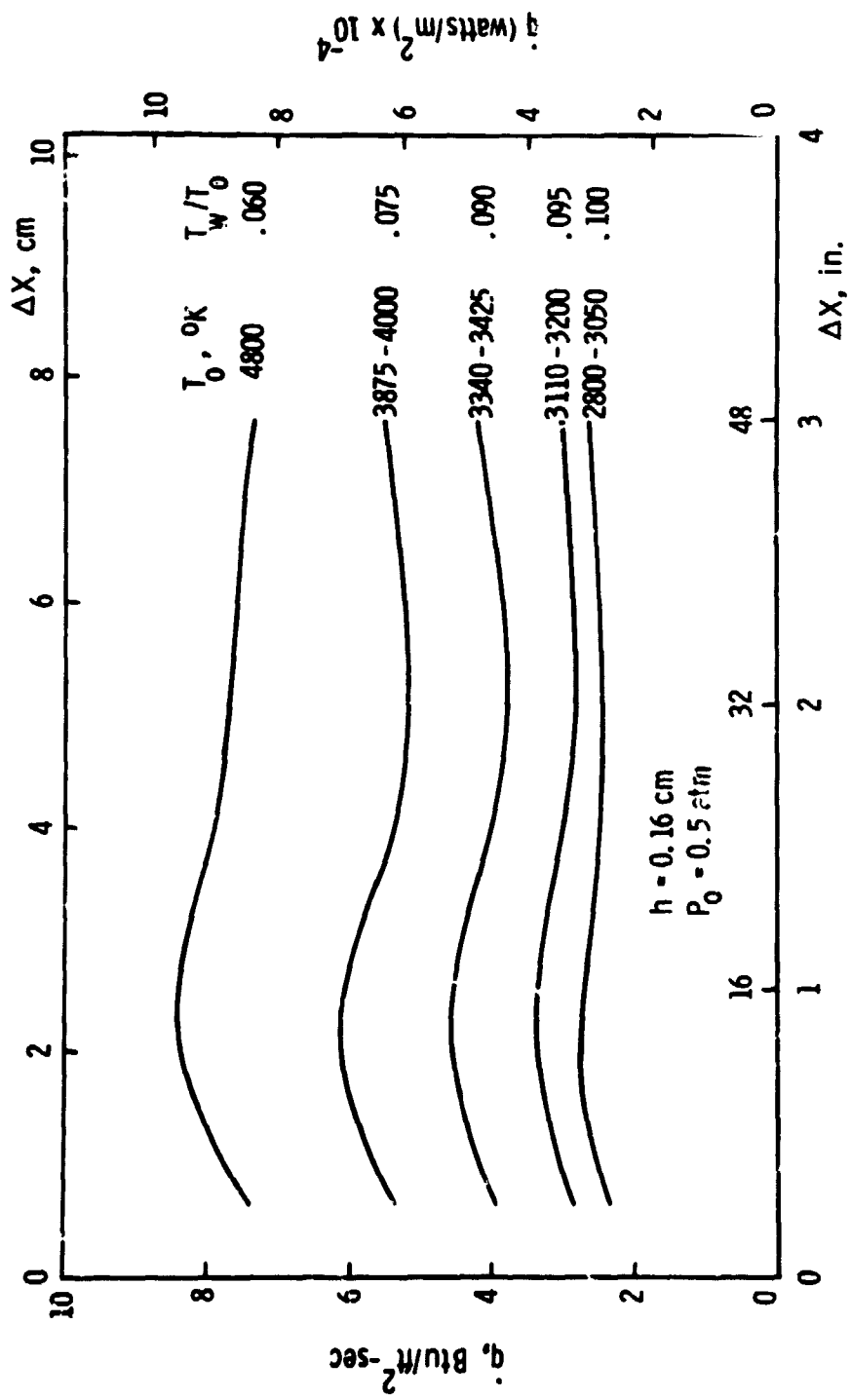
Figure 10c Effect of enthalpy variation on heat-transfer distribution: Model I.
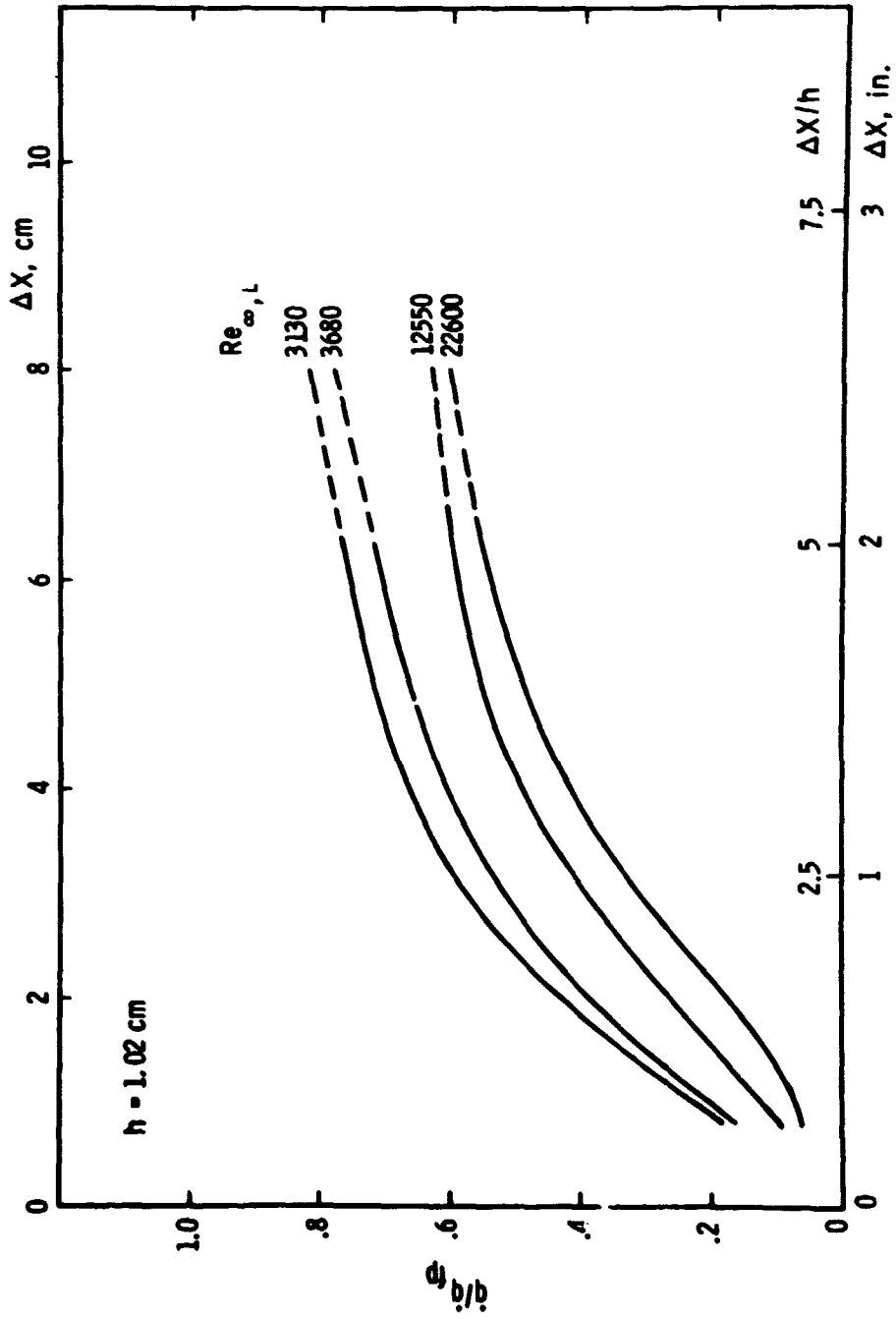
Figure 11a. Effect of Reynolds number on heat-transfer distribution: Model I.
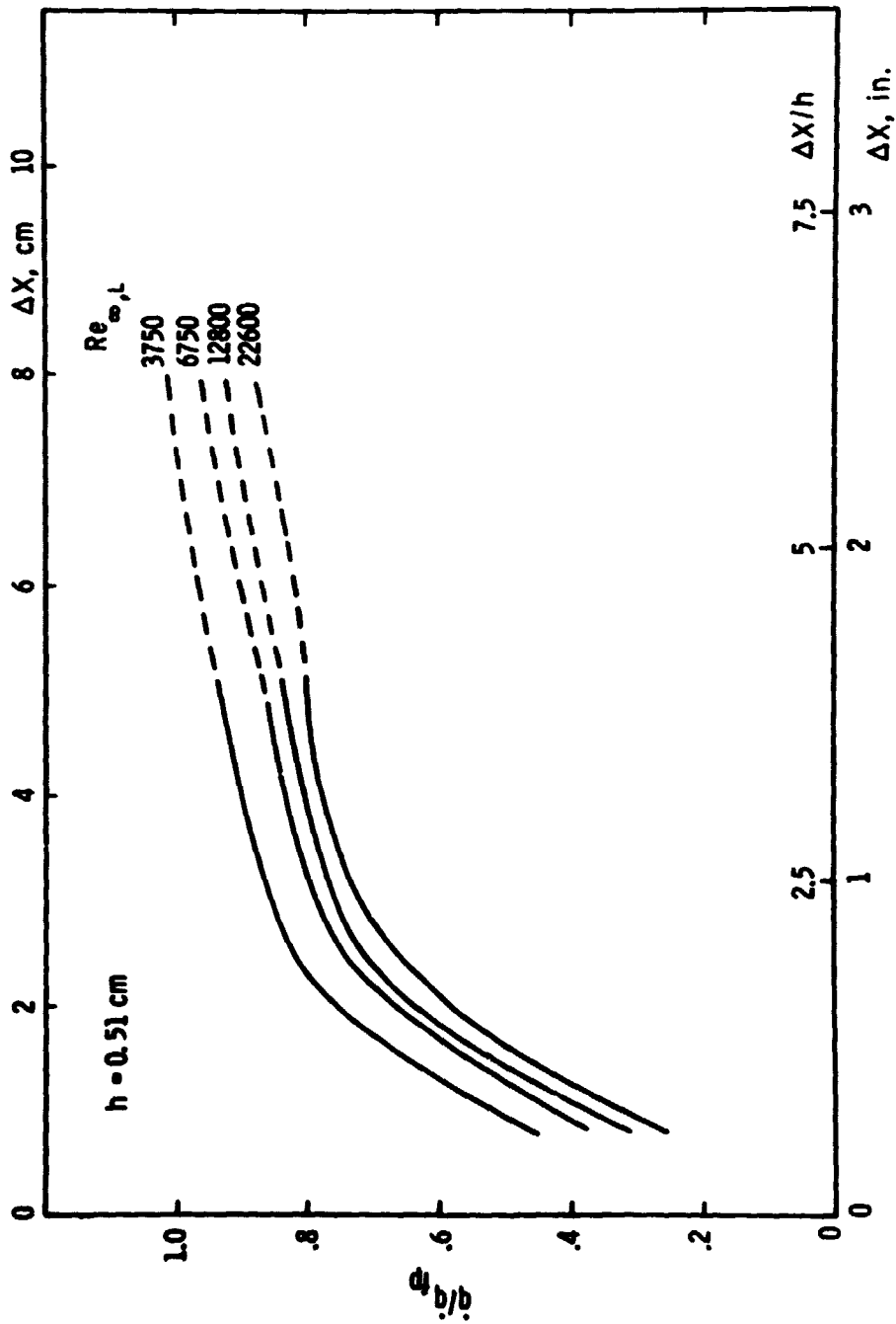
Figure 11b. Effect of Reynolds number on heat-transfer distribution: Model I.
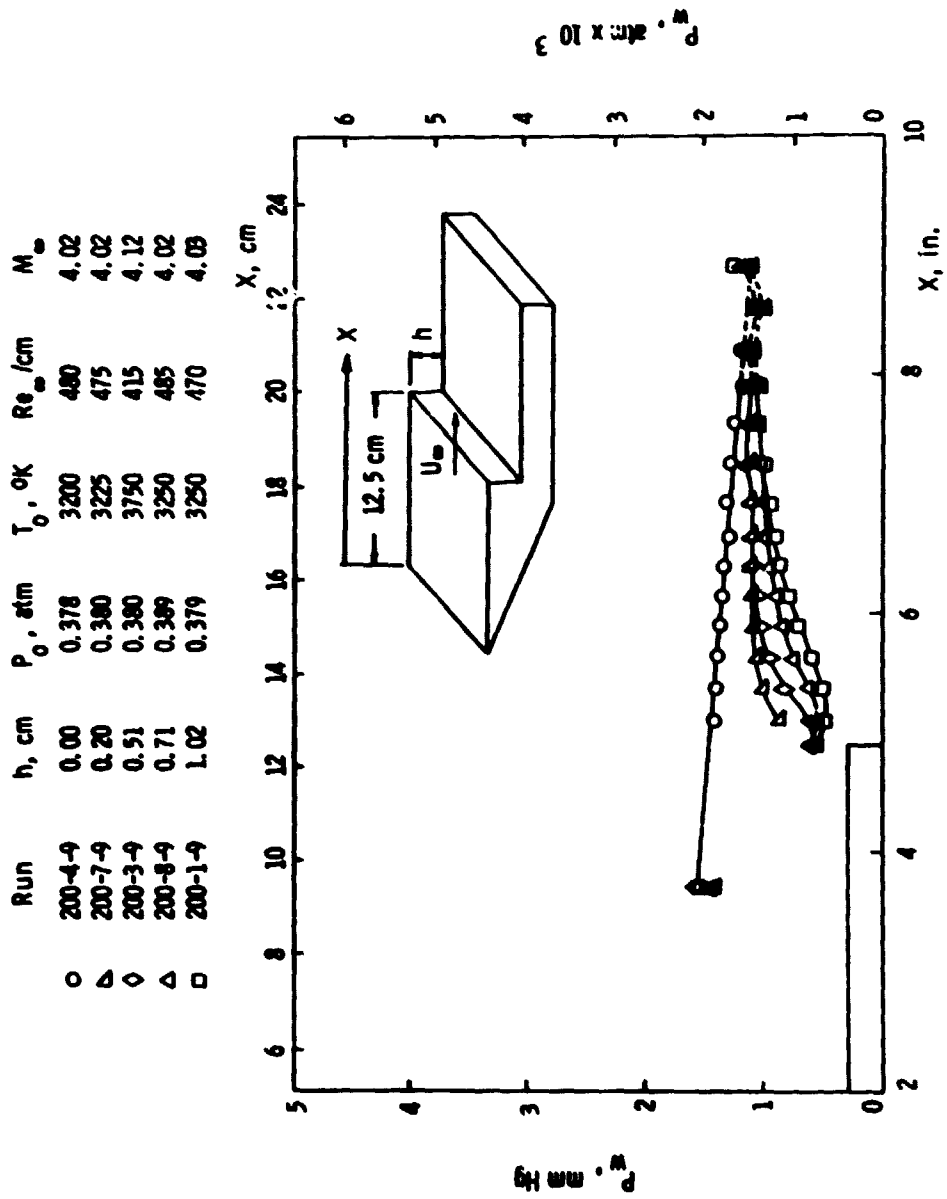
Figure 12a. Wall pressure distribution in the separated region: Model I.
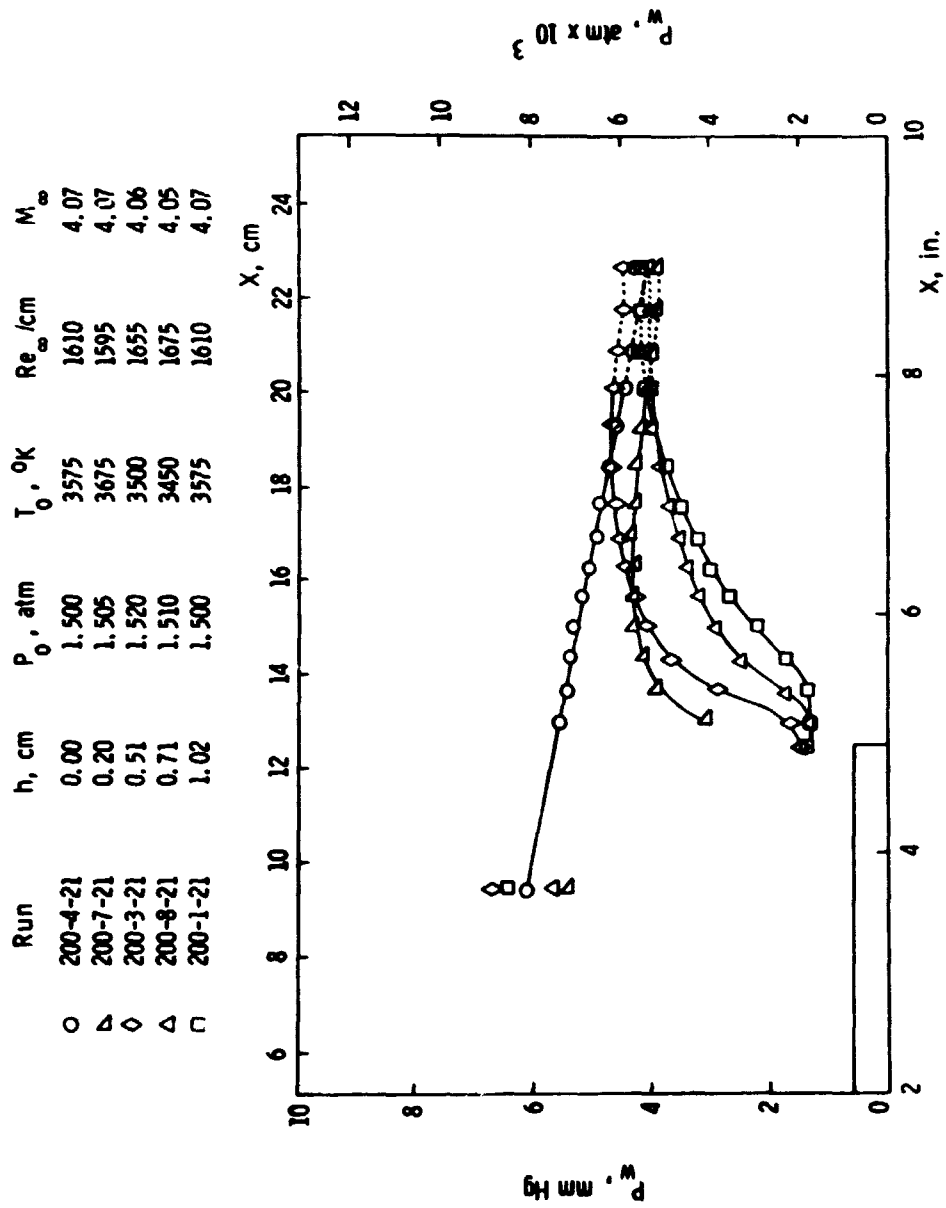
Figure 12b. Wall pressure distribution in the separated region: Model I.

	Run	h, cm	P_o, atm	T_o, °K	Re_∞ /cm	M_∞
O	200-4-21	0.00	1.500	3575	1610	4.07
△	200-7-21	0.20	1.505	3675	1595	4.07
◇	200-3-21	0.51	1.520	3500	1655	4.06
◁	200-8-21	0.71	1.510	3450	1675	4.05
□	200-1-21	1.02	1.500	3575	1610	4.07

50
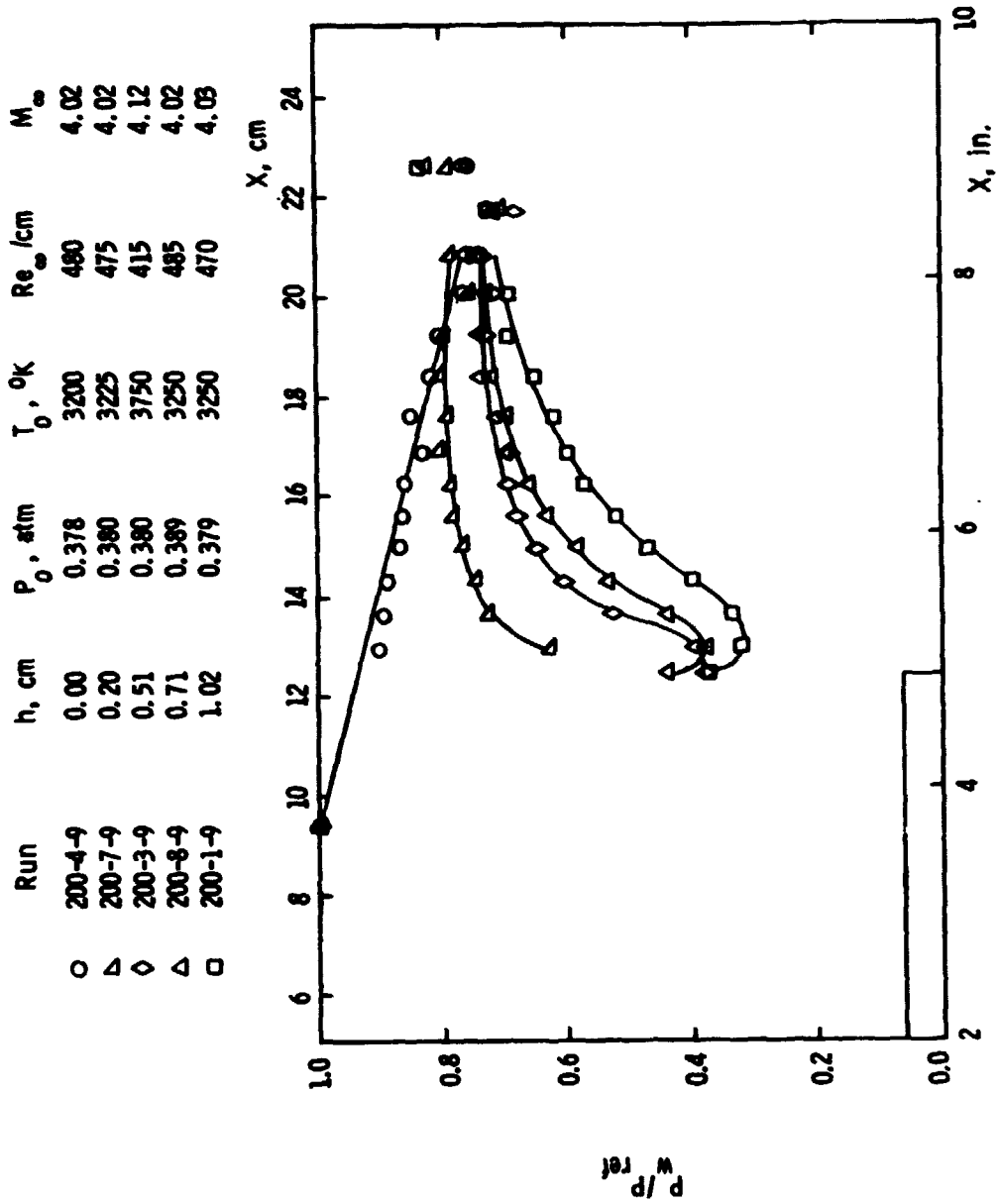
Figure 13a. Wall pressure distribution in the separated region: Model I.
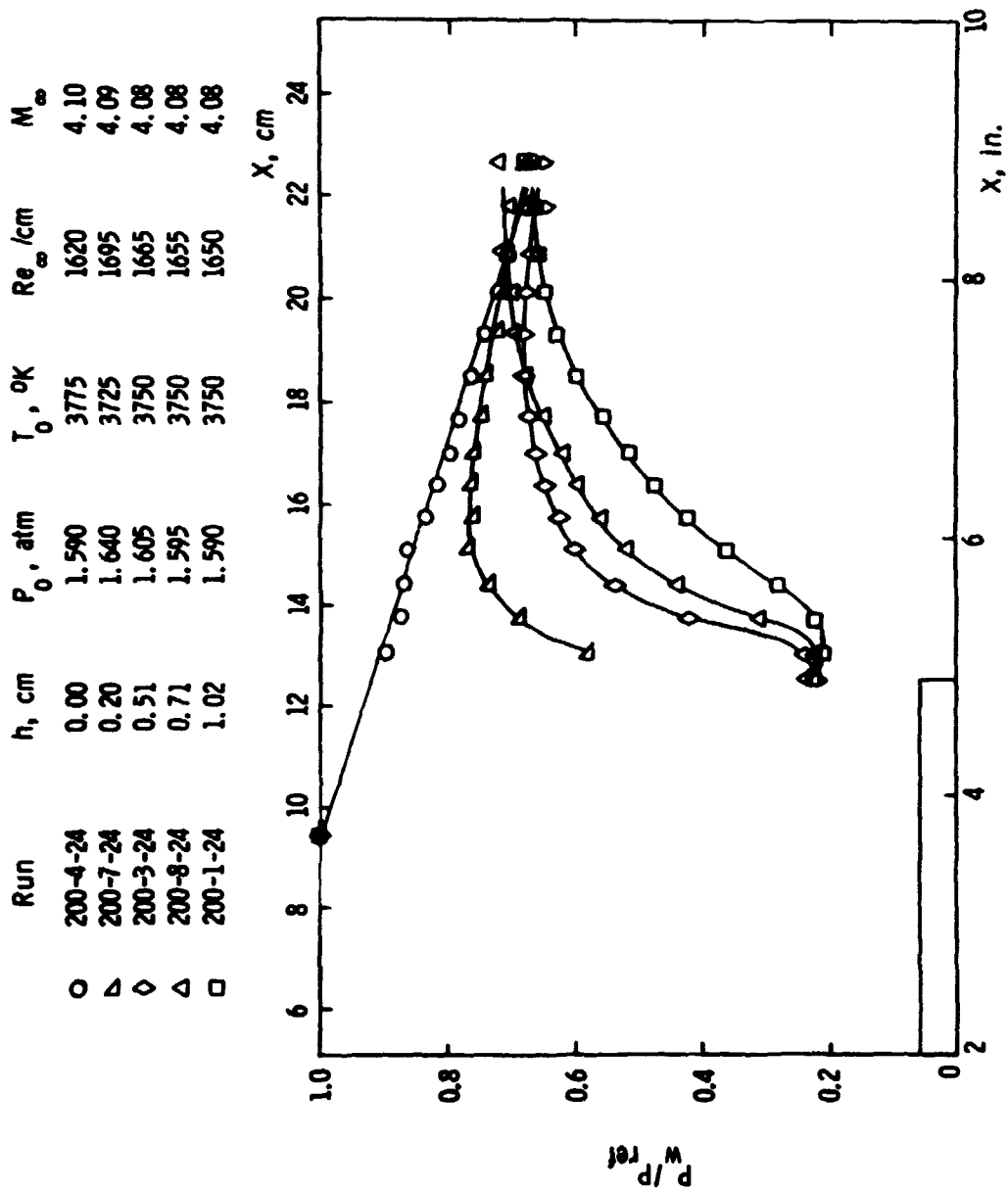
Figure 13b. Wall pressure distribution in the separated region: Model I.
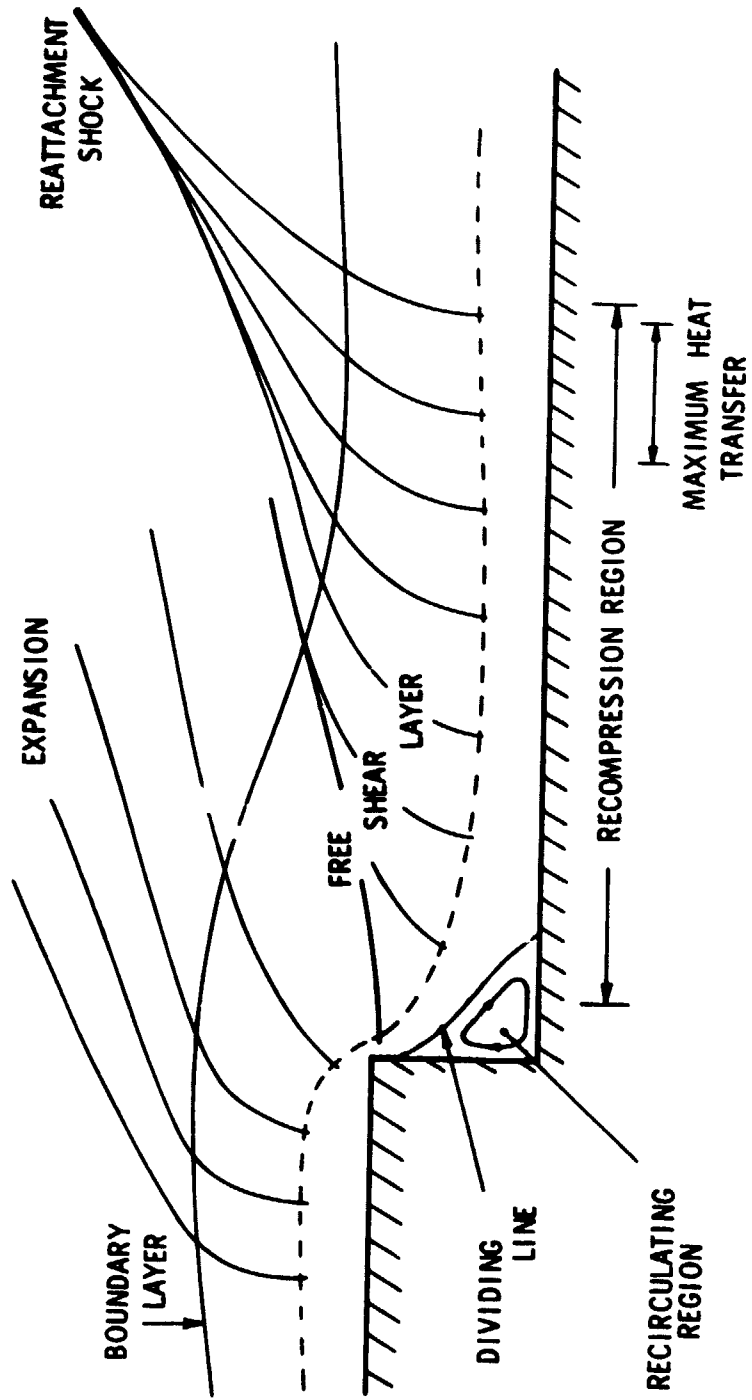
Figure 14. Hypothetical scheme of flow field. Laminar boundary layer, $h/\delta \sim O(1)$.

53
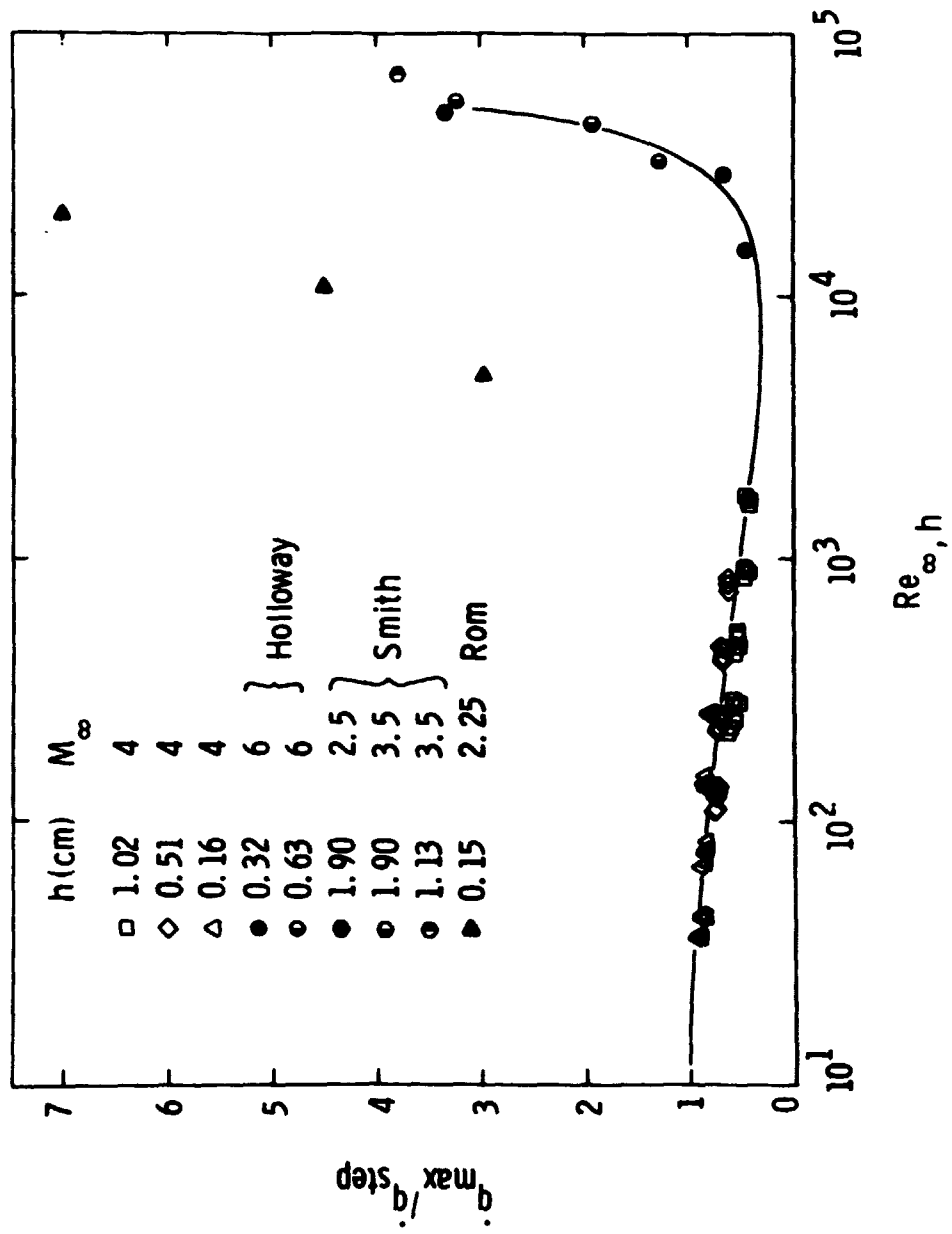
Figure 15. Maximum heating rate as function of $Re_{\infty,h}$.
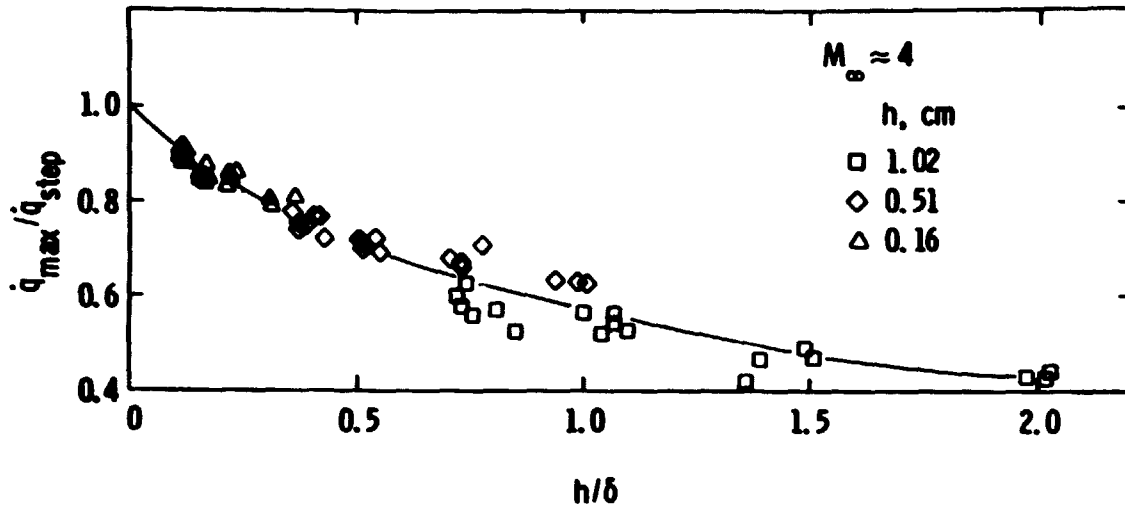
Figure 16. Maximum heating rate as function of h/δ.
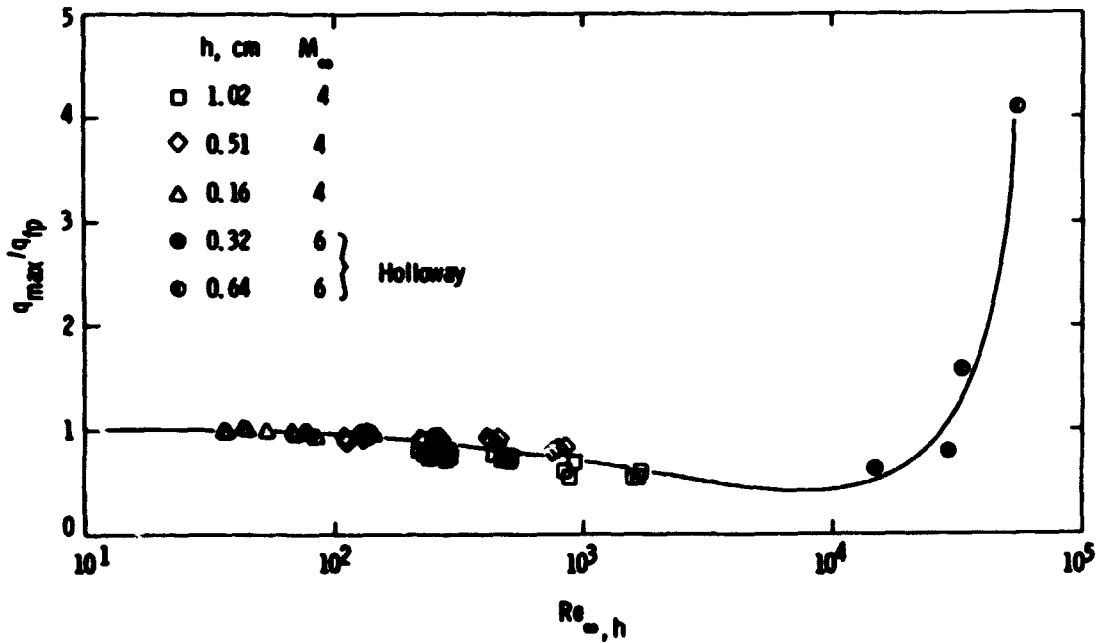
Figure 17. Maximum heating rate as function of $Re_{\infty,h}$.
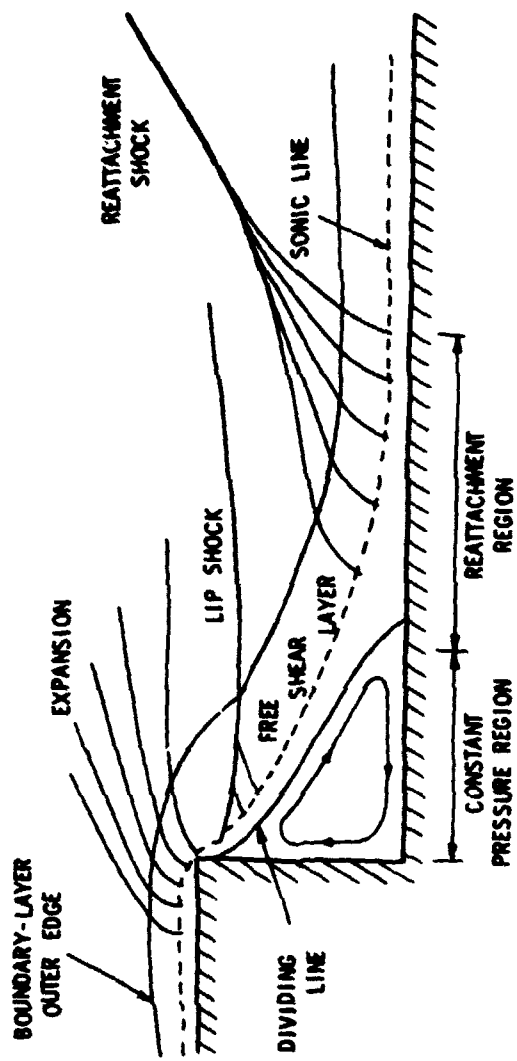
Figure 18. Hypothetical scheme of flow field. Laminar boundary layer, $h/\delta > 1$.
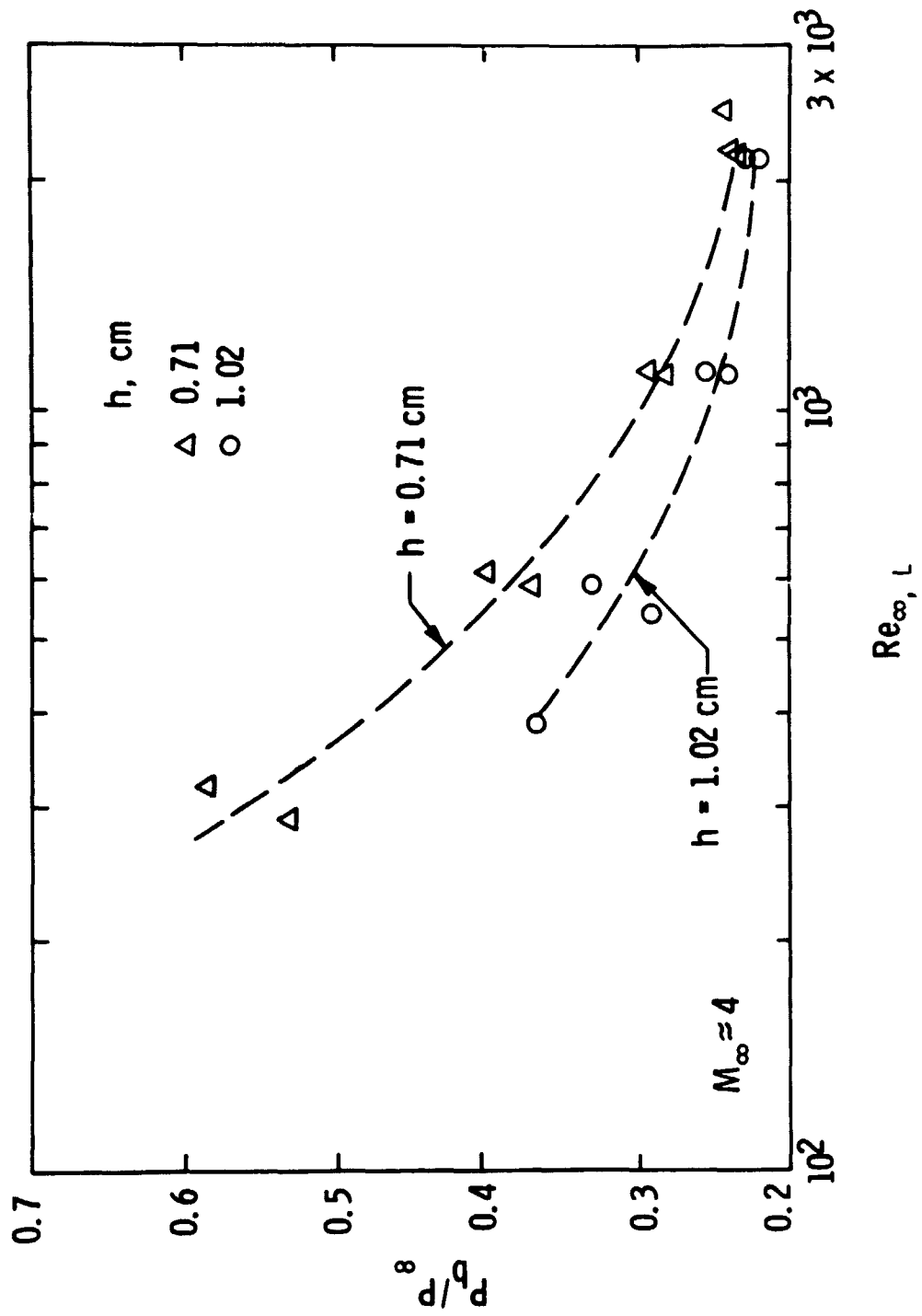
Figure 19. Base pressure as function of $Re_{\infty,L}$.
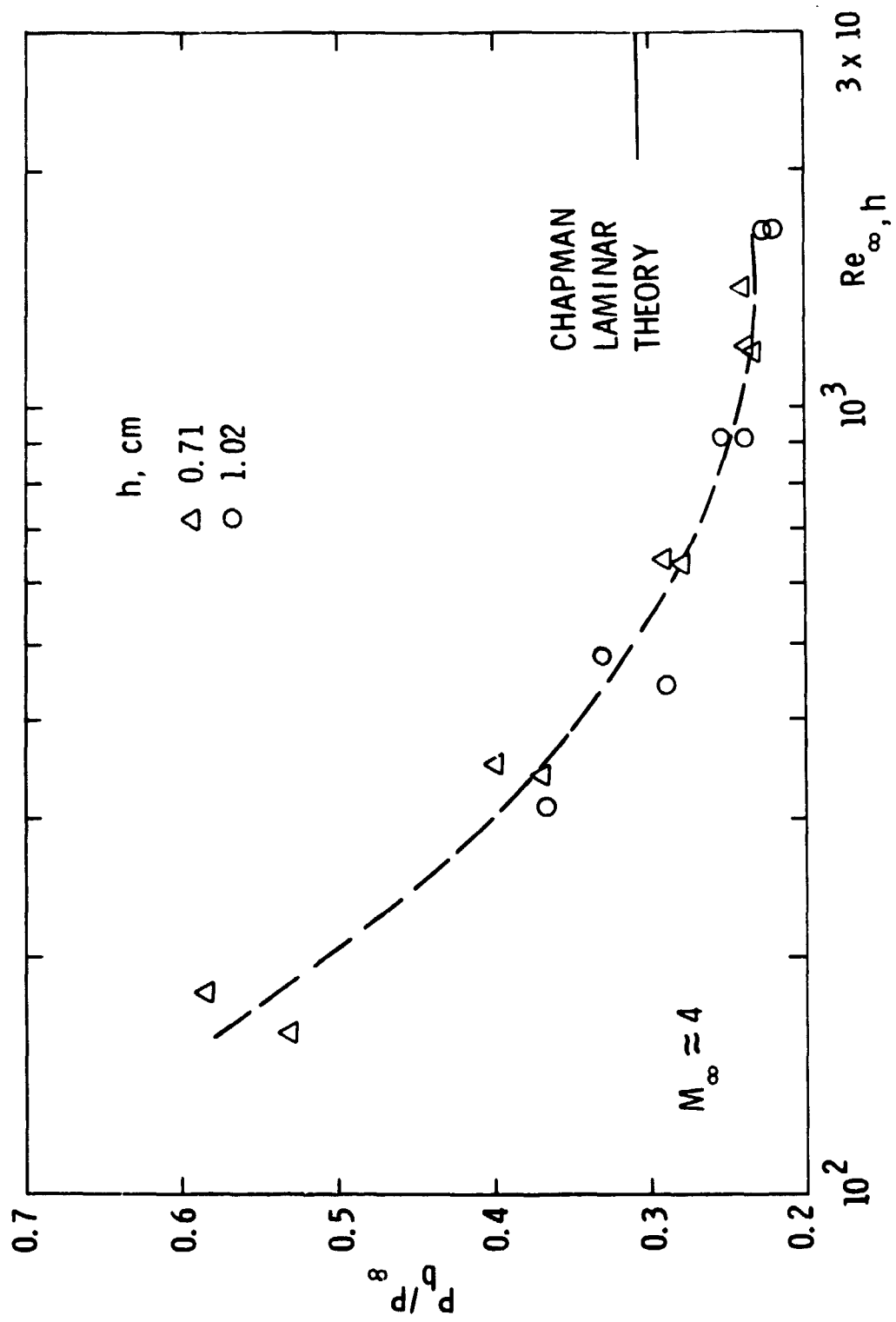
Figure 20. Base pressure as function of $Re_{\infty,h}$.
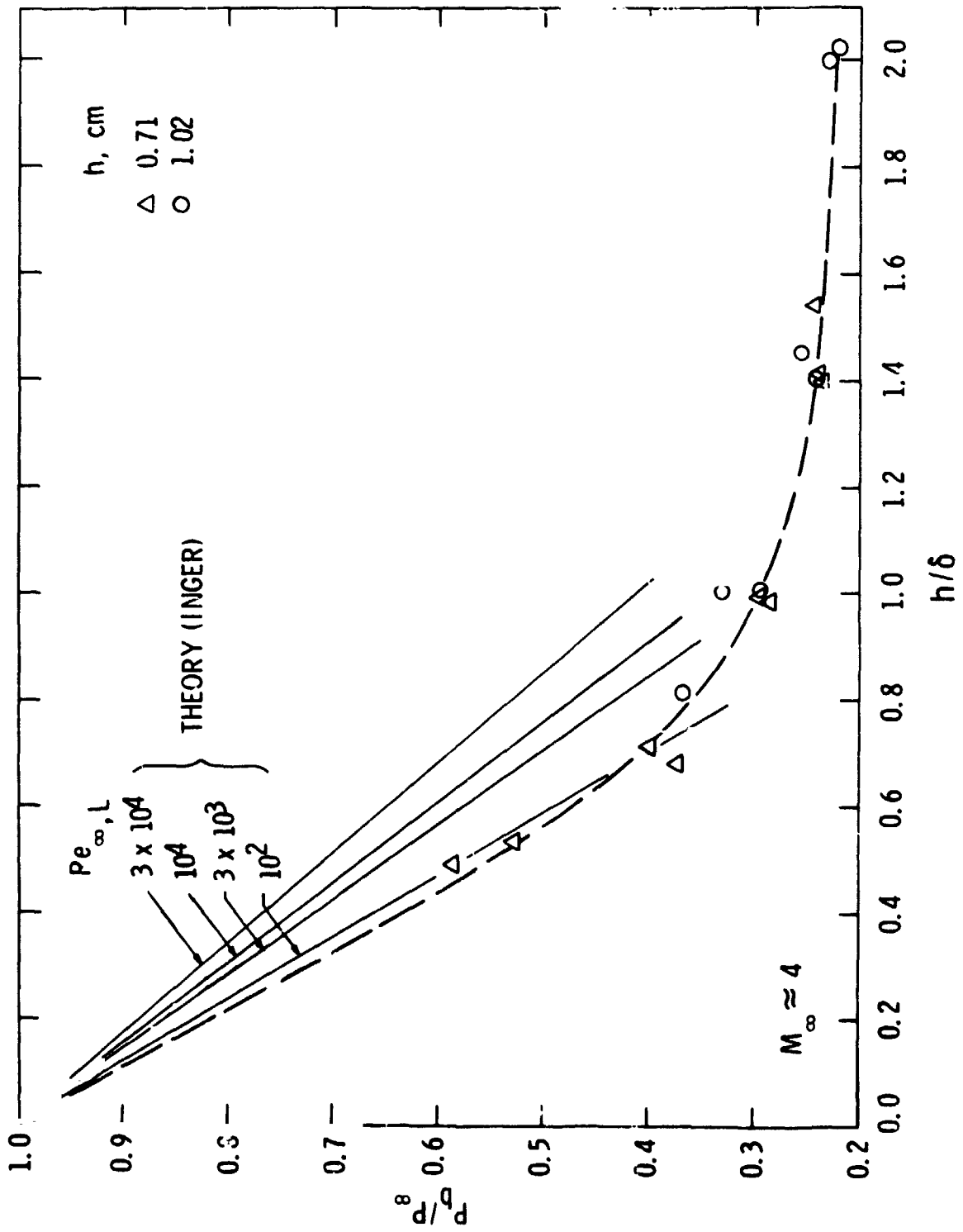
Figure 21. Base pressure as function of h/δ.

Figure 22a. Effect of mass suction on heat-transfer distribution downstream of the 1.02 cm step: Model II.

Run	h, cm	w	P_0, atm	T_0, °K	Re_∞/cm	M_∞
190- 7-12	1.02	0.22	0.348	3220	452	3.98
190- 8-12	1.02	0.00	0.379	3185	492	3.98
190-10-12	0.00	0.00	0.385	3250	491	3.99

60
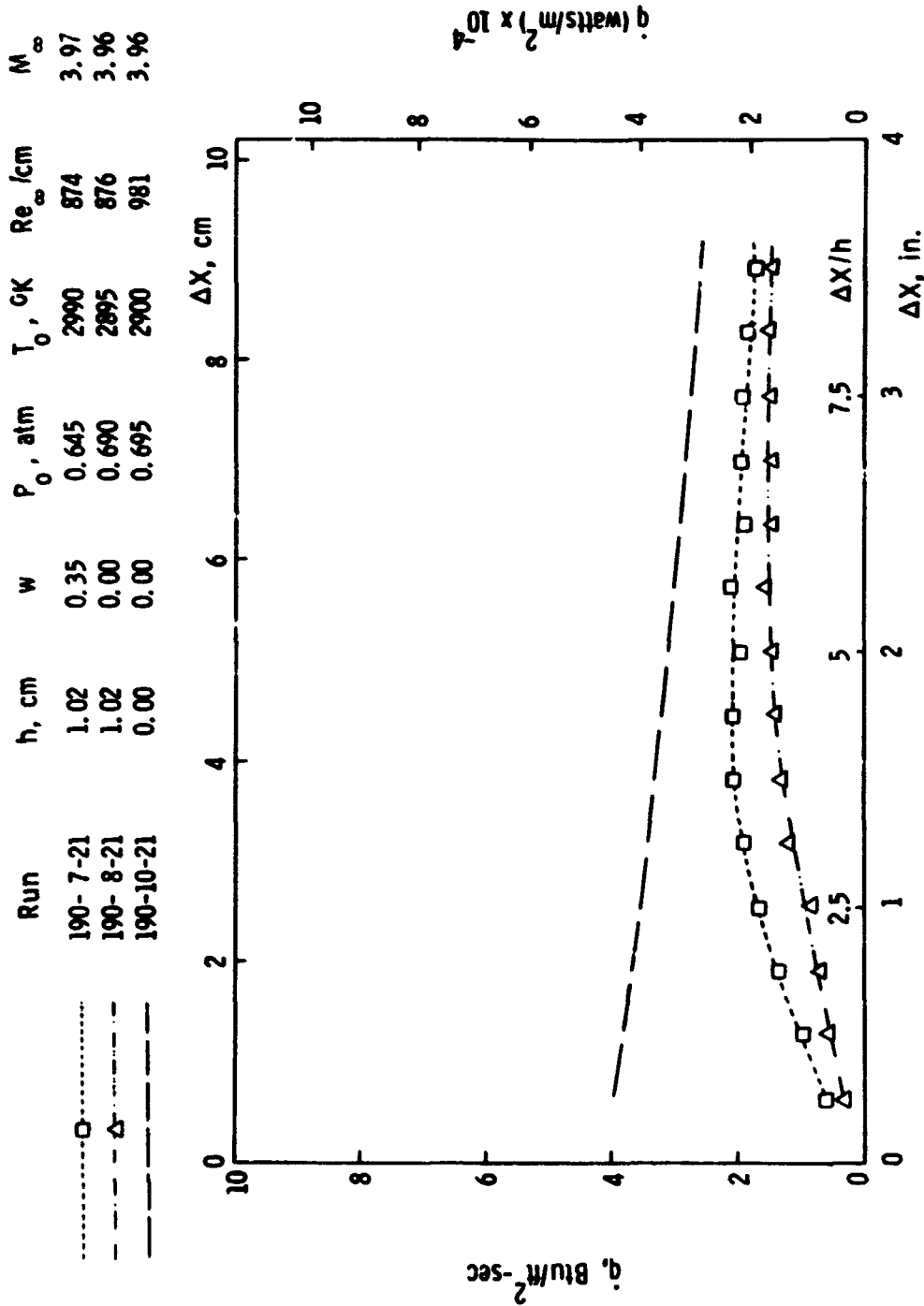
Figure 22b. Effect of mass suction on heat-transfer distribution downstream of the 1.02 cm step: Model II.

Run	h, cm	w	P_0, atm	T_0, $^\circ K$	Re_∞/cm	M_∞
190- 7-21	1.02	0.35	0.645	2990	874	3.97
190- 8-21	1.02	0.00	0.690	2895	876	3.96
190-10-21	0.00	0.00	0.695	2900	981	3.96
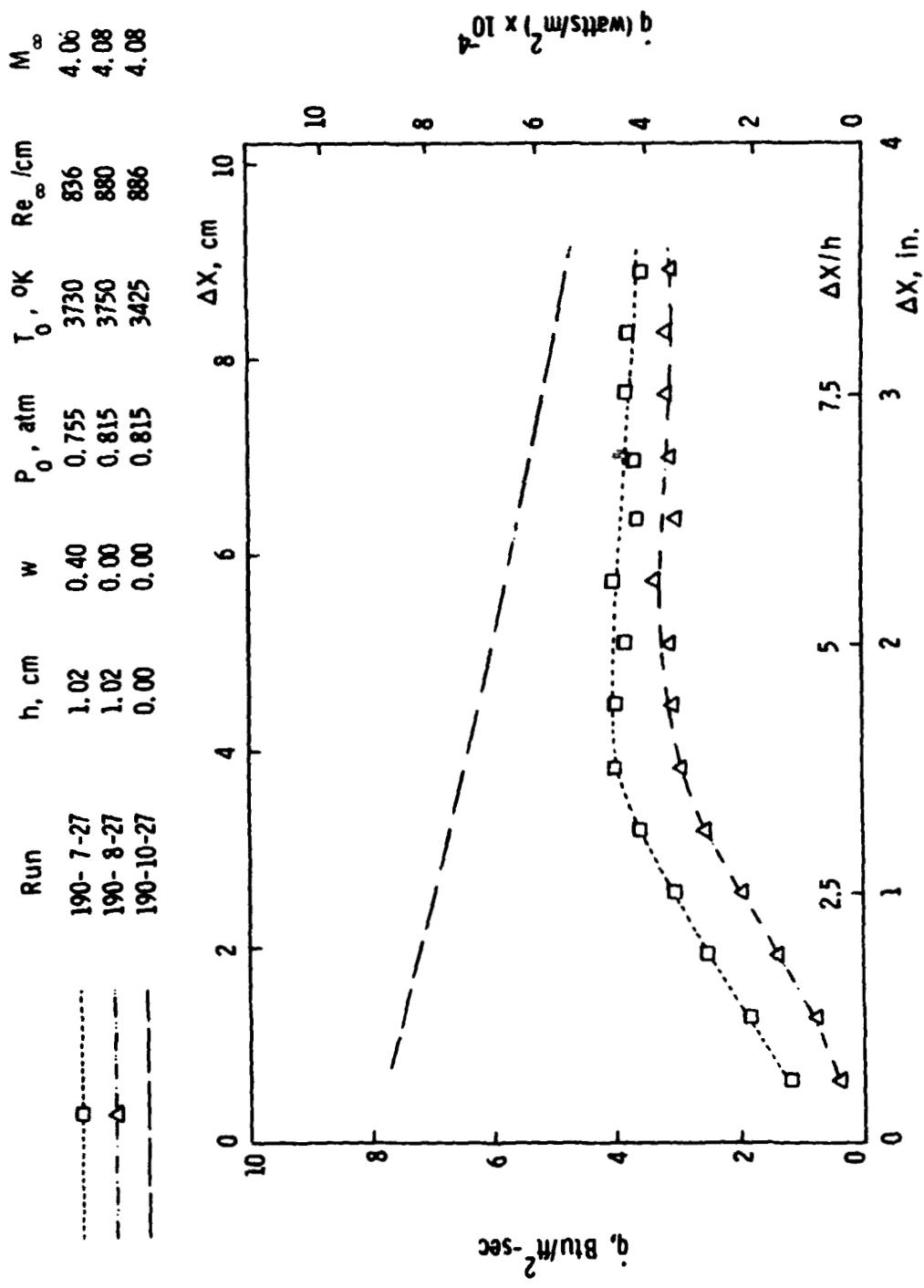
Figure 22c. Effect of mass suction on heat-transfer distribution downstream of the 1.02 cm step: Model II.

Figure 22d. Effect of mass suction on heat-transfer distribution downstream of the 1.02 cm step: Model II.

63
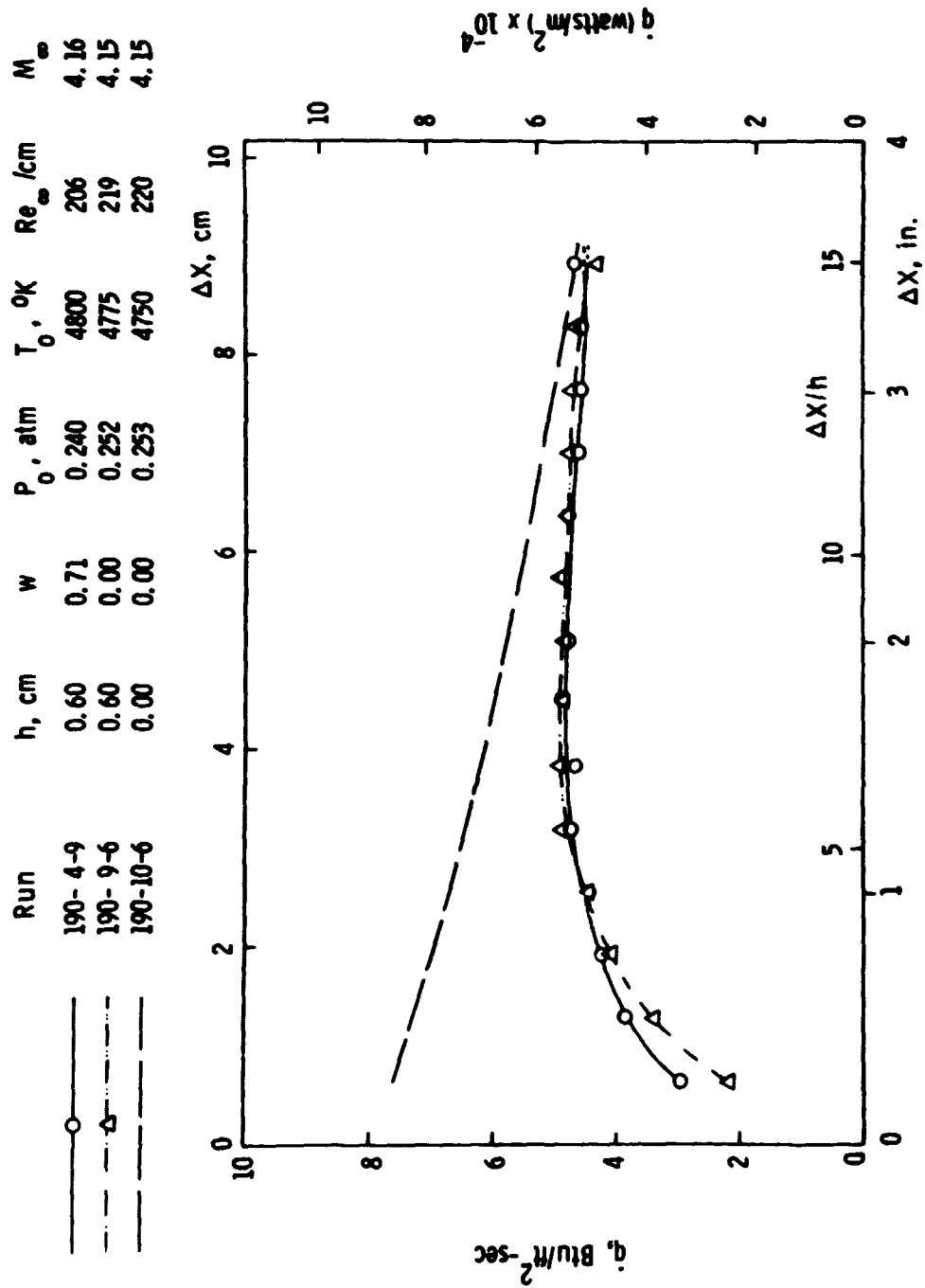
Figure 23a. Effect of mass suction on heat-transfer distribution downstream of the 0.6 cm step: Model II.
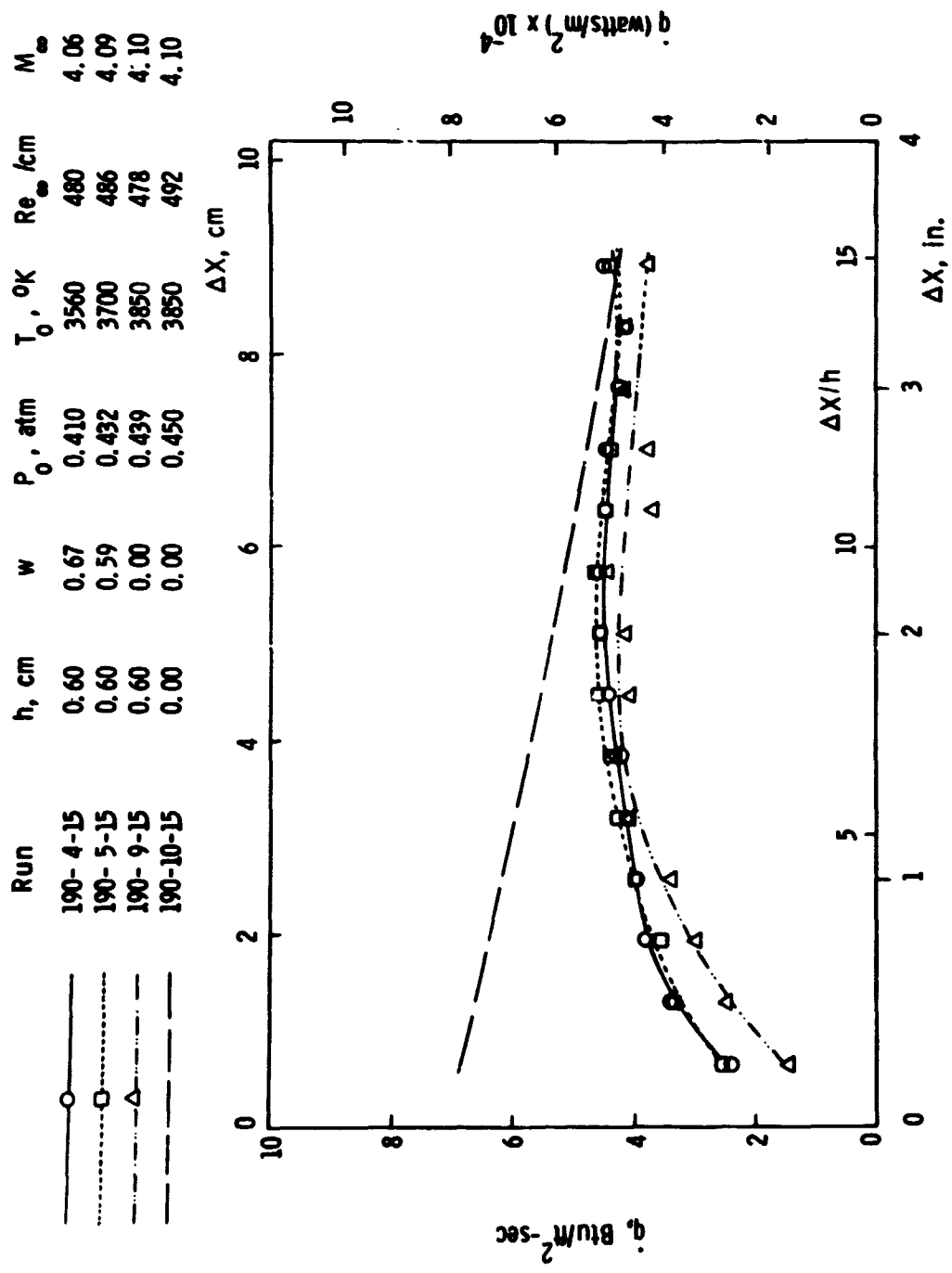
Figure 23b. Effect of mass suction on heat-transfer distribution downstream of the 0.6 cm step: Model II.
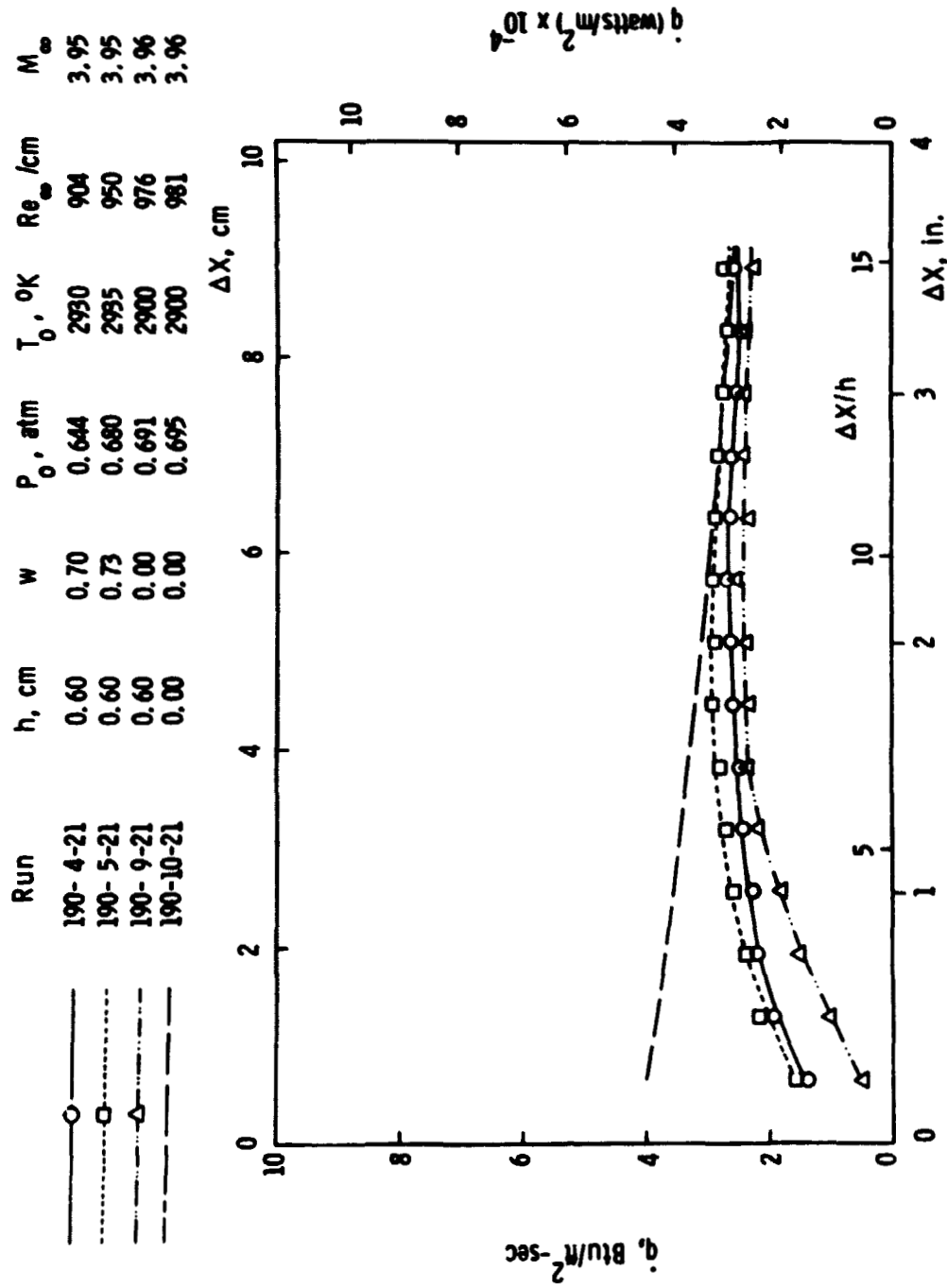
Figure 23c. Effect of mass suction on heat-transfer distribution downstream of the 0.6 cm step: Model II.

Figure 23d. Effect of mass suction on heat-transfer distribution downstream of the 0.6 cm step: Model II.
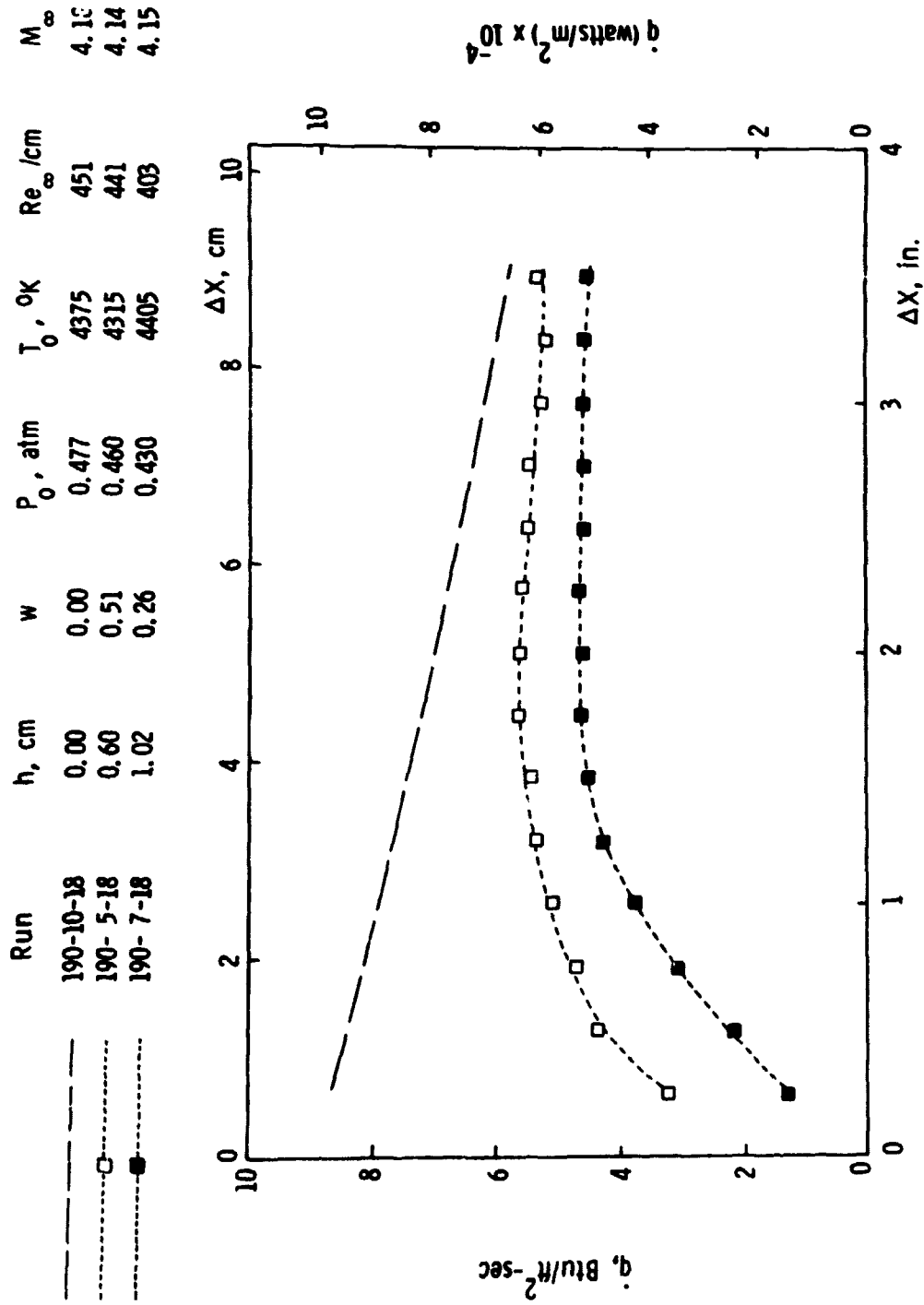
Figure 24a. Effect of step height on post-step heat-transfer distribution: Model II.

Figure 24b. Effect of step height on post-step heat-transfer distribution: Model II.

Run	h, cm	w	P_0, atm	T_0, °K	Re_∞/cm	M_∞
190-10-24	0.00	0.00	0.775	3450	917	4.01
190- 5-24	0.60	0.79	0.770	3470	905	4.02
190- 7-24	1.02	0.36	0.714	3420	850	4.01
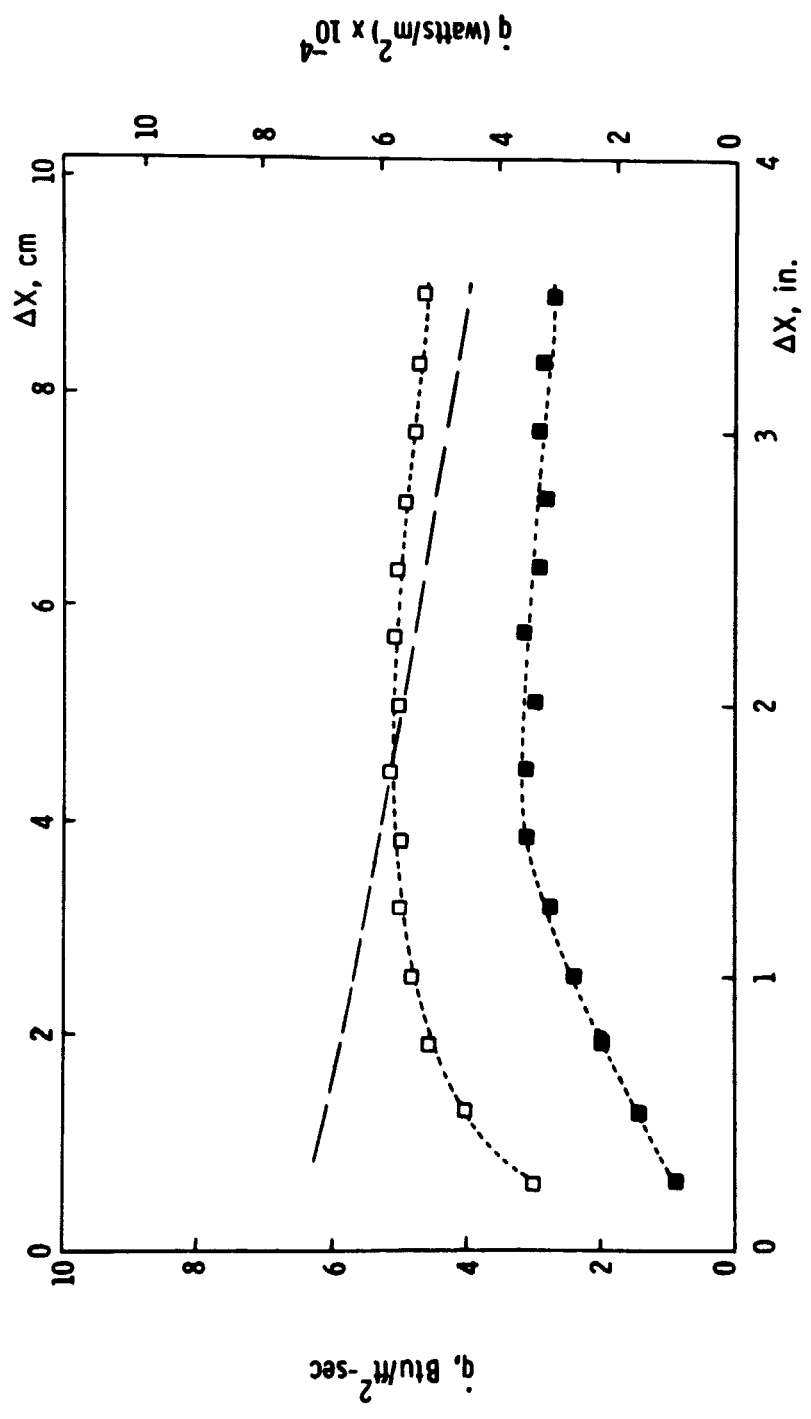
Figure 24c. Effect of step height on post-step heat-transfer distribution: Model II.
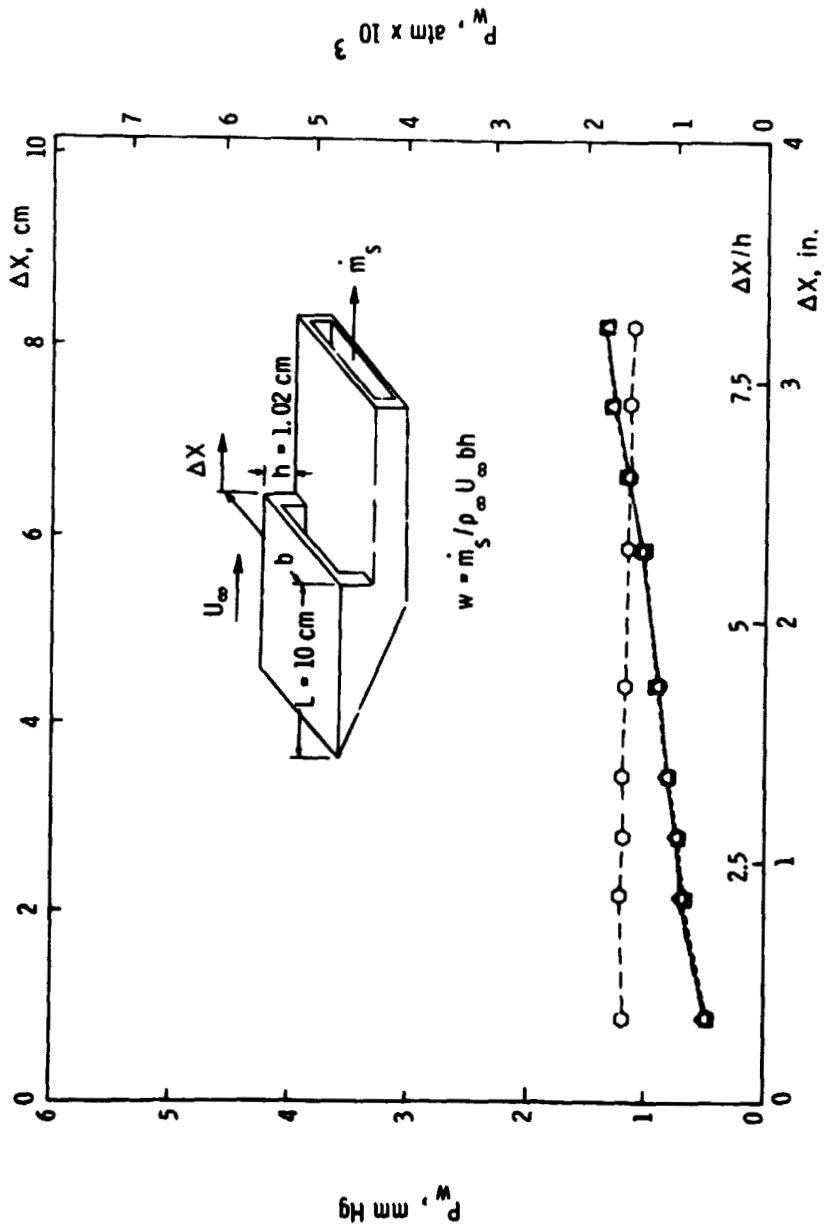
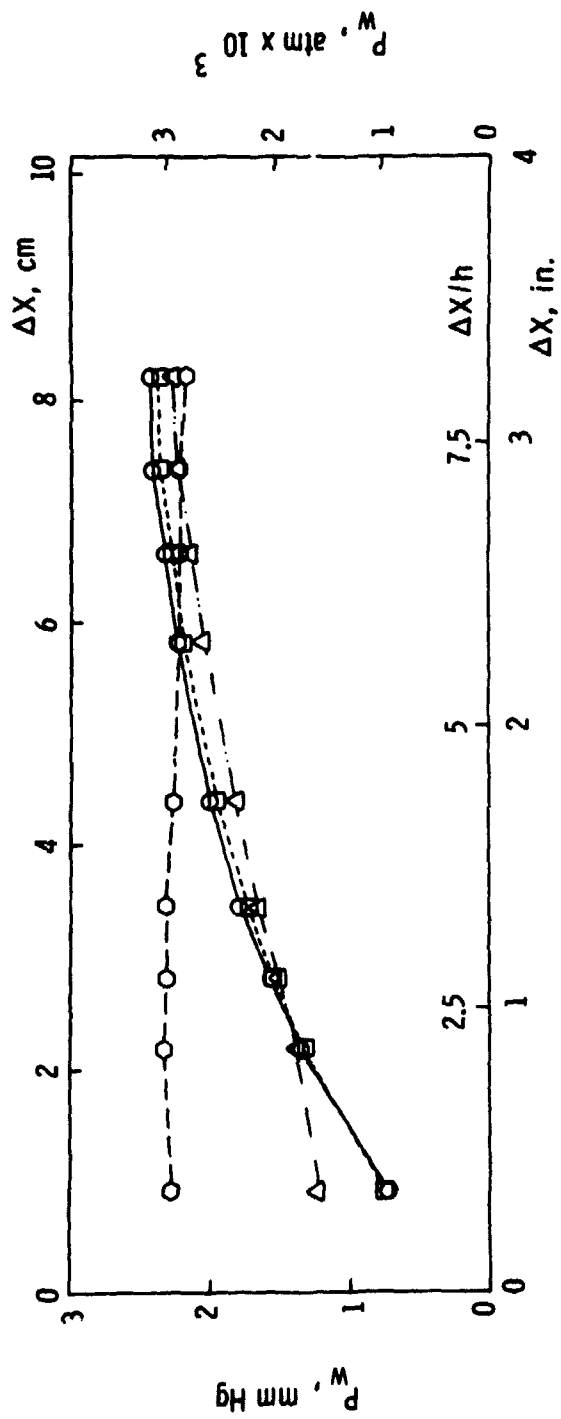Figure 25a. Effect of mass suction on pressure distribution downstream of the 1.02 cm step: Model II.

71

Figure 25b. Effect of mass suction on pressure distribution downstream of the 1.02 cm step: Model II.

Run	h, cm	w	P_o, atm	T_o, °K	Re_∞/cm	M_∞
197-1-21	1.02	0.39	0.680	2825	987	3.96
197-4-21	1.02	0.38	0.680	2950	937	3.96
197-3-21	1.02	0.00	0.675	2920	948	3.95
197-5-21	0.00	0.00	0.680	2950	937	3.96

72

Figure 25c. Effect of mass suction on pressure distribution downstream of the 1.02 cm step: Model II.

STREAMLINE

DIVIDING LINE

VORTICES

b) NO SUCTION CASE

DIVIDING LINE

STREAMLINE

$\dot{m}_s$

δ
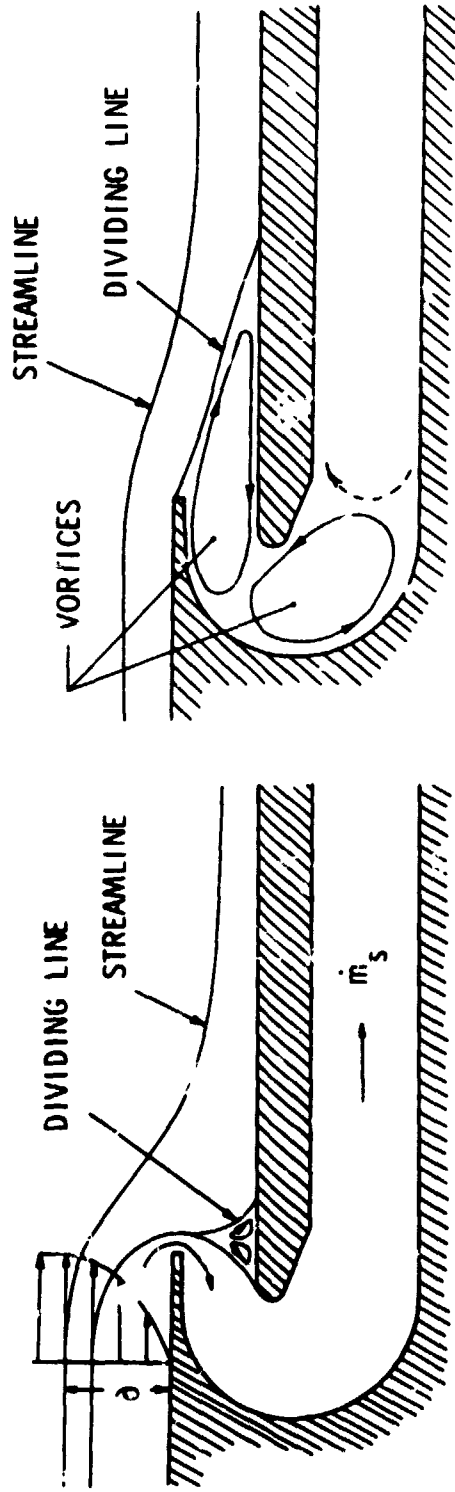
a) SUCTION CASE

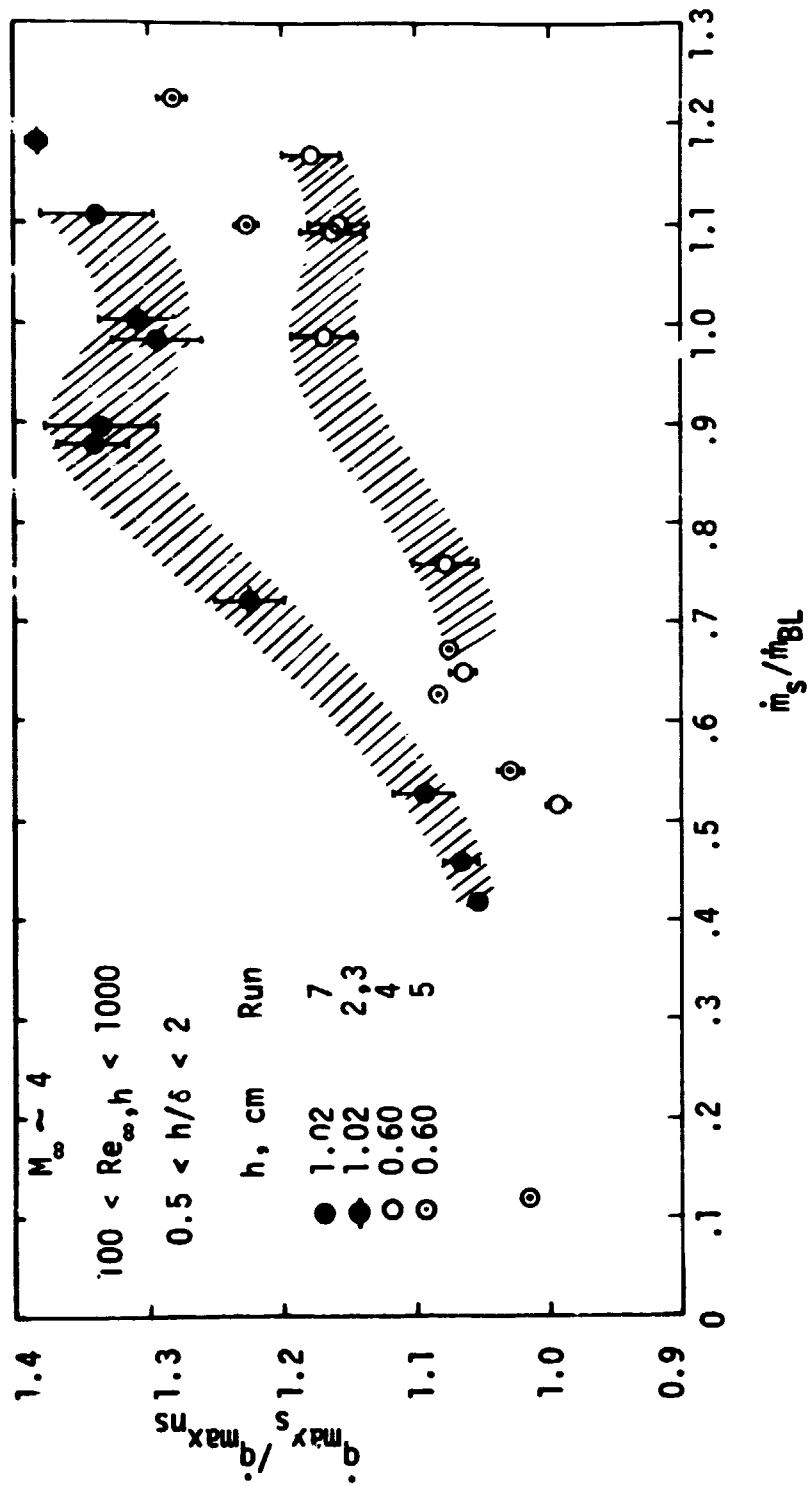Figure 26. Hypothetical flow fields in tests on Model II.

Figure 27. Increase in maximum heating rate as function of boundary-layer removal.
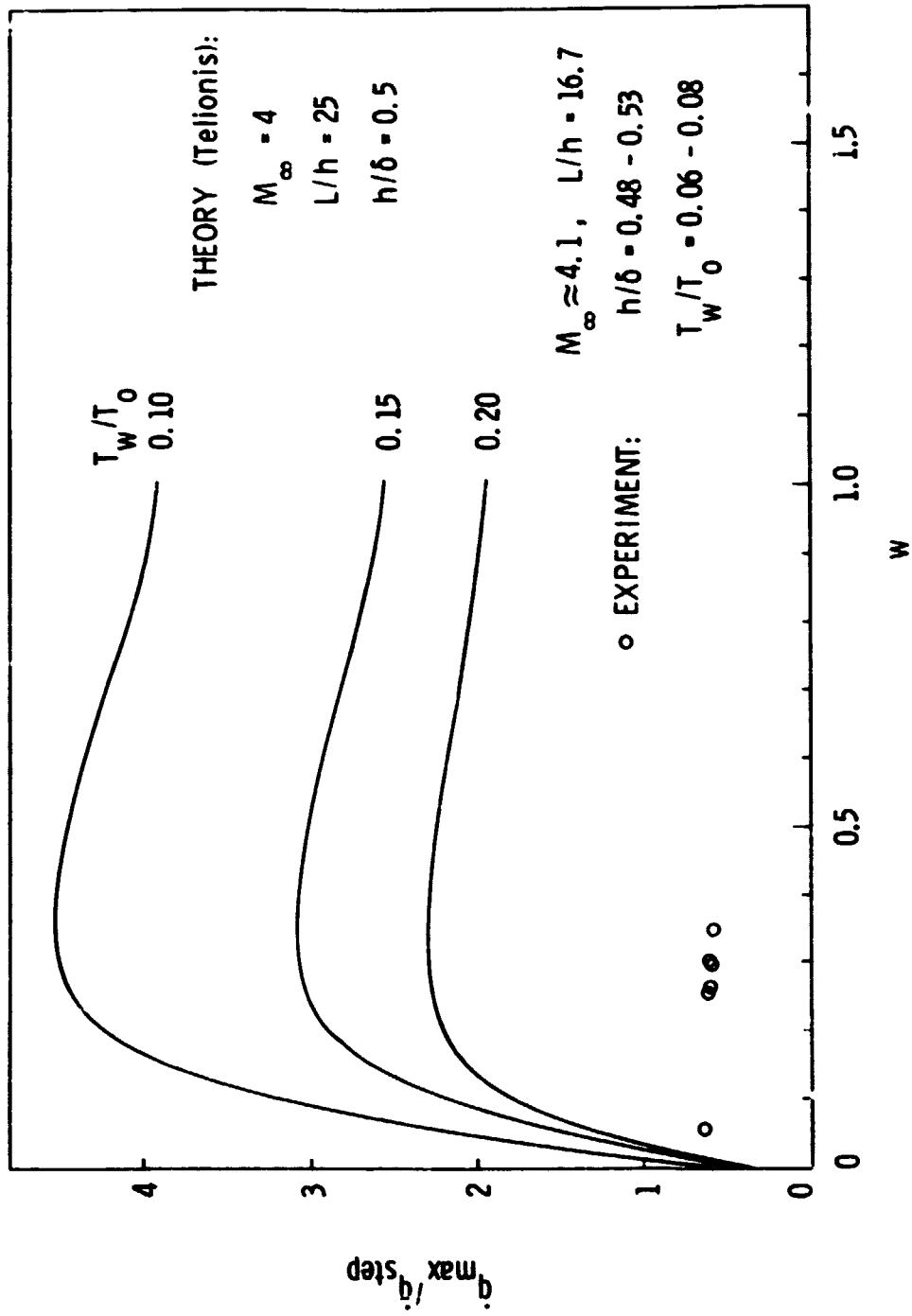
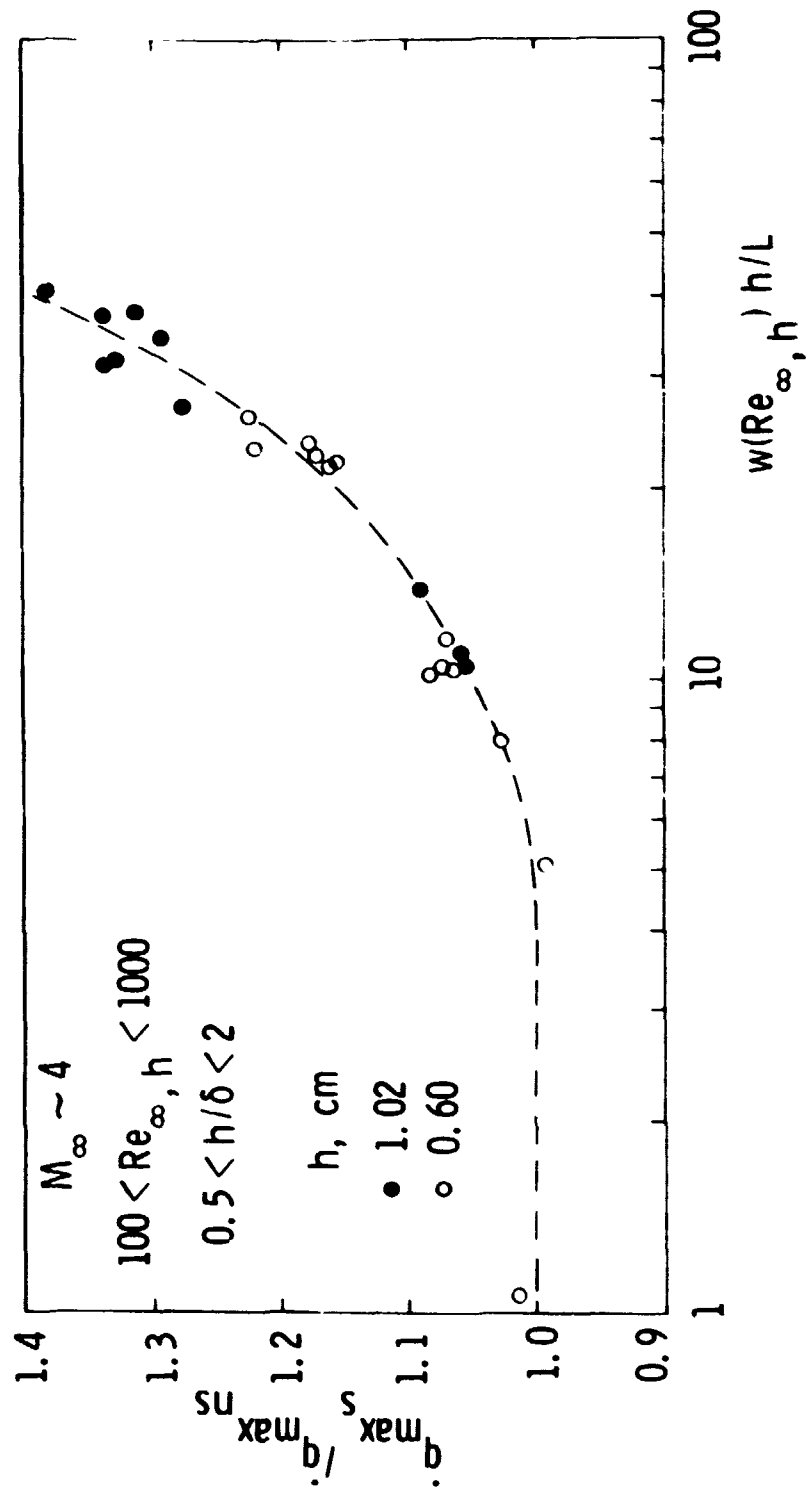Figure 28. Increase in maximum heating rate as function of w.

Figure 29. Correlation of maximum heating-rate increase due to mass suction.